

Chapter 2

Theoretical Framework

Jet physics, in particular at a hadron collider such as the LHC, cannot be understood without being thoroughly familiar with the theory of the strong interaction: quantum chromodynamics or short QCD. The material presented in this chapter is intended to provide the required proficiency to comprehend experimental and phenomenological publications on the subject of jet physics, some of which will be discussed in detail in the later chapters of this book. Basic knowledge of other aspects of the Standard Model (SM) of particle physics is implied or expected to be looked up in one of the many relevant textbooks. Hints for further reading will be given at the relevant occasions.

Before presenting a brief outline of the following sections, some notations need to be specified. Natural units, i.e. $\hbar = c = 1$ will be employed throughout so that energy, momentum, and mass all have units of $\text{eV} = e \cdot 1 \text{ V} \approx 1.6 \times 10^{-19} \text{ J}$. In this context, it is particularly useful to recall that $\hbar c = 1 \approx 200 \text{ MeV} \cdot \text{fm}$ can be exploited to translate energy units into units of length and time. Cross sections are given in the customary unit of “barn”,¹ $1 \text{ b} = 10^{-24} \text{ cm}^2$, with metric prefixes of “pico” or “femto” as appropriate for measurements in particle physics. The coordinate system that will be used is shown in Fig. 2.1, which defines the x , y , and z axes as well as some angular quantities. Symbols written as \vec{p} represent three-vectors, while p normally denotes a four-vector. The notation for matrices is **M**.

This chapter starts with a historical overview of the development of QCD, followed by a brief reminder of the basics of QCD theory. The next section deals with the central aspects of perturbative QCD. Subsequently, Monte Carlo event generators are introduced, followed by a thorough discussion of jet algorithms. The chapter is completed by a section on theoretical uncertainties and associated techniques for their evaluation.

¹The use of the unit “barn” goes back to December 1942, when it was introduced during wartime by M.G. Holloway and C.P. Baker. Because of its connection to nuclear physics this information was classified until 1948 [1].

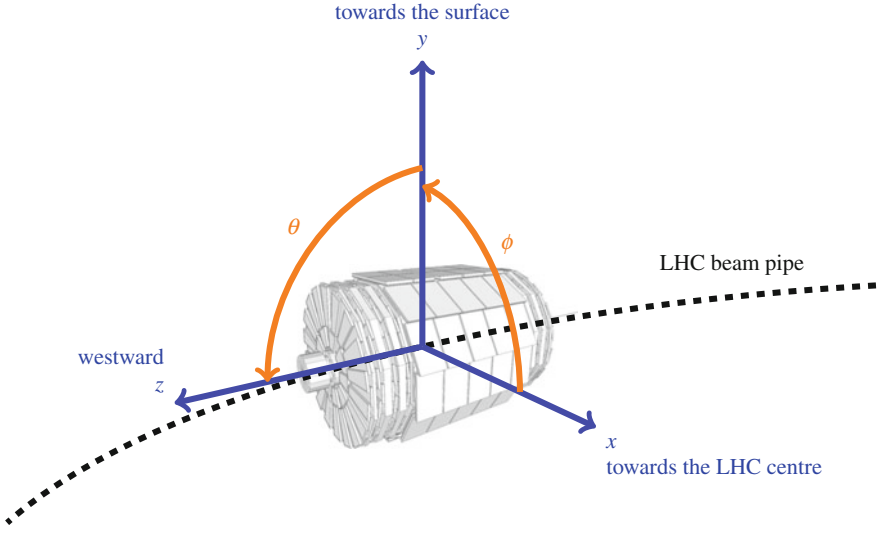


Fig. 2.1 Illustration of the coordinate system used by the LHC experiments at the example of the CMS detector: The experiments define a right-handed coordinate system with its origin at the nominal interaction point (IP) in the centre of the detector and the z axis pointing along the direction of the counterclockwise beam. The x axis points from the IP to the centre of the LHC ring, and the y axis points upwards, perpendicular to the plane of the LHC ring. Cylindrical coordinates (r, ϕ) are used in the transverse plane, ϕ being the azimuthal angle around the beam pipe. The pseudorapidity is defined in terms of the polar angle θ as $\eta = -\ln \tan(\theta/2)$; the rapidity, differing from η for massive objects, is defined as $y = 1/2 \cdot \ln [(E + p_z)/(E - p_z)]$. (Illustration courtesy of D. Haitz [2], background image source: CERN, CMS)

2.1 Historical Overview

Striving to describe as many phenomena in nature by as few fundamental assumptions as possible, physicists followed in the footsteps of chemists by replacing the roughly 100 chemical “elements” of the periodic table by merely two “elementary particles”: the positively charged proton and the negatively charged electron composing the atomic nuclei and shells, respectively. To properly account for atomic weights and to compensate the strongly repellent electrical force between the protons inside a nuclei, the list had to be complemented with electrically uncharged neutrons discovered by J. Chadwick in 1932 [3]. Theoretical developments by P.A.M. Dirac referring to the quantum mechanical description of spin- $\frac{1}{2}$ particles like the electron lead to the prediction of anti-particles [4] and the discovery of the anti-electron, the positron, by C.D. Anderson, also in 1932 [5]. Refining the technologies to observe cosmic rays, the muon was found unexpectedly in 1936 by C.D. Anderson and S. Neddermeyer [6] and first was mistaken for the so-called mu meson hypothesised one year earlier by H. Yukawa as carrier particle of the strong nuclear force [7]. However, it could be shown that the muon had the wrong properties and in particular did not take part in nuclear reactions. The real mu meson, the pion, was observed only eleven

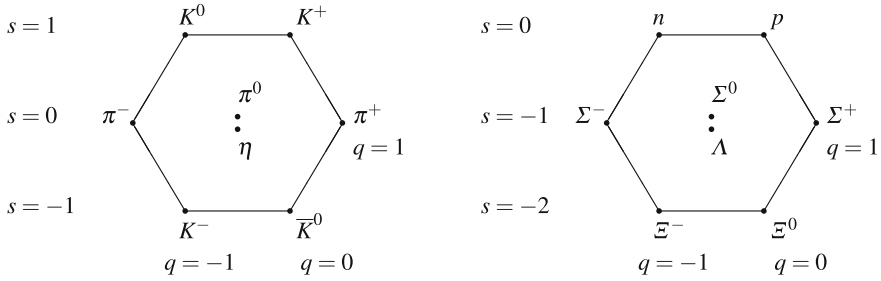


Fig. 2.2 Octets of spin-0 mesons (left) and spin- $\frac{1}{2}$ baryons (right) arranged according to their electrical charge q on the left-leaning diagonal and strangeness s on the horizontal lines. (Adapted from Source: 2007 Wikipedia, Laurascudder [16])

years later in 1947 by C. Lattes, G. Occhialini, and C. Powell again while studying cosmic radiation [8, 9]. In parallel, sophisticated technologies were developed in the thirties and forties to accelerate charged particles, which later on gave an enormous impetus to the field named *elementary particle physics*. Unfortunately, the huge number of new “elementary” particles discovered in the fifties and sixties, most of them subject to nuclear forces and hence collectively called *hadrons* in contrast to *leptons*, rendered it again difficult to find the ordering principles behind this *particle zoo*.

A clearer picture only started to emerge with the arrangement of the known spin-0 mesons and spin- $\frac{1}{2}$ baryons into octets, cf. Fig. 2.2, according to their electrical charge q and the new quantum property of *strangeness* s that seemed to be conserved in the production process via nuclear collisions, but not in particle decays, which are ascribed to the weak force. M. Gell-Mann coined the term the *Eightfold Way* for this scheme and applying it to the spin- $\frac{3}{2}$ baryons, cf. Fig. 2.3, he and independently Y. Ne’eman declared at the 1962 Rochester conference that a baryon Ω^- with charge $q = -1$ and strangeness $s = -3$ must exist [10], which was discovered two years later in 1964 [11]. The basis for the successful explanation of the observed hadron spectra essentially is their association with an approximate flavour $SU(3)$ symmetry group. For this connection, Gell-Mann and independently G. Zweig invented hadron constituents such that all hadrons known at that time could be composed out of either three such constituents for the baryons, or out of a constituent-anticonstituent pair for the mesons [12–14]. Gell-Mann thought of these constituents as *kworks*, which he later rewrote [15] into *quarks* after reading this expression in James Joyce’s “Finnegans Wake”. These quarks were postulated to come in the three flavours *up*, *down*, and *strange*, which are conserved in strong (nuclear) and electromagnetic reactions, but not in weak decays.² The strangeness of a particle then simply counts the number of antistrange minus the number of strange quarks, where the minus sign is chosen in analogy to the sign of the quark’s electrical charge. Peculiarly, however, the postulated quarks had to carry fractional electric charges of $+2/3$, $-1/3$ and $-1/3$, a feature which was never observed in nature.

²Supposing there ought to be four constituents in analogy to the four leptons, e , μ , ν_e , and ν_μ , known in 1963, Zweig dubbed them *aces*, but the name did not stick.

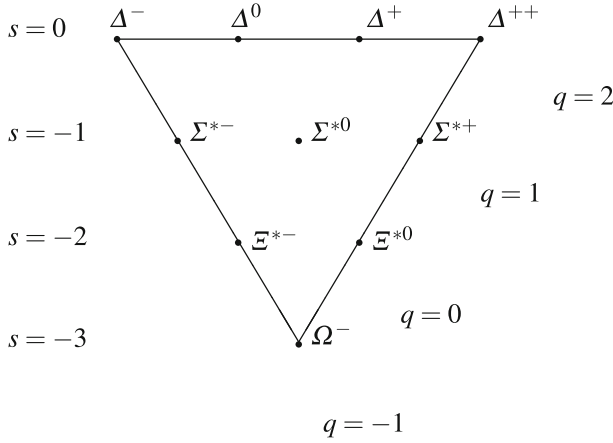


Fig. 2.3 Decuplet of spin- $\frac{3}{2}$ baryons arranged according to their electrical charge q on the left-leaning diagonal and strangeness s on the horizontal lines. (Adapted from Source: 2007 Wikipedia, Laurascudder [16])

Support for this quark constituent picture came from measurements of deep-inelastic electron-nucleon scattering (DIS) by the SLAC-MIT experiment at the Stanford Linear Accelerator Center [17, 18]. They confirmed a conjecture by J.D. Bjorken from 1969 that the scattering cross section does not depend on the absolute energy or the momentum transfer (squared), Q^2 , of the interaction but on dimensionless quantities like energy ratios or angles [19]. This “scaling” behaviour of the measured structure functions leads to a strikingly different prediction than a cross section falling steeply with increasing momentum transfer as expected from the product of elastic scattering and structure functions representing a finite size of the nucleon charge distribution. Interpreting the momentum transfer of the electron-nucleon scatter in terms of the spatial resolution at which the nucleons are probed, the scaling behaviour translates into an independence of the resolution scale and strongly suggests the presence of point-like scattering centres in a similar way that E. Rutherford concluded on the existence of an atomic nucleus decades before. In the slightly different context of high-energy hadron collisions such point-like constituents had also been proposed by R.D. Feynman who had given them the name *partons*, hence the name *quark-parton model* (QPM).

The so far missing dynamical description of strong interactions was greatly advanced by M. Veltman and G. ’t Hooft who proved in 1971 that non-Abelian gauge field theories based on the special unitary group $SU(N)$ are renormalisable [20]. The candidate quantum field theory (QFT) of the strong interaction suggested by Gell-Mann and H. Fritzsch in 1972 was just of this type [21]. In contrast to the previous approximate $SU(3)$ flavour symmetry that is explicitly broken by the different quark masses, the new threefold quantum number called *colour*, originally suggested by O. Greenberg [22], is associated with an exact $SU(3)$ symmetry of nature and each quark carries one of the three colours *red*, *green*, or *blue*. By attributing a different colour to each quark of a baryon, one can elegantly solve the so-called spin-statistics

problem. The Δ^{++} resonance shown in Fig. 2.3 top right has a spin of $\frac{3}{2}$ and consists of three u quarks leading to a fully symmetric wave function, in contradiction to the Pauli principle that demands it to be fully antisymmetric. Using the new colour degree of freedom for quarks, the wave function of the Δ^{++} can be antisymmetrised.

In analogy to quantum electrodynamics (QED), the gauge field theory of the electromagnetic interaction that is based on the unitary group $U(1)$, the theory of the strong interaction is called quantum chromodynamics (QCD). Similarly to QED, the strong force between the colour-charged quarks is mediated via eight massless exchange bosons of spin-1, the *gluons*.³ However, as a consequence of the non-Abelian character of the $SU(3)$ QCD gauge group, the eight gluons carry colour charges and interact amongst themselves via triple and quartic gluon vertices. This is a striking difference to the electromagnetic force, which is mediated by electrically uncharged photons.

Despite the additional colour degree of freedom, however, there do not seem to be any new hadrons associated with it. For an explanation the dynamics mediated by the self-interacting gluons has to be scrutinised. In QFT the *beta function* encodes the logarithmic dependence of a coupling parameter g on the relevant energy scale μ of a physical process:

$$\beta(g) = \frac{\partial g}{\partial \log(\mu)} . \quad (2.1)$$

D.J. Gross, H.D. Politzer, and F. Wilczek calculated in 1973 and 1974 in a perturbative expansion the beta function of QCD to lowest order and found that it has a negative sign in contrast to the beta function of QED [24–27]. As a consequence the strong force increases with distance, inversely to the electromagnetic force, and becomes small at very high energies, i.e. at subnuclear dimensions. This property is called *asymptotic freedom*. Gross, Politzer, and Wilczek also noted that the approximate scaling of structure functions of deep-inelastic electron-nucleon scattering as observed in the SLAC-MIT experiment could now be understood in terms of a QFT. The gross violation of scaling behaviour predicted by any QFT is, in agreement with experiment, reduced to a mild logarithmic scaling violation in asymptotically free theories. Thus, accounting for the gluon degrees of freedom, Feynman’s point-like parton constituents of hadrons can be identified with the asymptotically free coloured quarks, antiquarks, and gluons of QCD.

On the other hand the approximately linear growth in strength of the strong force with increasing spatial separation between two colour charges leads to the fact that colour-charged objects are confined to subnuclear dimensions. This property of QCD is called *confinement*. Only entities that are colour singlets, i.e. without any net colour charge, are not subject to strong interactions and can be observed as free particles. This is in complete accordance with experiment where only colourless hadrons are observed. Moreover, all such combinations of three quarks (or antiquarks) in the form of baryons or of a quark-antiquark pair in the form of a meson exhibit integer

³The name “gluon” initially was introduced by Gell-Mann in a slightly different context without reference to colour [23].

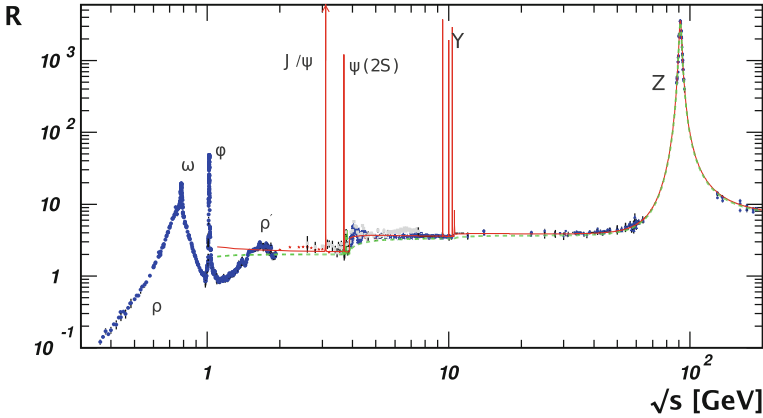


Fig. 2.4 World data on the ratio R of the total cross section of the reaction $e^+e^- \rightarrow \text{hadrons}$ to the cross section of the reaction $e^+e^- \rightarrow \mu^+\mu^-$ as a function of the centre-of-mass energy \sqrt{s} . (Adapted from the 2015 update of Ref. [28])

multiples of the electric charge, which explains why particles with non-integer electrical charges have never been observed in nature. Nevertheless, the fractional charges of the quarks have a direct influence on measurable quantities, notably the ratio R of the total cross section of the reaction $e^+e^- \rightarrow \text{hadrons}$ compared to $e^+e^- \rightarrow \mu^+\mu^-$. At centre-of-mass energies below the production threshold for the pairwise ($q\bar{q}$) production of *charm* or *bottom* quarks, one obtains $R = N_C \cdot \sum_q e_q^2 \cdot (1 + \delta_{m_q, \text{QCD}})$ where $N_C = 3$ is the number of colours and e_q is the charge of the up, down, and strange quarks. $\delta_{m_q, \text{QCD}}$ accounts for finite quark-mass and QCD corrections. When the collision energy surpasses the threshold for charm-anticharm or bottom-antibottom pair production, a corresponding step in this ratio is observed, cf. Fig. 2.4.

Today, QCD has been firmly established as the gauge theory of the strong interaction, one of the four fundamental forces of nature, and represents a cornerstone of the Standard Model of particle physics. It has a broad range of applications from high transverse momentum interactions between coloured quarks and gluons at TeV energies down to the low energy formation of hadrons and mesons. Numerous excellent text books and review articles have appeared in the course of time and provide extensive coverage of QCD and related topics.⁴ General principles of QFT are discussed in Refs. [30–34], while Refs. [35–44] are specialised on QCD. The foundations of perturbative QCD are laid out in Ref. [45]. The reviews [46, 47] and the books [48, 49] are recommended specifically in the context of QCD at the LHC. For a historical perspective on QCD Refs. [50, 51] can be consulted. The experimental foundations of particle physics in general are explained in Ref. [10] in their historical context including reprints of numerous original articles. The reference for the current state

⁴References in this book have been managed with the help of JABREF [29].

of research is the Review of Particle Physics by the Particle Data Group (PDG) [28], which is also available online.⁵

2.2 Basic Elements of QCD

As a gauge field theory, QCD is defined via its *Lagrangian density* \mathcal{L}_{QCD} , which is composed of four terms:

$$\mathcal{L}_{\text{QCD}} = \mathcal{L}_{\text{quarks}} + \mathcal{L}_{\text{gluons}} + \mathcal{L}_{\text{gauge}} + \mathcal{L}_{\text{ghost}} , \quad (2.2)$$

where

1. $\mathcal{L}_{\text{quarks}}$ describes the interaction of spin- $\frac{1}{2}$ quark fields q_a of mass m_q with spin-1 gluon fields \mathcal{A}_μ^A ,
2. $\mathcal{L}_{\text{gluons}}$ represents the kinetic term of the gluon fields \mathcal{A}_μ^A ,
3. $\mathcal{L}_{\text{gauge}}$ defines the chosen gauge,
4. and $\mathcal{L}_{\text{ghost}}$ is the so-called *ghost* term that is a remedy necessary in non-Abelian gauge theories to treat the degeneracy of equivalent gauge field configurations.

Here and in the following, spinor indices are suppressed, Greek letters $\mu, \nu, \dots \in \{0, 1, 2, 3\}$ represent space-time indices, and $a, b, c \in \{1, \dots, 3\}$ and $A, B, C \in \{1, \dots, 8\}$ are the indices of the triplet and octet representations, respectively, of the colour $SU(3)$ gauge symmetry group. Summation over identical indices is implied. As in QED, the first term can be written with the help of the covariant derivative $(\mathcal{D}_\mu)_{ab}$ as

$$\mathcal{L}_{\text{quarks}} = \sum_{q \in \{u, d, s, c, b, t\}} \bar{q}_a (i\gamma^\mu (\mathcal{D}_\mu)_{ab} - m_q) q_b , \quad (2.3)$$

where the sum runs over all six quark flavours $\{u, d, s, c, b, t\}$ and γ_μ are the *Dirac matrices*. Defining the diagonal metric tensor g as $g^{\mu\nu} = \text{diag}(1, -1, -1, -1)$, the γ matrices satisfy the anticommutation relation

$$\{\gamma^\mu, \gamma^\nu\} = 2g^{\mu\nu} . \quad (2.4)$$

In contrast to QED, however, the covariant derivative

$$(\mathcal{D}_\mu)_{ab} = \partial_\mu \delta_{ab} + ig_s T_{ab}^A \mathcal{A}_\mu^A \quad (2.5)$$

not only exhibits colour indices a, b and the gauge coupling g_s of the strong interaction, but also, instead of one photon field for the sole generator of the $U(1)$

⁵PDG: <http://pdg.web.cern.ch/pdg>.

Further useful resources for data, programmes, etc. are:

HEPDATA: <http://durpdg.dur.ac.uk/HepData>,

HEPFORGE: <http://www.hepforge.org/>.

group, eight gluon fields \mathcal{A}_μ^A with factors \mathcal{T}_{ab}^A corresponding to the generators of the $SU(3)$ gauge group of QCD. A representation of the generators is given via $\mathcal{T}^A = \lambda^A/2$ by the Hermitian⁶ and traceless *Gell-Mann matrices* λ^A :

$$\begin{aligned} \lambda^1 &= \begin{pmatrix} 0 & +1 & 0 \\ +1 & 0 & 0 \\ 0 & 0 & 0 \end{pmatrix}, & \lambda^2 &= \begin{pmatrix} 0 & -i & 0 \\ +i & 0 & 0 \\ 0 & 0 & 0 \end{pmatrix}, & \lambda^3 &= \begin{pmatrix} +1 & 0 & 0 \\ 0 & -1 & 0 \\ 0 & 0 & 0 \end{pmatrix}, \\ \lambda^4 &= \begin{pmatrix} 0 & 0 & +1 \\ 0 & 0 & 0 \\ +1 & 0 & 0 \end{pmatrix}, & \lambda^5 &= \begin{pmatrix} 0 & 0 & -i \\ 0 & 0 & 0 \\ +i & 0 & 0 \end{pmatrix}, & \lambda^6 &= \begin{pmatrix} 0 & 0 & 0 \\ 0 & 0 & +1 \\ 0 & +1 & 0 \end{pmatrix}, \\ \lambda^7 &= \begin{pmatrix} 0 & 0 & 0 \\ 0 & 0 & -i \\ 0 & +i & 0 \end{pmatrix}, & \lambda^8 &= \frac{1}{\sqrt{3}} \begin{pmatrix} +1 & 0 & 0 \\ 0 & +1 & 0 \\ 0 & 0 & -2 \end{pmatrix}. \end{aligned} \quad (2.6)$$

The (2×2) submatrices of the first three λ_A can be recognised as *Pauli matrices*. The generator matrices \mathcal{T}^A satisfy the commutation relations

$$[\mathcal{T}^A, \mathcal{T}^B] = i f^{ABC} \mathcal{T}^C, \quad (2.7)$$

where f^{ABC} are the corresponding *structure constants* of $SU(3)$ with values of

$$\begin{aligned} f^{123} &= 1 \\ f^{147} &= -f^{156} = f^{246} = f^{257} = f^{345} = -f^{367} = \frac{1}{2} \\ f^{458} &= f^{678} = \frac{\sqrt{3}}{2}, \end{aligned} \quad (2.8)$$

while all other f^{ABC} not related to these by index permutations are zero. The kinetic term of the gluons then reads

$$\mathcal{L}_{\text{gluons}} = -\frac{1}{4} \mathcal{G}_{\mu\nu}^A \mathcal{G}_A^{\mu\nu}, \quad \text{with} \quad \mathcal{G}_{\mu\nu}^A = \partial_\mu \mathcal{A}_\nu^A - \partial_\nu \mathcal{A}_\mu^A - g_s f^{ABC} \mathcal{A}_\mu^B \mathcal{A}_\nu^C \quad (2.9)$$

being the field strength tensor. In a pictorial representation,⁷ these two “classical” parts correspond to the free quark- and gluon-field terms, and the quark-gluon interaction term as depicted in Figs. 2.5 and 2.6. In addition, the non-Abelian group structure of QCD leads to the cubic and quartic gluon self-interaction vertices, which are proportional to g_s and g_s^2 , respectively.

Although not obvious from the Gell-Mann matrices or the structure constants, it can be shown that the probabilities for a quark emitting a gluon, or gluons splitting into a quark-antiquark or a gluon pair are identical with respect to each colour.

⁶A Hermitian matrix \mathbf{A} is equal to its complex conjugate transpose, i.e. $\mathbf{A} = \mathbf{A}^{*T} = \mathbf{A}^\dagger$.

⁷Feynman diagrams in this book have been drawn with the help of JAXODRAW [52].

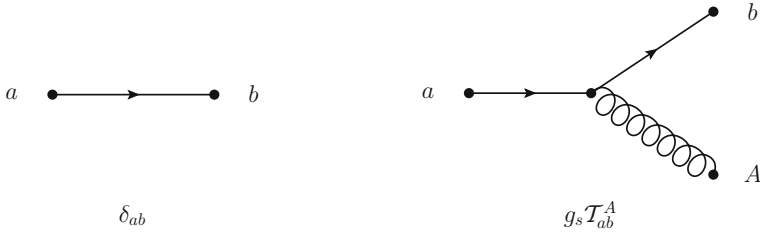


Fig. 2.5 Free quark-field and quark-gluon interaction term

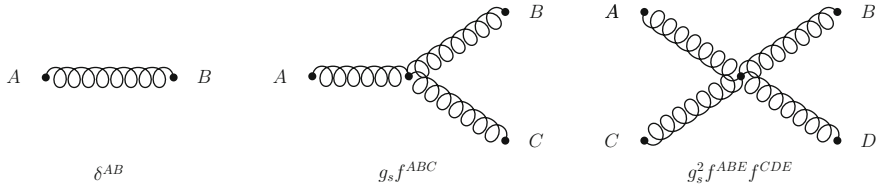


Fig. 2.6 Free gluon-field and cubic and quartic gluon self-interaction terms

Following the conventional normalisation of the colour $SU(3)$ matrices via the trace $\text{Tr} \{T^A T^B\} = T_F \delta^{AB}$ with $T_F = 1/2$, the relative factors for these processes are given by $C_F = 4/3$, $T_F = 1/2$, and $C_A = 3$. The ratio of a gluon emission by a gluon relative to the emission by a quark is therefore approximately $C_A/C_F = 9/4 = 2.25$, i.e. gluons radiate stronger than quarks by more than a factor of two. Similarly, gluons split into a gluon pair more often than into a quark-antiquark pair by roughly a factor of $C_A/T_F = 6$.

Of course, this classical QCD Lagrangian exhibits the property of local gauge invariance, i.e. invariance under a simultaneous redefinition of the quark and gluon fields. As a consequence of this internal symmetry, it is impossible to define the gluon field propagator without explicitly specifying a choice of gauge. A popular choice is given as a generalisation of the covariant Lorentz gauge $\partial^\mu \mathcal{A}_\mu^A = 0$ by the class of R_ξ gauges, imposed by adding the term

$$\mathcal{L}_{\text{gauge}} = -\frac{1}{2\xi} (\partial^\mu \mathcal{A}_\mu^A)^2 \quad (2.10)$$

to the classical Lagrangian. Following L.D. Faddeev and V.N. Popov [53] this must be accompanied by the ghost term

$$\mathcal{L}_{\text{ghost}} = \partial_\mu \eta^{A\dagger} (\mathcal{D}_{AB}^\mu \eta^B) \quad (2.11)$$

because of the non-Abelian character of the QCD gauge group. The ghosts η^A , with conjugate-transpose $\eta^{A\dagger}$, represent complex scalar fields that nevertheless obey Fermi–Dirac statistics. They do not have a physical meaning, but should be

considered as a mathematical trick to cancel nonphysical degrees of freedom otherwise present in calculations with covariant gauges.

This completes the Lagrangian for a consistent QFT of the strong interaction. Further invariant terms to add to the QCD Lagrangian are conceivable in principle. Renormalisability, however, forbids all additions that require coefficients with negative mass dimensions. Moreover, mass terms for the gluon fields, $m_A^2 \mathcal{A}_\mu^A \mathcal{A}^{A\mu}$, would violate gauge invariance. The only leftover possibility makes use of the *dual field strength tensor* defined as

$$\tilde{\mathcal{G}}_{\mu\nu}^A = \frac{1}{2} \varepsilon_{\mu\nu}{}^{\rho\sigma} \mathcal{G}_{\rho\sigma}^A, \quad (2.12)$$

where $\varepsilon_{\mu\nu}{}^{\rho\sigma}$ is the four-dimensional antisymmetric *Levi-Civita symbol*. With the help of this definition the so-called θ -term is written as

$$\mathcal{L}_\theta = \theta \frac{g_s^2 T_F}{16\pi^2} \mathcal{G}_{\mu\nu}^A \tilde{\mathcal{G}}^{A\mu\nu}. \quad (2.13)$$

This contribution would give rise to violations of the discrete symmetries of parity P and time reversal T by the strong interaction, which have never been observed in nature. Since T -violations are equivalent to a violation of the combined symmetry of charge conjugation C followed by P , experimental upper limits on the CP -violating electric dipole moment of the neutron lead to the conclusion that $|\theta|$ must be smaller than 10^{-10} [28]. Since no obvious reason is known for the smallness of this parameter, this is called the *strong CP problem*. New phenomena like *axions* as suggested by R. Peccei and H. Quinn in Refs. [54, 55] could provide an explanation.

2.3 Perturbative QCD

Given the complete QCD Lagrangian, quantitative predictions can be obtained either by means of lattice gauge theory (LGT), which applies QCD to a world discretised in space and time, or by using perturbative QCD (pQCD), which is valid in the asymptotically free regime, i.e. at high momentum transfers or respectively small distances, where quarks and gluons are weakly coupled. Computations in LGT are extremely complex and time-consuming and for a long time were not possible without severe approximations. For predictions in the context of collisions at the LHC, they are of very limited practical importance at present. On the other hand, such interactions at high- p_T are an ideal testing ground for a perturbative analysis of the strong interaction. In practice, however, the calculations are complicated by the occurrence of singularities that need to be properly addressed.

2.3.1 The Strong Coupling Constant

All Feynman rules required for a perturbative analysis can be deduced from the presented QCD Lagrangian. The relevant parameter in such a perturbative expansion is the gauge coupling g_s or equivalently the *strong coupling constant* α_s , which is defined in analogy to the QED *fine structure constant* α as $\alpha_s = g_s^2/4\pi$. With the knowledge of this fundamental parameter of QCD, in addition to the quark masses, tree-level amplitudes are calculable. Complications arise when loop diagrams come into play, because the momenta in a loop are not fully constrained by four-momentum conservation. The remaining integral over a loop momentum is logarithmically divergent for arbitrarily large momenta, which corresponds to an infinitely fine resolution. The strategy to overcome such *ultraviolet divergencies* that occur for example in self-energy corrections to quark and gluon lines, cf. Fig. 2.7, or in vertex corrections like in Fig. 2.8, is called *renormalisation*. Since QCD was proven to be a renormalisable QFT [20], the infinities can be absorbed into a finite number of parameters that need to be taken from experiment: the renormalised quark masses and coupling constant. Expressed in renormalised quantities, the Lagrangian of QCD must have exactly the same structure as the “bare” one presented in the previous section, such that counterterms cancel the divergencies to all orders in perturbation theory. As a consequence, precise higher order predictions can be made using the measured renormalised parameters. Details on the theoretical procedures are beyond this work and can be found for example in Ref. [35] specialised on QCD, or in Ref. [30] for QFT in general. For a historical perspective it might be interesting to look up Ref. [56].

The most powerful tool for theoretical predictions, perturbative QCD, can thus be applied and provides meaningful results as long as $\alpha_s \ll 1$. For a given observable \mathcal{X} the expansion can be written as:

$$\mathcal{X} = c_0 + c_1\alpha_s + c_2\alpha_s^2 + \cdots = \sum_{i=0}^n c_i \cdot \alpha_s^i \quad (2.14)$$

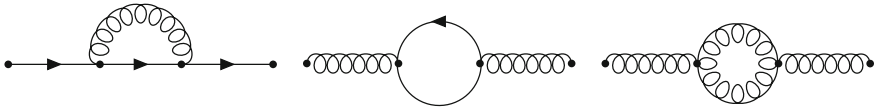
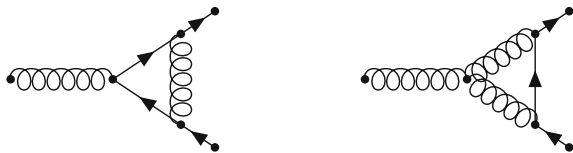


Fig. 2.7 Quark (*left*) and gluon (*middle and right*) self-energy corrections

Fig. 2.8 Quark-gluon vertex corrections



with the c_i being the perturbative coefficients of this expansion. A price to pay for the renormalisation of the theory, however, is the introduction of a regulator for the infinities, the *renormalisation scale* μ_r . The renormalised parameters, e.g. the strong coupling constant, and hence the predictions in pQCD depend logarithmically on this nonphysical scale unless all orders could be summed up. The exact dependence of $\alpha_S(\mu_r^2)$ on μ_r is given by QCD through the *renormalisation group equation* (RGE), which determines the *running* of the renormalised coupling constant $\alpha_S(\mu_r^2)$

$$\mu_r^2 \frac{\partial \alpha_S(\mu_r^2)}{\partial \mu_r^2} = \beta(\alpha_S(\mu_r^2)), \quad \text{with} \quad \beta(\alpha_S) = -\alpha_S^2 \cdot (b_0 + b_1 \alpha_S + b_2 \alpha_S^2 + \mathcal{O}(\alpha_S^3)). \quad (2.15)$$

The β function of QCD is a prime example of a quantity that can be evaluated in perturbation theory. The first three coefficients of the expansion are

$$b_0 = \frac{33 - 2N_F}{12\pi}, \quad b_1 = \frac{153 - 19N_F}{24\pi^2}, \quad b_2 = \frac{77139 - 15099N_F + 325N_F^2}{3456\pi^3}, \quad (2.16)$$

where N_F denotes the number of quark flavours with masses m_q smaller than the scale μ_r . Notably, the first term is $-b_0 < 0$ as long as $N_F \leq 16$, in contrast to QED where the corresponding coefficient is $8/3 > 0$. The non-Abelian nature of QCD manifests itself in this negative sign of the β function. In total, the coefficients are known up to four-loop order [57] and are renormalisation-scheme dependent starting with b_2 , which is quoted here in the *modified minimal subtraction* ($\overline{\text{MS}}$) scheme [20, 58, 59]. Retaining only the leading term b_0 , Eq. (2.15) is solved by

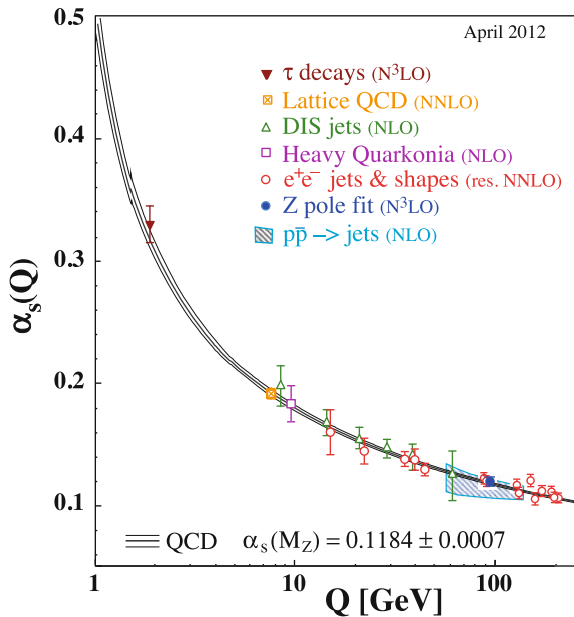
$$\alpha_S(Q^2) = \frac{\alpha_S(\mu_r^2)}{1 + b_0 \ln(Q^2/\mu_r^2) \alpha_S(\mu_r^2)}, \quad (2.17)$$

which relates the strength of the coupling at a scale Q to the one at scale μ_r , assuming both scales to be in the perturbative regime. With $b_0 > 0$, the coupling becomes weaker at higher scales Q , or, in other words, the effective colour charge gets smaller when the distance decreases. The consequence is asymptotic freedom, a key property of QCD, caused by the genuine quantum effect of anti-screening of colour charges through gluon self-interactions. The 2012 world average value of the strong coupling constant, quoted at the scale of the Z -boson mass M_Z , is given by

$$\alpha_S(M_Z) = 0.1184 \pm 0.0007, \quad (2.18)$$

derived from hadronic τ -lepton decays, lattice QCD calculations, DIS data, e^+e^- annihilation processes, and electroweak precision fits [60]. To be considered for this average, the perturbative expansion of the theory, to which data are compared, must be known at least to next-to-next-to-leading order. Figure 2.9 shows the respective

Fig. 2.9 Running of the strong coupling constant as of 2012. Determinations of the strong coupling constant α_s are shown as a function of the relevant energy scale Q of the respective process. The range in Q extends up to 208 GeV from e^+e^- annihilation data taken at the LEP collider. The hatched band indicates recent extractions from $p\bar{p}$ collisions at the Tevatron. (Taken from Ref. [60])



determinations of α_s as a function of the relevant energy scale Q . In addition, some results from fits at lower theoretical precision are included in the plot to demonstrate the running of the strong coupling constant.

At small momentum transfers Q , i.e. large distances, the perturbatively defined strong coupling constant grows beyond the validity of the perturbative approach. Defining the value where $\alpha_s(Q)$ formally diverges as Λ_{QCD} , an analytic solution to Eq. (2.15) can be given at one-loop level as

$$\alpha_s(Q) = \frac{1}{b_0 \cdot \ln(Q^2/\Lambda_{\text{QCD}}^2)}, \quad (2.19)$$

where experimentally $\Lambda_{\text{QCD}} \approx 200 \text{ MeV}$ for $N_F = 5$ in the $\overline{\text{MS}}$ scheme. This value, which is close to typical hadron masses and sizes,⁸ draws the dividing line between perturbative QCD and the manifestly non-perturbative regime of QCD. This growth of the coupling constant at small scales Q makes QCD the theory of the strong interaction that confines the quarks and gluons into ordinary hadronic matter. The transition from weakly interacting quarks and gluons inside hadrons to the formation of colour-neutral hadrons can not be described by perturbation theory. The alternative approach of LGT is not restricted to expansions around $\alpha_s \ll 1$, but requires vast amounts of computing power and despite severe approximations such an approach originally was considered hopeless. Drastic technical improvements and an exponential growth of computing capacities over the last decades, however, lead to almost

⁸Recall that $\hbar c = 1$ in natural units roughly corresponds to 200 MeV/fm.

“real world” applications nowadays. For example, it has become possible in recent years to calculate hadron masses *ab initio* [61], e.g. of the proton and neutron, provided mass scales for the three light quarks are set via the precisely measured pion, kaon, and Σ baryon masses. Combining pQCD with LGT, the latter can also be used to determine the strong coupling constant at small scales Q with seemingly very small uncertainties as visible in Fig. 2.9. The uncertainty of $\alpha_S(M_Z)$ as given in Eq. (2.18) has, in fact, become very small compared to previous determinations because of the estimates of LGT, cf. Ref. [60]. This will further be discussed in Chap. 7 on future perspectives.

2.3.2 Cross-Section Predictions

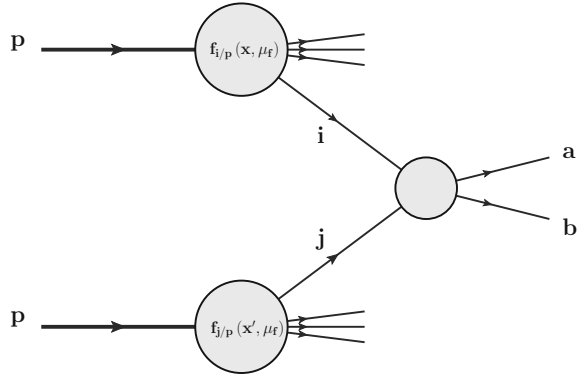
Perturbation theory so far is applicable to reactions between partons. In nature, however, confinement prohibits to observe free quarks and gluons. Instead only hadrons with a complex internal structure are available for the production of high- p_T collisions. The situation is saved by the *factorisation theorem* of QCD [45, 62], by which a cross-section computation can be separated into two parts, a short-distance partonic cross section tractable with pQCD, and a manifestly non-perturbative part that parameterises long-distance effects through universal functions extractable from measurements in a process independent way. In this approach, the partonic content of the colliding hadrons is described by parton distribution functions (PDFs), $f_{i/h}(x, \mu_f)$, which quantify the probability to find a parton i with longitudinal momentum fraction x within a hadron h at a resolution characterised by the factorisation scale μ_f . Transverse degrees of freedom in the initial state usually can be neglected compared to the collinear momentum component and are integrated over. Specialising to pp collisions and assuming that collinear factorisation holds, the cross section of a high- p_T scattering process can be written in the following form:

$$d\sigma_{(pp \rightarrow X)} = \sum_{i,j} \int dx dx' f_{i/p}(x, \mu_f) \cdot f_{j/p}(x', \mu_f) \times d\hat{\sigma}_{(ij \rightarrow X)}(x, x', \mu_f, \mu_r, \alpha_S(\mu_r)), \quad (2.20)$$

where i, j are the initial-state parton flavours and $f_{i/p}, f_{j/p}$ are the proton PDFs as functions of the fractional momenta x, x' of i and j , respectively. The sum extends over all contributing initial-state partons $i, j \in \{q, \bar{q}, g\}$, and the factorisation scale μ_f defines the resolution, below which the physics is absorbed into the non-perturbative PDFs. At higher resolution, any physics process is described by pQCD in the form of a parton-level cross section $d\hat{\sigma}_{(ij \rightarrow X)}$ that depends on the momentum fractions x, x' , the factorisation and renormalisation scales μ_f and μ_r , and the strong coupling constant $\alpha_S(\mu_r)$. A pictorial representation is given by Fig. 2.10.

The typical scale Q associated with the partonic process is assumed to be in the perturbative domain, i.e. much larger than Λ_{QCD} . The squared partonic centre-of-mass energy is given by $\hat{s} = x x' s$, where $s = (P_1 + P_2)^2$ is the squared hadronic centre-of-mass energy and P_1, P_2 are the four-momenta of the incoming hadrons.

Fig. 2.10 Sketch of one parton i of proton one and one parton j from proton two participating in a high- p_T scattering reaction $A(ij \rightarrow ab)$



The collinear factorisation ansatz is the key element for quantitative predictions in perturbative QCD. Based on the property of asymptotic freedom, the desired cross sections with relevant scale Q can be expanded as a power series in the strong coupling constant $\alpha_s(Q)$. Conventionally, the lowest-order contribution is denoted as leading order (LO), the subsequent ones as next-to-leading order (NLO), next-to-next-to-leading order (NNLO) and so forth. More precisely, these terms should be labelled as e.g. NNLO QCD corrections. For transverse momenta at the TeV scale or under particular kinematic conditions, electroweak (EW) tree-level effects of $\mathcal{O}(\alpha\alpha_s, \alpha^2)$ and loop effects of $\mathcal{O}(\alpha\alpha_s^2)$ might become equally or even more important than a QCD NNLO term. Figure 2.11 provides some examples of tree-level QCD and EW Feynman diagrams. For further details Refs. [48, 63, 64] are recommended.

The universal PDFs required in this factorised ansatz must be extracted from data. Their dependence on the factorisation scale μ_f , however, is again prescribed by QCD via the Dokshitzer–Gribov–Lipatov–Altarelli–Parisi (DGLAP) [65–68] evolution equations:

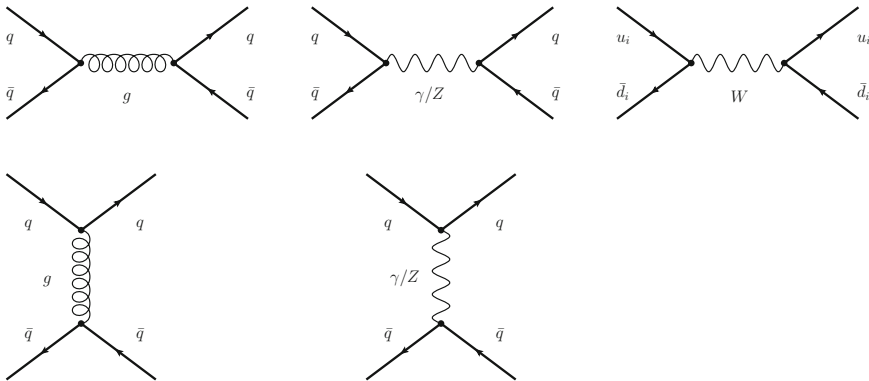


Fig. 2.11 Some tree-level QCD Feynman diagrams and corresponding EW corrections

$$\mu_f^2 \frac{\partial f_i(x, \mu_f)}{\partial \mu_f^2} = \sum_{j=\{q, \bar{q}, g\}} \int_x^1 \frac{dz}{z} \frac{\alpha_S}{2\pi} P_{ij}(z) f_{j/p}(x/z, \mu_f), \quad (2.21)$$

where the P_{ij} are the regularised Altarelli–Parisi (AP) splitting functions

$$\begin{aligned} P_{qq}(z) &= C_F \left(\frac{1+z^2}{(1-z)_+} + \frac{3}{2} \delta(1-z) \right), \\ P_{qg}(z) &= T_F (z^2 + (1-z)^2), \quad P_{gq}(z) = C_F \left(\frac{1+(1-z)^2}{z} \right), \\ P_{gg}(z) &= 2C_A \left(\frac{z}{(1-z)_+} + \frac{1-z}{z} + z(1-z) \right) + \delta(1-z) \frac{11C_A - 4N_F T_F}{6}, \end{aligned} \quad (2.22)$$

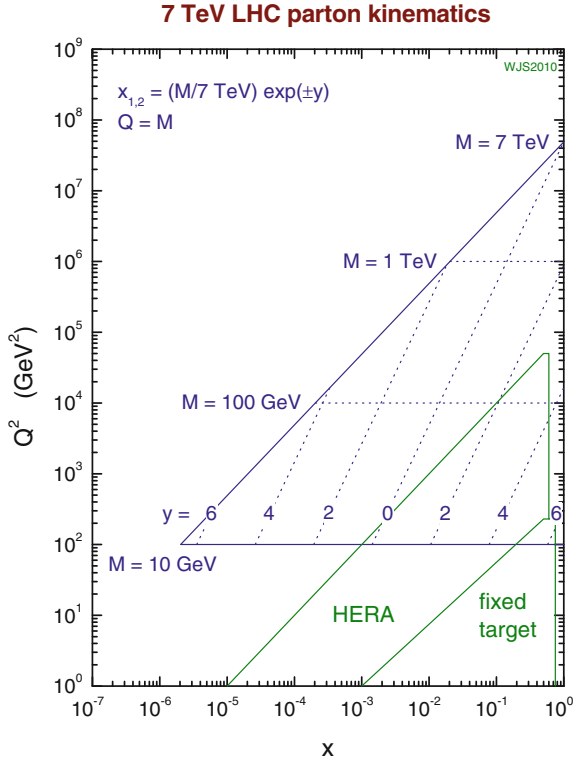
with $P_{q\bar{q}} = P_{qq}$ and $P_{g\bar{q}} = P_{gq}$.⁹ The splitting functions, listed here at one-loop, i.e. LO approximation, are known up to three-loop accuracy [69, 70]. When calculating the LO, NLO, ... estimates of a partonic cross section, the QCD evolution of the PDFs has to be used at the same relative order.

The LO DGLAP evolution allows for an interpretation by means of simple branching processes. A parton i resolved at a scale μ_f may have originated from the branching of a parton j resolved at some higher scale. This transition of parton j to i is accompanied by the emission of an additional QCD parton. When applying the DGLAP equations to solve for the scale evolution, these emissions are ignored by considering inclusive processes only.

First investigated in the context of DIS under kinematic conditions with a large transverse momentum squared Q^2 , the task was to sum up all leading terms that give rise to logarithmically enhanced contributions proportional to $(\alpha_S \log Q^2)^n$ to the cross section. With respect to the parton kinematic plane in (x, Q^2) as shown in Fig. 2.12 indicating the accessible phase space for fixed-target, HERA, and LHC experiments, the DGLAP evolution equations connect PDF sensitive measurements at different scales Q^2 . On the other hand, for very small momentum fractions x probed at large energies \sqrt{s} in the forward or backward directions with respect to the beams, some PDFs, e.g. the gluon one, rise dramatically. Summing up the leading logarithmic contributions proportional to $(\alpha_S \log(1/x))^n$ the PDF evolution is described by the Balitsky–Fadin–Kuraev–Lipatov (BFKL) [71, 72] equations. For the purpose of the high- p_T processes considered here the DGLAP equations are sufficient.

⁹The subscript “+” indicates the use of the *plus prescription* defined via the distribution $\int_0^1 \frac{f(x)}{(1-x)_+} dx = \int_0^1 \frac{(f(x)-f(1))}{(1-x)} dx$ for any sufficiently smooth function f .

Fig. 2.12 Kinematic plane in parton fractional momentum x and squared energy scale Q^2 accessible to collisions in DIS at fixed-target experiments and at the HERA ep collider, and at the LHC for 7 TeV centre-of-mass energy. (Taken from Source: 2010 Stirling [73])



2.3.3 Parton Luminosity

Even without specifying the partonic production process $d\hat{\sigma}_{(ij \rightarrow X)}$ in Eq. (2.20), a lot can already be learned from the parton kinematics and the PDFs. Specifying the incoming parton four-momenta in the centre-of-mass system as $p_1 = \sqrt{s}/2 \cdot (x, 0, 0, x)$ and $p_2 = \sqrt{s}/2 \cdot (x', 0, 0, -x')$, the rapidity y of a final state particle of mass $M = \sqrt{\hat{s}}$ is given by $y = 1/2 \cdot \ln(x/x')$ and the momentum fractions read $x, x' = (M/\sqrt{s}) \cdot e^{\pm y}$ as shown in Fig. 2.12 with $x_1 = x$ and $x_2 = x'$. With these parton momentum fractions the hadron beams effectively are parton beams of variable energy, where the energy profile is given by the PDFs. Assuming that the partonic cross section $d\hat{\sigma}_{(ij \rightarrow X)}$ only depends on \hat{s} , it is useful to define the differential *parton luminosity*¹⁰

$$\frac{d^2 L_{ij}}{d\hat{s} dy} = \frac{1}{s} \frac{1}{1 + \delta_{ij}} \left[f_{i/p}(x, \mu_f) f_{j/p}(x', \mu_f) + (x \leftrightarrow x') \right] \quad (2.23)$$

¹⁰This should not be confused with the luminosity, which is a characteristic of a collider.

and its integral $dL_{ij}/d\hat{s}$. The pre-factor with the Kronecker δ corrects for double-counting in case of identical parton flavours i and j . The inclusion of s into the definition allows the comparison between different colliders. Using $d\hat{s} dy = s dx dx'$, the factorised cross section Eq. (2.20) can be transformed into

$$d\sigma_{(pp \rightarrow X)} = \sum_{i,j} \int d\hat{s} dy \left[\frac{dL_{ij}}{d\hat{s} dy} \right] \times d\hat{\sigma}_{(ij \rightarrow X)}(\hat{s}, \mu_f, \mu_r, \alpha_S(\mu_r)), \quad (2.24)$$

or

$$\sigma_{(pp \rightarrow X)} = \sum_{i,j} \int d\hat{s} \left[\frac{dL_{ij}}{d\hat{s}} \right] \times d\hat{\sigma}_{(ij \rightarrow X)}(\hat{s}, \mu_f, \mu_r, \alpha_S(\mu_r)), \quad (2.25)$$

respectively. The term in square brackets, i.e. the parton luminosity, has units of a cross section. Provided reasonable estimates of the other numerical factors are possible, cf. Ref. [37] or [74], the parton luminosities allow order-of-magnitude estimations for cross sections as a function of the centre-of-mass energy.

2.3.4 Final State

One entity from Eq. (6.8) that has not yet been discussed is the final state X of a collision. The simplest reaction that can be considered is the Drell–Yan process [75], where a quark and an antiquark annihilate to produce a lepton pair: $\hat{\sigma}(q\bar{q} \rightarrow \ell^+\ell^-)$. Figure 2.13 shows relevant LO and NLO Feynman diagrams. In this case there are no strongly interacting particles in the final state and the theory prediction can directly be compared to the measured leptons. Merely the proton remnants, which fragment into hadrons along the beam lines, have to be described by non-perturbative models. At high transverse momenta, the two leptons are well separated from any such proton debris and high-precision comparisons with theory are possible.

However, in the vast majority of reactions at least some colour-charged partons are produced so that a further step covering the transition from the partonic final state to measurable particles, the so-called “particle level”, is needed. Here, “measurable” refers to colour-neutral particles with mean decay lengths such that $c\tau > 10$ mm, where c is the speed of light and τ the mean lifetime of a particle. One possibility to account for this transition is to reuse the concept underlying the PDFs that describe

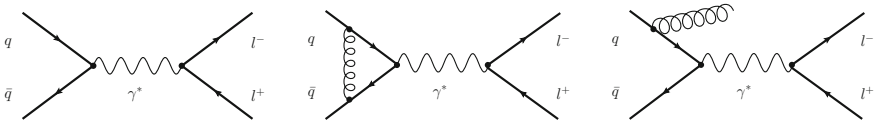


Fig. 2.13 Feynman diagrams for the Drell–Yan process $q\bar{q} \rightarrow \ell^+\ell^-$ at LO and NLO: tree-level amplitude (*left*), virtual correction (*middle*), and real correction (*right*)

the partonic content of a hadron, only in an inverted sense. The necessary functions $D_{k \rightarrow h}(z, \mu_F)$ are called fragmentation functions (FFs) and are the final-state analogues of the PDFs [76]. They parameterise the probability of finding a hadron h within the fragmentation products of parton k , carrying the fraction z of the parton momentum. With this definition, Eq. (2.26) reads

$$\begin{aligned} d\sigma(pp \rightarrow X) = \sum_{i,j,k} \int dx dx' dz f_{i/p}(x, \mu_f) \cdot f_{j/p}(x', \mu_f) \times d\hat{\sigma}_{(ij \rightarrow k)}(x, x', z, \mu_f, \mu_r, \alpha_S(\mu_r)) \\ \times D_{k \rightarrow X}(z, \mu_F), \end{aligned} \quad (2.26)$$

where, like for the PDFs, fragmentation functions depend on a non-physical resolution or fragmentation scale μ_F . Again, these functions can currently not be determined by first principles in QCD, but once they have been measured, they are valid universally. Experimentally favourable conditions prevail for example in e^+e^- collisions, where $q\bar{q}$ pairs are created via the inverse of the Drell–Yan process described above.

Other possibilities to account for the transition to measurable particles make use of the concepts of *energy flow* [77] and *particle jets* [78–82]. Instead of scrutinising the detailed production of identified particles—an experimentally very challenging endeavour—for the majority of processes it is sufficient to know how much energy or momentum is carried away by hadrons into a specific direction. Focusing on the normalised spatial distribution of the energy flow, the “shape” of an event (or an ensemble of events) can be compared to QCD radiation patterns. The influence of non-perturbative (NP) effects on such *event shapes* is expected to be power-suppressed with respect to some process-relevant energy scale Q [83]. Event shapes are very popular study subjects in e^+e^- collisions, lead to the discovery of the gluon [84–86] at the e^+e^- colliders of DESY in Hamburg, and are at the basis of one of the $\alpha_S(M_Z)$ determinations entering the world average reported in Ref. [28]. They are further discussed in Sect. 6.6.

QCD also predicts that the large-distance NP effects are mostly decoupled from the hard reaction so that highly energetic partons fragment into a collimated stream or “jet” of hadrons, which inherits energy and momentum from its parent parton. More precisely, the transverse momenta of individual hadrons with respect to the jet direction are expected to be typically of the order of Λ_{QCD} . Of course, the term “collimated” requires a mathematical prescription that, given some distance measure, unambiguously decides which objects belong to a jet. Since such particle jets are **THE** primary subject of this work, the whole Sect. 2.5 is dedicated to their introduction.

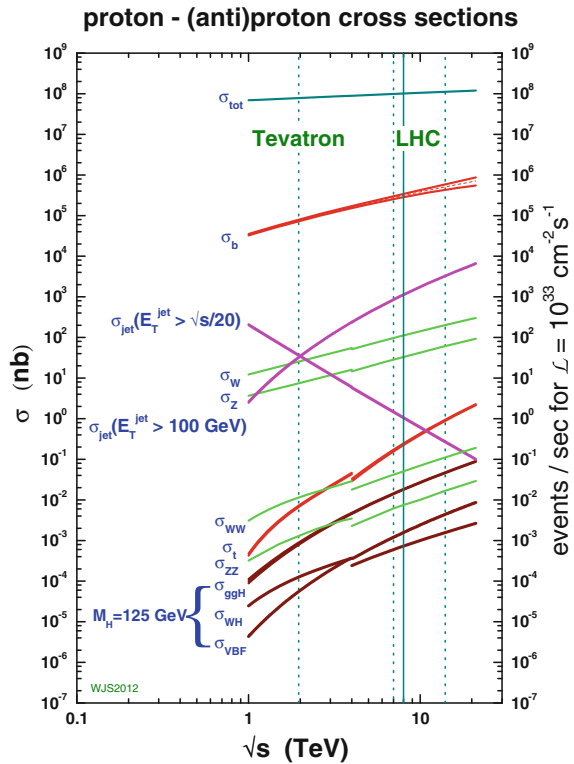
If complete knowledge of the final state of a collision event is mandatory, for example in detailed simulations of a complex experimental apparatus, perturbative methods must be complemented with models for the NP effects. This is the domain of *general-purpose Monte Carlo (MC) event generators*, which will be introduced in the next Sect. 2.4.

2.4 General-Purpose Monte Carlo Event Generators

For a first overview it is interesting to compare the cross sections for a set of standard processes as a function of the centre-of-mass energy. Such an overview is given in Fig. 2.14, where typical values can be read off, in decreasing order, for the production of b quarks, jets, W and Z bosons, top quarks, and Higgs bosons separately for the three major production processes. In addition, the total cross section is indicated as well as two diboson production channels and jet production above a minimal jet p_T that scales with $\sqrt{s}/20$. The plot spans about a dozen orders of magnitude between the total cross section and Higgs production, i.e. only each trillionth event of any pp collision produces one of the famous Higgs particles discovered in 2012 by the ATLAS and CMS experiments at the LHC [87, 88]. On the other hand, top quarks, discovered with a handful of events at the Tevatron collider in 1995 [89, 90], are produced roughly at a rate of one per second at the LHC with $\sqrt{s} = 8$ TeV.

The cross sections presented in Fig. 2.14 are sufficient for a rough estimation of event types and rates to expect for a new collider. For the conception of an experiment such as the ones at the LHC, much more comprehensive predictions are indispensable, not only for the precise design with the help of detailed simulations, but also

Fig. 2.14 Typical cross sections and event rates for SM processes including Higgs boson production as a function of the centre-of-mass energy in $p\bar{p}$ (below 4 TeV) and pp collisions (above 4 TeV). (Taken from Source: 2012 Stirling [73])



in the later operational phase for an accurate understanding of the recorded data. On the theory side, the most complete description of a collision event is given by general-purpose MC event generators. Based on physically motivated probability distributions, they generate every step in the reaction chain leading from the initial interaction between the two incoming beam particles to the final state that is composed of a list of specific particle types with their respective masses and four-momenta. Everything beyond the final-state particle level, i.e. for flight distances larger than 10 mm, cf. Sect. 2.3.4, is part of the detector simulation discussed in Sect. 3.4.1.

2.4.1 *Non-perturbative Modelling*

Three general-purpose MC event generators are in widespread use at the LHC: PYTHIA (The Lund Monte Carlo for high- p_T Physics), HERWIG (Hadron Emission Reactions With Interfering Gluons), and SHERPA (Simulation of High-Energy Reactions of PArticles). The first two have undergone decades of development from early versions in the FORTRAN programming language, PYTHIA [91–94], HERWIG [95–98], up to the ones in current use based on C++, PYTHIA8 [99, 100] and HERWIG++ [101], which most recently was renamed to HERWIG7 [102]. The new contender, SHERPA, was directly developed in a C++ framework [103].

Within the scope of this work it is hardly possible to do justice to all these developments and even less so to explain the concepts and models in great detail. To complement the following short recapitulation, it is advised to consult the excellent overview of MC event generators in Ref. [104] or the corresponding chapter of Ref. [105]. References [106, 107] are recommended as reviews or lectures that include also the latest developments, A pre-LHC summary can be found in Ref. [108].

Coming back to the simple example of Drell–Yan lepton-pair production, a sketch of a MC event generation is shown in Fig. 2.15. The small central blob in red represents a high- p_T , short-distance interaction, where in this case the pair of leptons is created. Even though the two leptons do not interact any further, the situation is complicated by the fact that the initial parton lines radiate gluons that evolve into cascades of partons. This process is described perturbatively by the concept of *parton showers* (PS) [109, 110]. If the high- p_T scattering products are partons as well, then the initial-state radiation (ISR) must be complemented by final-state radiation (FSR). Considered as a whole, the parton showers represent in their simplest form a perturbative leading-logarithmic approximation (LLA) to the full result. In contrast to the fixed-order partonic cross sections that well describe the high- p_T component of a scattering reaction, the LLA works explicitly well for the situation of collinear or soft radiation around a parton. In the basic use case, the MC event generators combine LO predictions with PS (LO+PS). Exploiting the freedom in the choice of shower resolution scale and inclusion of colour-coherence effects, several implementations exist. PYTHIA contains two incarnations with Q^2 - and p_T -ordered PS, respectively [111–113], while HERWIG employs angular-ordered showers [95, 114]. SHERPA’s

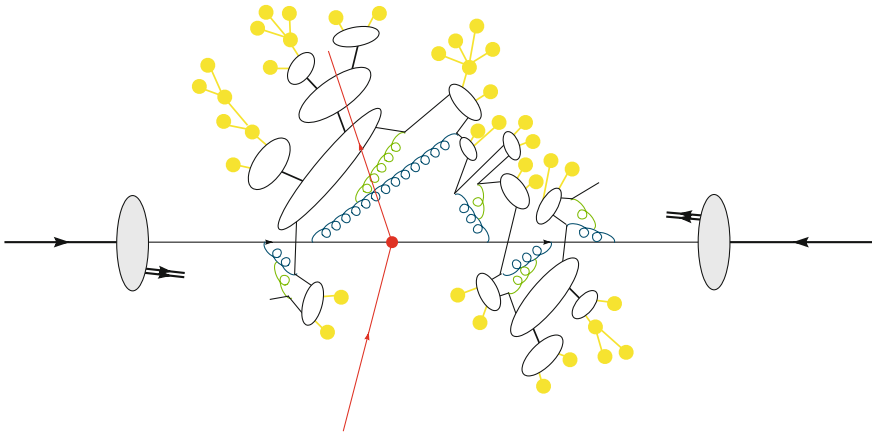


Fig. 2.15 Sketch of a MC event generation: One parton from each colliding hadron (*grey blobs*) interact and result in two high- p_T leptons (*red*). Gluon radiation off the incoming partons initiate parton showers, whose partons are combined into colourless clusters (*hollow ellipses*) that finally are fragmented into potentially further decaying hadrons (*yellow circles*). (*Sketch courtesy of S. Gieseke*)

version is based on the concept of dipole showers [115, 116] first developed in Ref. [117].

Finally, all partons in an event must form colourless compounds, represented by hollow ellipses in Fig. 2.15, that must be transformed into hadrons (yellow circles), which according to their lifetimes might still decay or not. For this manifestly non-perturbative step of *fragmentation*, frequently also called *hadronisation*, only models exist. In PYTHIA this step is performed with the *Lund string fragmentation* [118–120]. The alternative model is *cluster fragmentation*, which is used in HERWIG [121] as well as in SHERPA [122]. The pictorial view of Fig. 2.15 is based on the HERWIG version.

Unfortunately, this picture has to be refined further in order to account for additional, relatively diffuse “soft” particle production observed in hadron-hadron collisions, but absent from the theoretical description so far. Neither ISR and FSR nor the fragmentation of the beam remnants can sufficiently explain the effect. Moreover, the amount of extra particles (and energy) depends not only on the centre-of-mass energy but also on the energy scale of the primary interaction, which is characterised by the leading jet p_T . In phenomenological studies everything not associated to the high- p_T reaction is investigated and generically denoted as the *underlying event* (UE). Traditionally, this is done by geometrically subdividing an event into different regions of azimuthal angle, “towards”, “away”, and “transverse”, with respect to the jet or particle leading in p_T as illustrated in Fig. 2.16. At the same time the p_T of the leading object is defined to be the so-called event scale, i.e. the measure of the momentum transfer in the partonic scattering. The transverse region then is used to measure the soft particle production that supposedly does not originate from the

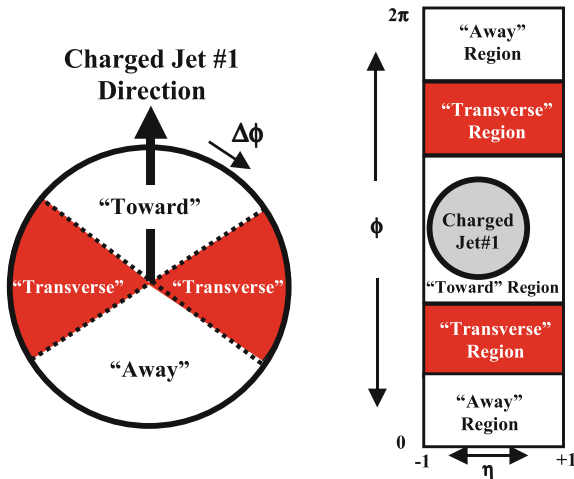


Fig. 2.16 Illustration of the “toward”, “away”, and “transverse” regions: The highest- p_T jet of an event defines the zero direction of the azimuthal angle in the transverse plane of a hadron-hadron collision. The leading jet as well as the balancing jet in the opposite direction dominate the particle and energy flow in these “toward”- and “away”-side named regions. Perpendicular to the latter is the “transverse” region (red) that is expected to receive predominantly particles from the underlying event. All particles and energies within the respective azimuthal angular intervals are summed up within a pseudorapidity range that usually coincides with the acceptance region of tracking devices, hence “charged” jet. (Taken from Ref. [123])

high- p_T scatter. Studies along this line were performed at a series of centre-of-mass energies at the Tevatron [123–126] and at the LHC by the ATLAS [127–130], CMS [131–135], and ALICE experiments [136].

Predictions so far are based on the naive picture of only one interacting parton from each colliding hadron to participate in a high- p_T reaction. It is known though that this picture must fail when approaching small transverse momenta, because the respective cross sections grow beyond all limits and finally violate unitarity. The assumption of two simultaneous high- p_T interactions is an interesting subject of study on its own and is closer examined in Sect. 6.4. To simulate the underlying event, the MC event generators accompany the primary reaction by multiple parton interactions (MPI) depending on the overlap in the transverse plane of the percolating hadrons. Collisions with a small impact parameter lead to high transverse momenta and more MPI, while a merely grazing collision exhibits only few soft particles. Partons produced by this extra activity interfere with other partons in the event, including the ones from ISR, FSR, and the beam remnants, and cannot be uniquely separated. A sketch of the resulting hadron-hadron event composition is shown in Fig. 2.17.

The original impact parameter model presented in Ref. [138] is used in PYTHIA, with modifications described in Refs. [113, 139], as well as in SHERPA. The eikonal multiple partonic scattering model applied in HERWIG is explained in Ref. [140].

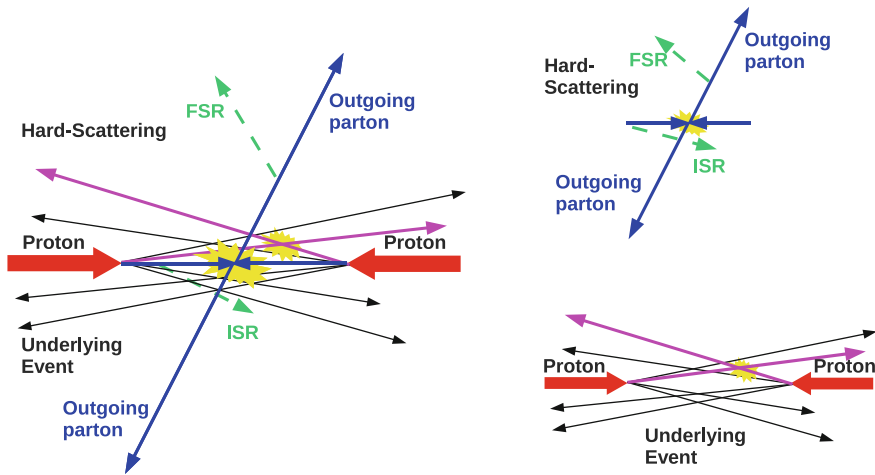


Fig. 2.17 Sketch of the composition (*left*) of a generated hadron-hadron collision. The “hard” parton-parton scattering, complemented with ISR and FSR, (*top right*) is accompanied by soft particle production from MPI and hadron remnant fragmentation (*bottom right*). Because of interference already at parton level it is not possible though to unambiguously attribute any interaction product to a particular effect. (Adapted from illustration courtesy of D. Piparo [137] following an original design of R. Field)

Together with numerous other parameters steering the parton showers, hadronisation, and decays, the MPI-based phenomenological models employed in the MC event generation must be adapted or *tuned* to data, e.g. from the various experimental results listed above. Two popular tools employed for such tunings are RIVET [141] and PROFESSOR [142]. RIVET contains numerous MC event analyses that follow as closely as possible the observable definitions and selection criteria of published measurements. Thereby, for each such measurement, it efficiently provides sets of MC predictions for arbitrary choices of parameters to tune. These predictions are then delivered to the PROFESSOR framework, which parameterises the generator response and returns the set of tuned parameters that best fits the input measurements.

Recent developments in MPI and in MC tuning are discussed in a workshop series, cf. Refs. [143–145]. Dedicated MC tuning efforts are reported in Refs. [146–149]; a comprehensive review can be found in Ref. [150].

2.4.2 Perturbative Concepts

The standard perturbative concept applied so far to MC event generation consists in attaching parton showers to a LO prediction, which works well for the situation of collinear or soft radiation around few high- p_T partons. At LHC energies, however, high- p_T partons are produced abundantly. Therefore, more sophisticated strategies

were needed that allow the automated calculation of multi-parton fixed-order results and their combination with parton showers. Several tree-level *merging or matching schemes* were developed that consistently dress varying multi-parton states with parton showers and combine everything into an inclusive event sample: the Catani–Krauss–Kuhn–Webber (CKKW) approach [151, 152], the Lönnblad variant CCKW-L [153], and the MLM method [154]. A comparative review is presented in Ref. [155].

For most observables, however, NLO predictions in the strong coupling constant represent the first accurate theoretical estimate that allows an assessment of associated theoretical uncertainties. To improve the fixed-order part of MC event generation correspondingly, two challenges had to be overcome. First, methods had to be developed that deal with the more involved NLO calculations and properly cancel singularities between real-emission graphs and virtual one-loop corrections in a numerically stable way. A number of techniques have been established [156–159]. Secondly, when combining NLO matrix elements with parton showers, the obstacle of double-counting configurations that appear in both approaches needs to be resolved. For example, real-emission corrections as part of the fixed-order calculation have to be properly synchronised with the first, i.e. highest- p_T , shower splitting. Two strategies emerged, which are known as MC@NLO [160] and POWHEG [161–163] and which are compared for example in Ref. [164].

Thanks to this enormous progress made over the last years, sometimes dubbed “the NLO revolution”, the standard in terms of pQCD ingredients to MC event generation is the combination of NLO with parton showers including multi-parton tree-level corrections or even PS-matched NLO calculations of varying parton multiplicity [165–171]. Here, it should be noted that jet algorithms play an essential part in these developments by providing a safe mapping between m -parton and n -jet ($n \leq m$) final states.

2.5 Jet Algorithms

In common language a jet describes a collimated stream of objects forcefully moving into the same direction, like water molecules in a jet of water. An example of such a “jet d’eau” is the famous water fountain and symbol of the city of Geneva as shown in the photograph Fig. 2.18.

In experimental particle physics, jets are made of measured tracks or energy depositions as illustrated in Fig. 2.19. To decide unambiguously whether a measured object belongs to a jet or not, a mathematical prescription is required: a jet algorithm. Moreover, for comparisons to pQCD, which predicts cross sections in terms of quarks and gluons, an algorithm is needed that is applicable to theoretical calculations as well as to measurements from different experiments. The first prescription of such a jet algorithm was given by G. Sterman and S. Weinberg in 1977 [172] with respect to e^+e^- collisions, where particles (or energy depositions) are grouped together depending on their location with respect to an angular cone around a

Fig. 2.18 The Jet d'Eau, the famous symbol of Geneva, Switzerland, the hosting city of the CERN laboratory. The water fountain has its origin in a safety valve for a hydraulic power network from 1886. In its nowadays form as a landmark and tourist attraction it reaches a height of 140 m, for which 500 litres of water per second are ejected at a speed of 200 km/h

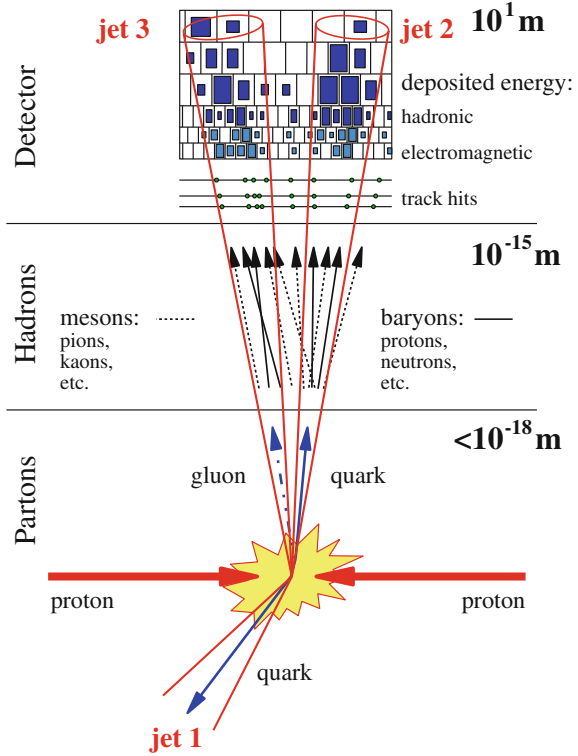


specific direction. In the following decade this prescription was extended by theorists as well as by experimental groups in order to analyse hadron-hadron collisions in terms of a number of cone-shaped jets of a chosen jet size or radius, R , which are localised around the highest concentrations of energy in an event. In the same period a novel type of algorithm based on iterative pairwise clusterings was introduced by the JADE Collaboration for the analysis of e^+e^- events at the PETRA collider [173]. A summary of the jet algorithms in use at that time is presented in Ref. [174]. Two classes of jet algorithms emerged:

1. cone algorithms that assign objects to the leading energy-flow objects in an event based on geometrical criteria;
2. sequential-recombination algorithms that iteratively combine the closest pairs of objects.

It was quickly realised, however, that the comparability of jet quantities between experiment and theory or among different experiments was questionable at best because of serious shortcomings in these early algorithms. For example, many cone

Fig. 2.19 Illustration of a jet to which bundles of partons, hadrons, or detector measurements are grouped together. (Taken from Ref. [48])



algorithms need starting points with a minimum energy or momentum for the cone directions, so-called “seeds”, which spoil their applicability in perturbation theory. In a series of workshops extending over almost 20 years and starting with the one at Snowmass in 1990 [175–177], the uncovered issues could be addressed and mostly solved leading to a number of requirements, which are listed below from a now-days perspective. An excellent recapitulation of the encountered problems and the developments can be found in Ref. [178].

2.5.1 General Desiderata

- Order independence: equal applicability to partons, particles, or measured tracks and energy depositions;
- Full specification: disclosure of all necessary details including the required software;
- Ease of implementation: avoidance of complex, proprietary code developments.

These rather general conditions are met by only permitting four-momenta as input objects and by using standardised public code for the jet clustering instead of proprietary implementations as done previously. The software library of reference in use at the LHC is FASTJET [179]. Furthermore, to compare parton-based theory predictions with experiment a clear definition must be given of the final state “truth level” to which measurements and theory are corrected [177], cf. the previous Sect. 2.3.4. The definitions in use by the ATLAS and CMS experiments are given in Sect. 3.2.2.

2.5.2 Theoretical Desiderata

- Well-defined finite cross sections at any order of pQCD: collinear and infrared safety;
- Longitudinal boost invariance: independence of jet observable of longitudinal boosts, in particular for hadron-hadron collisions;
- Boundary stability: insensitivity of jet kinematic boundaries from details of the hadronic final state e.g. the number of particles;
- Insensitivity to non-perturbative effects: limitation of impact of hadronisation and additional soft particle production (underlying event).

The by far most pressing issue that needed to be addressed is the *collinear and infrared safety* of a jet algorithm; otherwise the cancellation of collinear and soft singularities appearing in calculations of pQCD is spoiled and the most powerful computational technique for predictions, perturbation theory, is rendered useless. Hence, the outcome of a jet-clustering procedure must neither depend on the splitting or merging of collinear parton four-vectors nor on the addition of arbitrarily soft partons to the set of clustering objects. More formally, to be collinear- and infrared-safe an observable $F_m(p_1, \dots, p_m)$, defined as a function of m four-momenta p_i , must satisfy the following conditions:

$$\begin{aligned}
 F_m(p_1, \dots, \lambda p_i, p_j = (1 - \lambda)p_i, \dots, p_m) &= F_{m-1}(p_1, \dots, p_i, p_{j-1}, p_{j+1}, \dots, p_m) \\
 &\text{and} \\
 \lim_{\lambda \rightarrow 0} F_m(p_1, \dots, \lambda p_i, \dots, p_m) &= F_{m-1}(p_1, \dots, p_{i-1}, p_{i+1}, \dots, p_m)
 \end{aligned}
 \tag{2.27}$$

with $0 < \lambda < 1$. Examples of unsafe behaviour occurring notably for the cone-type jet algorithms, which partially are still employed at the Tevatron [176, 180, 181], are shown in Fig. 2.20. The first row demonstrates an issue in cone algorithms with energy (or p_T) thresholds for the seeds of the cone finding procedure. The two in terms of energy flow equivalent situations are distinguished by the number of reconstructed jets. The collinear splitting of a four-momentum leads to the disappearance of a jet (right plot) as compared to the left panel. In the second row, the emission of a soft gluon leads to the merging of two jets into one, spoiling the cancellation of divergences in the virtual corrections (left configuration) against the ones in

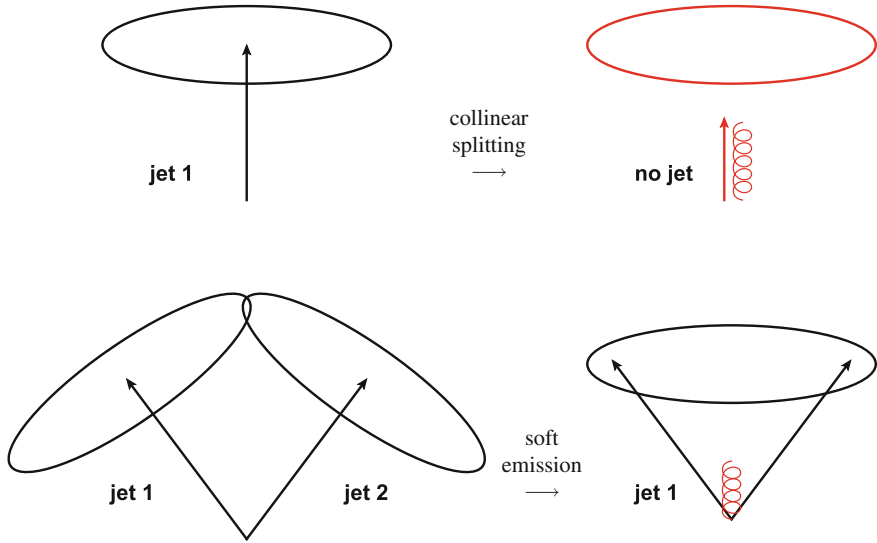


Fig. 2.20 Examples of collinear- and infrared-unsafe behaviour. *Upper row* The collinear splitting of a jet seed reduces the seed p_T 's below threshold. *Lower row* The emission of a soft gluon leads to the merging of two jets into one

real corrections (right configuration). A safe cone algorithm, SIScone for *seedless infrared-safe cone*, only exists since 2007 [182].

Longitudinal boost invariance and boundary stability are ensured by using the rapidity y instead of the pseudorapidity for the jet kinematics and by combining two clustering objects through four-vector addition. The combination prescription is called *recombination scheme* (RS), for which other possibilities have been employed in the past [175], but have been abandoned by now. The boundary stability is essential for the applicability of soft gluon resummation to stabilise fixed-order pQCD predictions near exclusive phase space boundaries. As an aside, collinear and infrared safety are necessary, but not sufficient conditions for finite predictions order by order. Unsmooth behaviour of a “safe” observable inside its allowed range, caused for example by a change in phase space limitations when going from an n - to an $n + 1$ -parton final state, can lead to infinities at these internal borders unless the calculation is complemented with soft gluon resummation [183].

Finally, jet algorithms are designed *per se* to delimit the impact of the non-perturbative hadronisation phase by collecting within one jet hadrons spread out in p_T by $\approx \Lambda_{\text{QCD}}$ relative to the jet axis. Obviously, the amount of leakage, the so-called *out-of-cone* effect (OOC), depends on the cone size R . On the other hand, the algorithm itself plays a role as well as can be seen from Fig. 2.21, which shows hadron-jet associations for a 3-jet event in e^+e^- collisions [184]. The same set of four-momenta is differently distributed over the three jets when using the JADE algorithm [173] (left) as compared to the k_t algorithm [185] (right). In particular, the

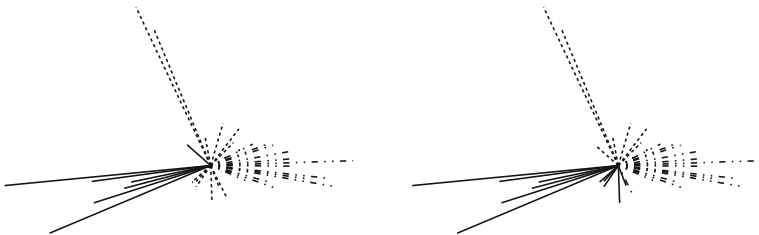
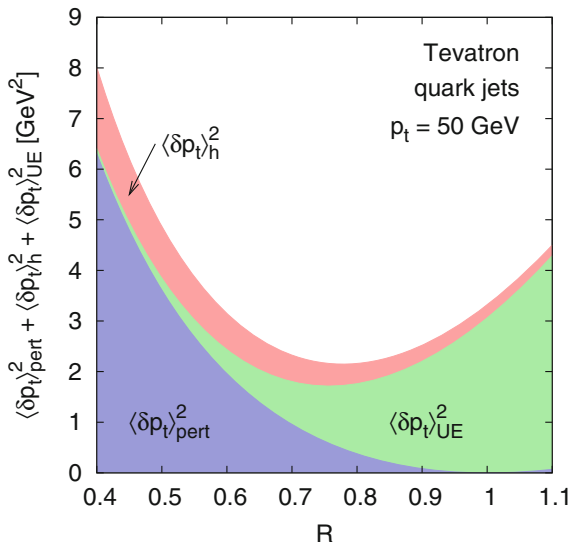


Fig. 2.21 A 3-jet final state in e^+e^- collisions as seen by the JADE (*left*) and k_t (*right*) jet algorithms. The particle assignments to the first, second, and third jet according to the algorithms are indicated by *full*, *dash-dotted*, and *dashed* lines. (Redrawn from Ref. [184])

JADE algorithm clusters soft particles together into the third jet although they are going into opposite directions, while the k_t algorithm is designed to undo perturbative parton splittings and prefers small angle over small mass clusterings. In effect it is found that the k_t algorithm is better behaved than JADE in terms of hadronisation corrections and resummability of large logarithms at small values of the resolution.

A detailed comparison of the impact of the jet radius R on the size of NP corrections to jet p_T cross sections has been performed in a collinear approximation in Ref. [186]. As shown in Fig. 2.22 it was found that perturbative radiation, hadronisation, and the underlying event affect jet transverse momenta for small R roughly proportional to $\ln R$, $-1/R$, and R^2 respectively. As a consequence, the value of the jet radius parameter R determines which aspects of jet formation are emphasised and is a matter of choice.

Fig. 2.22 Estimation of the squared average shift in p_T of a jet caused by perturbative radiation (pert), hadronisation (h), and soft particle production from the underlying event (UE) as a function of the jet cone size R . The effects are estimated in a collinear approximation for quark jets at Tevatron energies. (Taken from Ref. [186])



2.5.3 Experimental Desiderata

- Detector independence: No algorithmic dependence on detector details;
- Computational efficiency and predictability: predictable computing times that only mildly increase with growing numbers of input objects;
- Maximal reconstruction efficiency: lossless treatment of all input objects (no “dark jets”);
- Insensitivity to pile-up collisions: accurate correction for additional energy not coming from the primary interaction;
- Ease of calibration: accurate and straightforward estimation of diverse detector effects on the jet response.
- Minimal resolution smearing and angular biasing: avoidance of algorithmic distortions in addition to detector effects;

Early versions of jet construction by the UA1 and UA2 experiments at the Sp \bar{p} S were based on the cell structure of their calorimeters in a way making it difficult to compare consistently to theory or other experiments [187–189]. This could be remedied by using cone algorithms, which as an added bonus are computationally efficient even for a large number N of input objects. On the contrary, sequential-recombination algorithms like k_t , favoured in low multiplicity e^+e^- collisions, were believed to scale with N^3 in terms of computing time. It was discovered in Ref. [190] that much better implementations are possible where the N^3 dependence is drastically reduced to merely N^2 or $N \ln N$. As a consequence k_t type algorithms became even faster than cone-type ones and it could be envisioned to apply them in the experimental triggering procedure, where fast and predictable reconstruction times are a must.

An undesired feature related to the search for stable cones in some cone-type algorithms is the possibility to have so-called *dark jets*, i.e. measured energy depositions that are not reconstructed as jets [191]. This does not happen with sequential-recombination algorithms.

An experimental complication to jet measurements is caused by the quest for extremely rare processes like Higgs boson or very high- p_T jet production that demand correspondingly high instantaneous luminosities to be provided by a collider. Such luminosities cannot be achieved without piling up multiple proton-proton collisions per bunch crossing. In addition, the finite integration time of detector components in comparison to bunch separations of 50 or 25 ns (from 2015 onwards) leads to crosstalk from adjacent colliding bunches. As a result, each “event” is interspersed with energy depositions from such pile-up collisions (PU), which need to be subtracted. At low p_T even complete jets made of PU energy might be produced as illustrated in Fig. 2.23. An event-by-event identification of PU contributions is possible only for charged particles, which appear as reconstructed tracks that are not associated to the primary vertex of the event.

Jet algorithms that are insensitive to PU do not exist. Instead PU particles and energy are collected roughly proportional to the squared jet radius R^2 in a similar

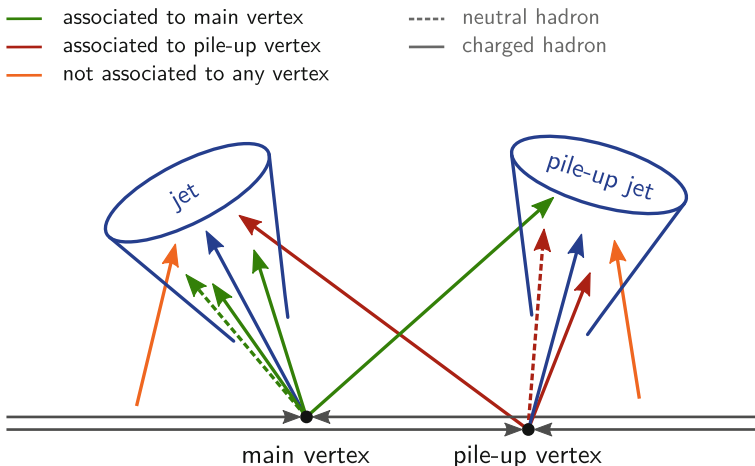


Fig. 2.23 Illustration of a pile-up collision in addition to a primary high- p_T interaction leading to additional particles and energy depositions within the same event. (Illustration courtesy of J. Berger [192])

fashion as for the UE. Since a complete subtraction of PU is impossible, it is advantageous to have a clear idea of the *jet area* A . Although not always exactly correct, for cone-type algorithms the area is estimated to be πR^2 , at least for the leading jets. For the k_t algorithm it is much more involved. However, as first proposed in Ref. [193] it is possible to define a jet area for each collinear- and infrared-safe jet algorithm by clustering in addition to the normal list of input objects large numbers of so-called *ghost particles* that have negligible four-momentum and are uniformly distributed in rapidity and azimuth. Figure 2.24 presents as example for one hadron-hadron collision event the jet areas so defined for the k_t [194], Cambridge/Aachen [195, 196], SIScone [182], and anti- k_t [197] jet algorithms. The exact definition for the three sequential-recombination algorithms is given in the next Sect. 2.5.4. The k_t algorithm first combines low- p_T objects and leads to larger, irregular-shaped areas, while anti- k_t starts clustering with the highest- p_T objects and produces round-shaped jet areas as if from a cone jet algorithm. The Cambridge/Aachen algorithm solely relies on angular distances and lies somewhere in the middle of the other two.

With respect to PU subtraction and ease of calibration a regular shape of the jet area is favourable, because it simplifies the experimental evaluation of average densities (per area) to implement corrections as described in Chap. 3. In combination with perturbative safety, fast computing speed, and good geometrical resolution characteristics, the cone-like sequential-recombination algorithm anti- k_t was therefore quickly adopted as the standard jet algorithm at the LHC.

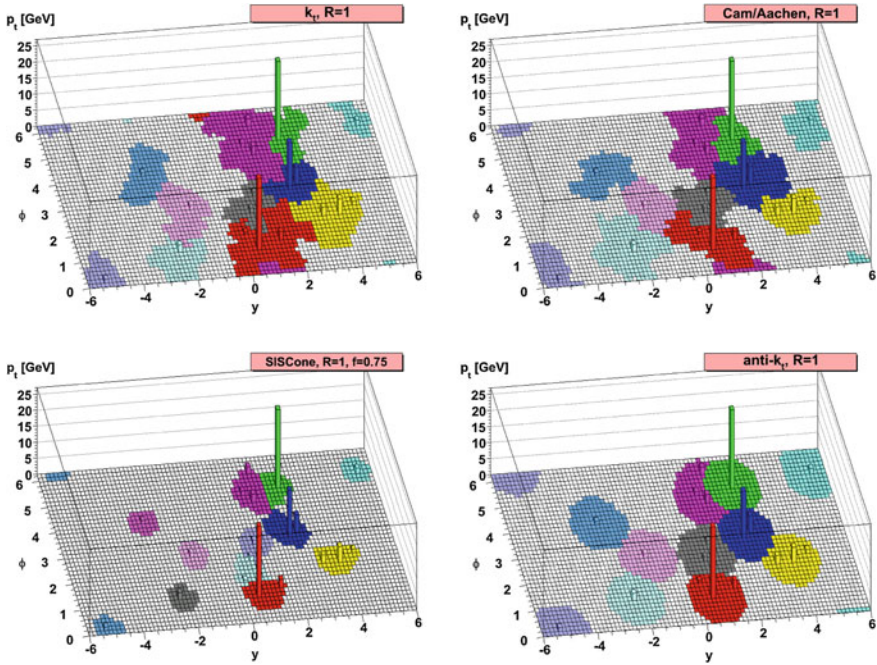


Fig. 2.24 Illustration of jet areas for the k_t , Cambridge/Aachen, SIScone, and anti- k_t jet algorithms. The tiles in rapidity and azimuth are coloured as a function of the number of ghosts clustered into a particular jet. (Taken from Ref. [193])

2.5.4 Sequential Recombination Algorithms

The sequential-recombination algorithms in use at the LHC can be described in a unified way. First of all two distance measures must be defined that give the relative distance d_{ij} between each pair of N input objects i and j and between each input object i and the beam direction, d_{iB} :

$$d_{ij} = \min \left(p_{T,i}^{2p}, p_{T,j}^{2p} \right) \frac{\Delta R_{ij}^2}{R^2}, \quad (2.28)$$

$$d_{iB} = p_{T,i}^{2p}. \quad (2.29)$$

Here, ΔR_{ij} is the purely “angular” distance in y and ϕ between i and j ,¹¹

$$(\Delta R_{ij})^2 = (y_i - y_j)^2 + (\phi_i - \phi_j)^2, \quad (2.30)$$

¹¹Of course, azimuthal angular separations are delimited to the interval $(-\pi, +\pi]$.

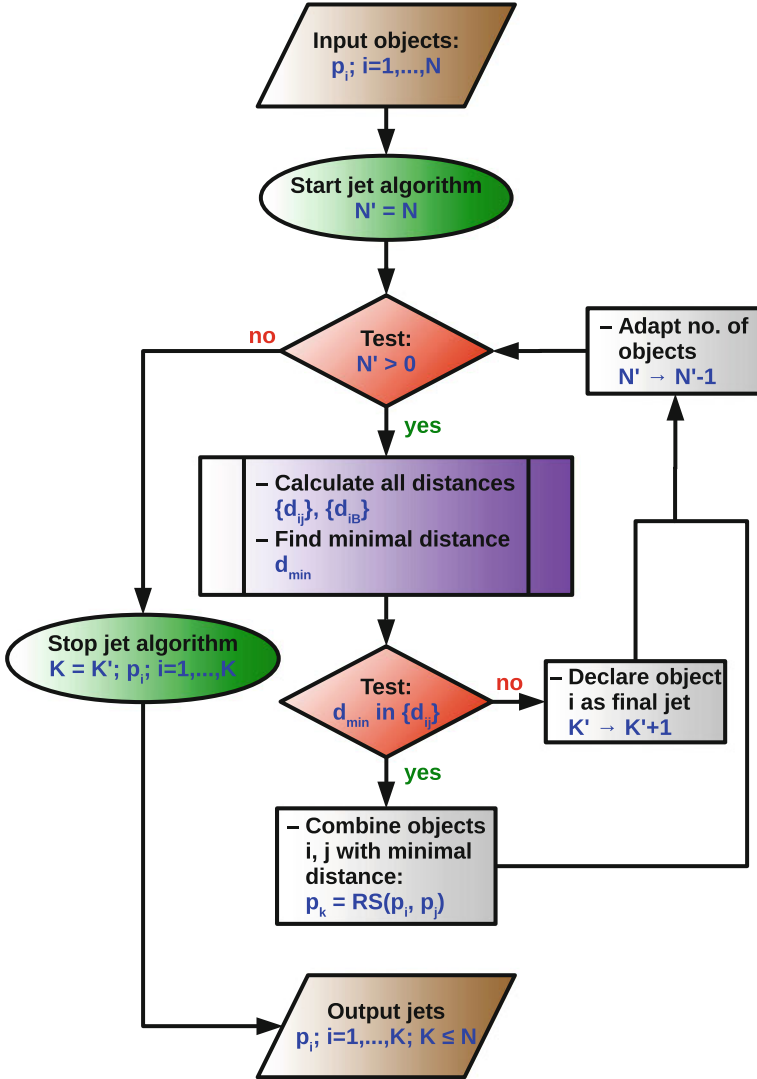


Fig. 2.25 Flowchart of a jet algorithm with sequential recombination. N input objects, usually given in the form of four-momenta p_i , are iteratively clustered following a recombination scheme RS. The final output is a list of K jets where $K \leq N$

which is scaled with respect to a parameter R that is equivalent to a cone radius and defines what will be referred to as *jet size* in the rest of this work. The power p decides whether low- or high- p_T objects are clustered first and differentiates between the k_t ($p = 1$), the Cambridge/Aachen ($p = 0$), and the anti- k_t ($p = -1$) jet algorithms.

Then, the minimal distance d_{\min} is found from all pair-wise distances d_{ij} and all beam distances d_{iB} simultaneously. If $d_{\min} \in \{d_{iB}\}$, then the input object is declared a final jet, removed from the list of clustering objects, and added to the list of K jets, which initially is empty. If $d_{\min} \in \{d_{ij}\}$, then the two objects are merged with four-vector addition as recombination scheme and the new object is added to the clustering list while the parent objects i and j are removed. These steps are repeated until there are no more objects left in the clustering list. The list of final jets then is returned as result. An illustrative flowchart of the described algorithms is displayed in Fig. 2.25.

The default jet sizes chosen in LHC Run 1 by the two omni-purpose experiments for the anti- k_t algorithm are $R = 0.4$ and 0.6 for ATLAS and $R = 0.5$ and 0.7 for CMS. For Run 2, CMS changed the smaller jet size to 0.4 enabling direct comparisons to ATLAS measurements.

If the substructure of a jet is of interest, for example because the jet is supposed to come from a heavy boosted object whose two- or three-prong decay products all end up in the same jet, then it might be unwise to enforce a round-shaped jet area. For such purposes other jet types are better suited and in particular the Cambridge/Aachen algorithm is widely used. Last but not least, jet areas itself can be exploited for measurements, for example as an alternative to the traditional method to determine the UE [198].

2.6 Theoretical Uncertainties

Given the amount of approximations and assumptions necessary before arriving at a prediction comparable to experimental data, a careful assessment of related uncertainties is mandatory. The most common theoretical uncertainties encountered in jet physics will be addressed in the next sections. They are related to:

1. the truncation of the perturbative series in a fixed-order calculation, colloquially but inadequately referred to as *scale uncertainty*;
2. the limited knowledge of hadron structure, *PDF uncertainty*;
3. the limited knowledge of the strong coupling constant, α_s *uncertainty*;
4. the modelling and tuning of non-perturbative effects, *NP uncertainty*.

Depending on the observable under study and the employed theoretical tools and techniques, further causes such as the fragmentation of heavy quarks, the top mass, decay constants, or limited statistical precision in numerical approximations may give rise to further uncertainties, cf. also Chap.9 of Ref. [199].

2.6.1 Scale Uncertainties

Because the perturbative expansion in the strong coupling constant α_S needs to be truncated, all fixed-order calculations suffer from the fact that the missing higher orders somehow have to be accounted for in an uncertainty. Apparently, a truncated expansion following Eqs. (2.14)–(2.16) depends on the more or less arbitrary choices of renormalisation scheme and scale μ_r , while the full result of a renormalisable theory does not. More precisely, it can be shown that a quantity expanded in α_S up to terms of power n varies with $\ln \mu_r^2$ proportional to α_S^{n+1} , i.e. one order higher than the expansion itself:

$$\frac{d\mathcal{X}}{d \ln \mu_r^2} (\alpha_S^n) = \mathcal{O}(\alpha_S^{n+1}) . \quad (2.31)$$

Naturally, this lead to the paradigm of estimating missing higher orders through this residual scale dependence. The differences between the central and varied results when changing the scale μ_r around a central value μ_0 by factors of $1/r$ and r are taken to be the scale uncertainty. However, there are a couple of questions related to this *ad hoc* procedure that, nevertheless, is in widespread use:

- What renormalisation scheme to choose?
- What should the central scale μ_0 be?
- Which factor r should be used for the variation?
- What is the statistical interpretation of this uncertainty?
- What should be done, if multiple choices for μ_0 are involved?
- What should be done with other nonphysical scales like μ_f appearing in calculations of pQCD?

Nowadays adopted standard in terms of renormalisation is the $\overline{\text{MS}}$ scheme, which is chosen for computational simplicity when dealing with one-loop corrections. In this scheme, the central scale μ_0 preferably should be of the order of the “hard” scale of the considered process to improve the accuracy of the perturbative expansion, cf. Ref. [45]. Conventionally, the variation factor r is chosen to be 2, which in many cases leads to reasonable results, see for example Ref. [200] for an examination of single-inclusive jet production. Figure 2.26 left shows the rapidity distribution of Z boson production as predicted to LO, NLO, and NNLO including scale uncertainty bands, where, on the contrary, the NLO prediction lies outside the estimated LO band. If the uncertainty is interpreted in the usual sense of a 1σ or 67% confidence level (CL), one such example might still be fine. However there are much worse cases in the same Ref. [201] and elsewhere. A review and comparison to a more rigorous statistical interpretation in terms of Bayesian degrees of belief (DoB) has been presented in Refs. [202, 203]. Figure 2.26 right presents the example of Higgs boson production via the gluon fusion process. Apparently, the computed higher orders at NLO and NNLO lie beyond the estimated uncertainties for $r = 2$ at lower order, and the uncertainties are largely underestimated even for $r = 4$ in comparison to the DoB as derived in the modified Cacciari–Houdeau approach (CH).

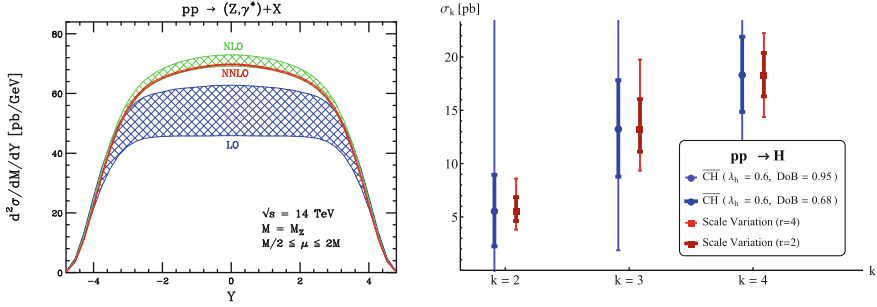


Fig. 2.26 Issues in scale variations: *Left* Predictions at LO, NLO, and NNLO including scale uncertainty bands for Z boson production as a function of the Z rapidity Y . *Right* Higgs production cross section $pp \rightarrow H$ via gluon fusion process at LO ($k = 2$), NLO ($k = 3$), and NNLO ($k = 4$). The light- and dark-blue error bars corresponding to the 1σ and 2σ degrees of belief estimated according to the modified Cacciari–Houdeau approach ($\overline{\text{CH}}$) are compared to the estimates using scale variations by factors of 2 and 4 shown as light- and dark-red error bars. (Taken from Refs. [201, 203])

The multi-scale problem partially is related to the merging and matching schemes of the NLO+PS event generation mentioned in Sect. 2.4.2. Discussions with respect to the involved merging/matching scale μ_m and corresponding uncertainties are still ongoing. The factorisation scale μ_f introduced in Sect. 2.3.2 on the other hand has a totally different physics origin from μ_r and can, in principal, be set independently. For jet production in ep DIS for example, μ_f usually is identified with Q , i.e. the momentum transfer between the scattered electron and the proton, while μ_r is chosen to be the jet p_T . At the LHC, μ_r and μ_f are mostly defined identically, but scale variations are performed independently avoiding overly large relative factors between the two, cf. Refs. [204, 205]:

$$1/r \leq \mu_r/\mu_f \leq r. \quad (2.32)$$

With $r = 2$ this leads to the following six variations of μ_r and μ_f from the default choice of $\mu_r = \mu_f = \mu_0$ between $\mu_0/2$ and $2\mu_0$: $(\mu_r/\mu_0, \mu_f/\mu_0) = (1/2, 1/2)$, $(1/2, 1)$, $(1, 1/2)$, $(1, 2)$, $(2, 1)$, and $(2, 2)$. The maximal downwards and upwards deviations from the central result are defined as scale uncertainty, where the dominant effect usually comes from the change in μ_r . Despite the above-mentioned issues the majority of experimental and theoretical particle-physics analyses in the past and still today employ this recipe, or a simplified variant, of scale uncertainties, which although far from optimal at least induce comparability. It is well-known though that scale variations anyway are incapable to account for the appearance of new production channels at the next perturbative order.

Other concepts of scale setting, *fastest apparent convergence* (FAC) [206, 207], *principle of minimal sensitivity* (PMS) [208, 209], and *Brodsky–Lepage–Mackenzie* (BLM) [210], have been investigated early on. The latter claims to eliminate scale

ambiguities in pQCD, but requires to find a proper scale that is different order-by-order for each relevant set of subprocesses and hence is rather impractical. A recent revival of interest in the BLM prescription lead to a reformulation in the form of the *principle of maximum conformality* (PMC) [211–213]. PMC promises to be a systematic method to eliminate the renormalisation scale and scheme ambiguities to all orders in pQCD. A widespread application of PMC is still outstanding, but taken at face value it emphasises once more that scale variations cannot really address the original aim of estimating a *missing higher order uncertainty*. Some progress in that direction has been reported in Refs. [214, 215].

2.6.2 PDF Uncertainties

Initially, the PDFs, necessary for the factorised, long-distance part in Eq. (2.20), were derived from in particular DIS experiments in the form of parameterised functions. The observation of an excess of jet production at high p_T by the CDF Collaboration in 1996 [216], cf. Fig. 2.27 left, triggered speculations with respect to new phenomena. However, at that time, the only means to exploit the potential freedom in these PDFs consisted in comparing the predictions of a few candidate functions like the ones used by the CDF Collaboration. A systematic approach to PDF uncertainties simply did not exist. In the end, the excess could be accommodated by adaptations in the gluon PDF [217] as shown in Fig. 2.27 right.

In the following 20 years enormous progress has been made towards statistically well-founded, systematic schemes to determine PDFs including uncertainty estimates. Numerous PDF fitting groups continuously develop and refine their methods, while simultaneously more and more precise data are integrated into the process.

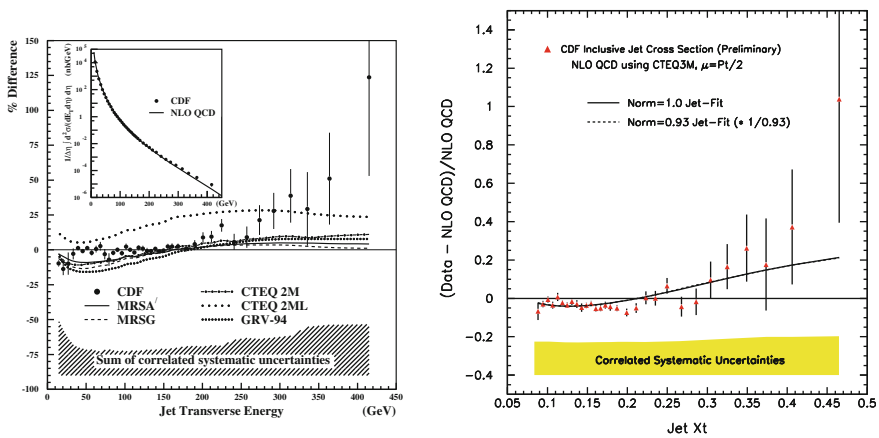


Fig. 2.27 Excess reported by CDF with respect to the predicted inclusive jet p_T spectrum (left) and explanation in terms of a modified gluon PDF (right). (Taken from Refs. [216, 217])

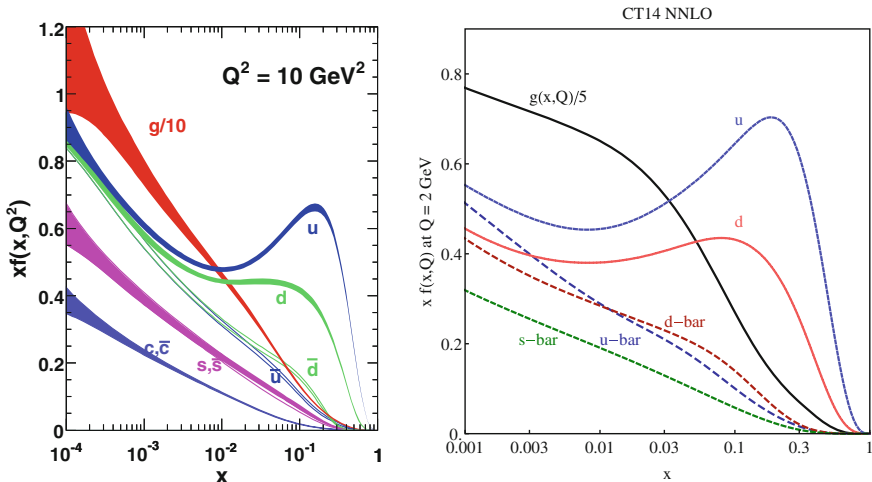


Fig. 2.28 MSTW2008 NLO PDFs including uncertainty bands at a scale of $Q^2 = 10 \text{ GeV}^2$ (left) and shape of the recent CT14 NNLO PDFs at $Q^2 = 4 \text{ GeV}^2$ (right). (Taken from Refs. [218, 219])

Figure 2.28 left exemplifies the MSTW2008 NLO PDFs including uncertainty bands at a scale of $Q^2 = 10 \text{ GeV}^2$. Their shape at higher scales like 10000 GeV^2 as needed at the LHC is completely determined by the DGLAP equations (2.21). An example of the most recent PDFs, displayed without uncertainties, is given in Fig. 2.28 right.

Table 2.1 gives an overview of the primary PDF sets available for comparisons to data at NLO. In most cases, NNLO versions and further variants exist as well. As exhibited in Fig. 2.28 the validity of the DGLAP equations is assumed starting from scales Q even below threshold for the production of b quarks.¹² The inclusion of the heavy quarks, charm and bottom, into pQCD predictions involving PDFs requires special care. Several solutions are proposed. The ABM and (G)JR PDF sets employ a fixed-flavour number scheme (FFNS) [220–222] with three respectively five flavours. All other PDF sets use a general-mass variable-flavour number scheme (GM-VFNS), several variants of which are reviewed in Ref. [223]. The maximum number of flavours is five, $N_{f,\text{max}} = 5$, except for NNPDF2.1 and 2.3, which have $N_{f,\text{max}} = 6$. Even beyond the top quark mass it can be justified to continue using $N_F = 5$ [224] as is the case for the jet analyses presented later in this work.

The PDF sets are supplied for usage in other programs via the unified Les Houches Accord PDF (LHAPDF) interface [239, 240], which in its latest version includes routines to evaluate uncertainties. Two primary strategies evolved to provide these uncertainty estimates from PDF fits:

1. The *Hessian* or *eigenvector method* [241, 242] where the correlated experimental data uncertainties on the fitted parameters for simplicity are provided within an orthonormalised parameter space.

¹² $m_{\text{charm}}^{\overline{\text{MS}}} = 1.275 \text{ GeV}$, $m_{\text{bottom}}^{\overline{\text{MS}}} = 4.18 \text{ GeV}$ [28].

Table 2.1 The NLO PDF sets used in comparisons to the data in Run 1 (upper eight rows) and newer sets for Run 2 (lower six rows) together with the corresponding number of flavours N_f , the assumed masses M_t and M_Z of the top quark and the Z boson, respectively, the default values of $\alpha_S(M_Z)$, and the range in $\alpha_S(M_Z)$ variation available for fits. A * behind the $\alpha_S(M_Z)$ values signifies that the parameter was fixed, not fitted. The FFNS (G)JR PDF sets use $N_f = 3$, but allow N_f to rise up to five in the evolution of α_S . VFNS variants of these PDFs exist as well

Base set	References	N_f	M_t (GeV)	M_Z (GeV)	$\alpha_S(M_Z)$	$\alpha_S(M_Z)$ range
ABM11	[225]	5	180	91.174	0.1180	0.110–0.130
CJ12	[226]	≤ 5	180	91.1876	0.1180*	–
CT10	[227]	≤ 5	172	91.188	0.1180*	0.112–0.127
HERAPDF1.5	[228]	≤ 5	180	91.187	0.1176*	0.114–0.122
GJR08	[229, 230]	3(5)	175	91.71	0.1145	–
MSTW2008	[218, 231]	≤ 5	10^{10}	91.1876	0.1202	0.110–0.130
NNPDF2.1	[232]	≤ 6	175	91.2	0.1190*	0.114–0.124
NNPDF2.3	[233]	≤ 6	175	91.1876	0.1180*	0.114–0.124
CJ15	[234]	≤ 5	180	91.1876	0.1180*	–
CT14	[219]	≤ 5	172	91.1876	0.1180*	0.113–0.123
HERAPDF2.0	[235]	≤ 5	173	91.1876	0.1180*	0.110–0.130
JR14	[236]	3(5)	173	91.1876	0.1158	–
MMHT2014	[237]	≤ 5	10^{10}	91.1876	0.1180*	0.108–0.128
NNPDF3.0	[238]	≤ 5	173	91.2	0.1180*	0.115–0.121

2. The *MC method* [243–245] where the input data are varied according to their precision, including correlations, to produce an ensemble of PDFs that statistically reflects the intrinsic uncertainty.

Since each eigenvector of the Hessian method corresponds to an uncertainty source independent of all other eigenvectors, the total impact on an observable \mathcal{X} can be evaluated by quadratic addition. If one-sided deviations caused by the + and – variations of one eigenvector are to be considered in an asymmetric uncertainty, the formula reads:

$$\begin{aligned}\Delta\mathcal{X}^+ &= \sqrt{\sum_{i=1}^{N_{\text{EV}}} [\max(\mathcal{X}_i^+ - \mathcal{X}_0, \mathcal{X}_i^- - \mathcal{X}_0, 0)]^2}, \\ \Delta\mathcal{X}^- &= \sqrt{\sum_{i=1}^{N_{\text{EV}}} [\min(\mathcal{X}_i^+ - \mathcal{X}_0, \mathcal{X}_i^- - \mathcal{X}_0, 0)]^2},\end{aligned}\quad (2.33)$$

where N_{EV} is the number of eigenvectors and the index 0 indicates the result for the central PDF stored as zeroth member. The CJ, CT, MSTW, and MMHT sets fall into this category and consist of this central PDF member no. 0 and $2 \cdot N_{\text{EV}}$ members for the uncertainty. The PDF uncertainties customarily are evaluated at 68 % confidence level (CL) except for the CT and CJ ones, which provide uncertainties only at 90 % CL. For a uniform treatment, the CT/CJ uncertainties must therefore be downscaled by a factor of $\sqrt{2} \operatorname{erf}^{-1}(0.9) \approx 1.645$. If symmetric errors are required, for example in covariance matrices, the formula

$$\Delta\mathcal{X}^\pm = \pm \sqrt{\sum_{i=1}^{N_{\text{EV}}} \left[\frac{\mathcal{X}_i^+ - \mathcal{X}_i^-}{2} \right]^2} \quad (2.34)$$

can be used instead. In case of the ABM and (G)JR PDF sets a symmetrisation has been performed beforehand such that in their case the Hessian uncertainties are to be derived according to the equation

$$\Delta\mathcal{X}^\pm = \pm \sqrt{\sum_{i=1}^{N_{\text{mem}}} [\mathcal{X}_i - \mathcal{X}_0]^2}, \quad (2.35)$$

where N_{mem} is the total number of members not counting the zeroth one.

For the MC method as employed by the NNPfDF sets, the usual formula for a standard deviation is applicable:

$$\Delta\mathcal{X}^\pm = \sqrt{\frac{1}{N_{\text{rep}} - 1} \cdot \sum_{i=1}^{N_{\text{rep}}} [\mathcal{X}_i - \langle\mathcal{X}\rangle]^2}, \quad (2.36)$$

where $N_{\text{rep}} = N_{\text{mem}}$ is the number of replicas, again not counting the zeroth one. $\langle\mathcal{X}\rangle$ corresponds to the average prediction for the observable \mathcal{X} , which in general is different from the predicted value for the averaged PDFs present as zeroth member.

The PDF sets listed in Table 2.1 can be further differentiated into “global” ones that evaluate a multitude of different data sets in a global combined fit, ABM, CT, (G)JR, MSTW/MMHT, and NNPfDF, and more specialised ones, CJ, HERAPDF. Out of the global ones, the (G)JR PDF sets are less used, because they lack a series with variations in the value of $\alpha_S(M_Z)$.

The CJ sets follow the general strategy of the CT ones, but include data with nuclear targets, e.g. deuterium, which requires supplementary assumptions or *nuclear correction factors* when extracting proton PDFs. Their advantage consists in larger amounts of data that constrain the high x region, which is particularly important when searching for new phenomena at very high p_T or mass.

The HERAPDF sets are restricted to the exclusive use of DIS measurements from the H1 and ZEUS experiments. Since these data are essential ingredients to all other PDF sets as well, they pose an ideal baseline for comparisons. Moreover, the computer code for performing the fits is publically available in the form of the open source framework HERAFITTER [246].¹³ The uncertainty estimation employed in this framework is more involved and is explained in detail in Sect. 4.5, where such a PDF fit including CMS jet data is described.

Standard model measurements, particularly the ones that promise to be valuable ingredients to fits of SM parameters, clearly should be confronted with predictions for each individual PDF set. In some cases, e.g. limit settings on physics beyond the SM, it might be desirable to provide only one number that in addition accounts for variations caused by the different PDF sets. For this purpose, the PDF4LHC working group has proposed a combination procedure [247] that was updated recently [248].

Effects of polarisation or *transverse momentum dependence* (TMD) in PDFs have been neglected so far. These topics are specially addressed in Refs. [45, 249, 250].

2.6.3 α_S Uncertainties

In addition to the parameters of the PDFs themselves the strong coupling constant enters into the fits. Correlations, specifically between the gluon PDF and the assumed value of $\alpha_S(M_Z)$, are expected and must be addressed when deriving a combined uncertainty. For this purpose, it must be differentiated whether $\alpha_S(M_Z)$ is considered a fixed input parameter, i.e. the “starred” values in Table 2.1, or a fitted output parameter in a PDF fit.

For the first case, three approaches are discussed in Ref. [251]:

- Quadratic addition of the PDF uncertainty and a $\Delta\alpha_S(M_Z)$ uncertainty computed with the same central PDF set.
- Quadratic addition of the PDF uncertainty and a $\Delta\alpha_S(M_Z)$ uncertainty computed with PDF sets fitted using the varied values of $\alpha_S(M_Z)$.
- Correlated propagation of the PDF and $\alpha_S(M_Z)$ uncertainty to the PDF error set.

The first recipe is totally ignorant of correlations, while the last one depends on the method for the estimation of PDF uncertainties, Hessian or MC method. For a variation of $\alpha_S(M_Z)$ by ± 0.0012 as recommended in Ref. [247] it is observed that all three recipes are rather close to each other with a slight underestimation of the

¹³ HERAFITTER recently was renamed to XFITTER.

uncertainty by variants one and two. For all practical purposes it is sufficient and recommended to apply the second recipe for the CT and NNPDF sets [252, 253].

In the second case where $\alpha_S(M_Z)$ was fitted together with the PDF parameters, the α_S uncertainty intrinsically is included already in the ABM PDF uncertainties. For the MSTW2008 PDF set, it is recommended to calculate the PDF+ $\alpha_S(M_Z)$ uncertainty from the envelope of five PDF sets with uncertainties produced under varying assumptions on $\alpha_S(M_Z)$ [231].

The newer CT, MMHT, and NNPDF sets all employ the same fixed value of $\alpha_S(M_Z) = 0.1180$. Here, the recommended procedure follows recipe two above, but with an enlarged uncertainty of $\Delta\alpha_S(M_Z) = \pm 0.0015$.

The latest 2015 update of the PDG gives the world average as:

$$\alpha_S(M_Z) = 0.1181 \pm 0.0013. \quad (2.37)$$

2.6.4 Non-perturbative Uncertainties

Since fixed-order predictions as used in fits of SM parameters are at parton-level only, corrections for non-perturbative effects must be applied. As described in Sect. 2.4.1 this implies model assumptions and parameter tuning and hence induces a corresponding uncertainty. Customarily, the corrections are estimated from the ratio of distributions for fully hadronised events over the distributions with MPI and hadronisation switched off in the respective LO+PS MC event generators. An envelope is constructed around the predictions by different event generators with various tunes to derive a medium correction and to attribute a systematic uncertainty of half-width of the spread for this factor.

The advent of MC event generators capable of combining NLO+PS with the NP modelling opens up new possibilities. A first step towards NP corrections from NLO+PS event generation has been taken in Ref. [254], cf. Fig. 2.29 left, where the results for LO+PS from HERWIG++ and PYTHIA6 are compared with those for NLO+PS from POWHEG +PYTHIA6. As expected the NP effects are negligible for high transverse momenta, but can become significant for jet p_T 's below 300 GeV. Interestingly, they are less pronounced in the NLO+PS case. However, it has to be kept in mind that the p_T dependence of the various effects of PS, MPI, and hadronisation differs as detailed in Sect. 2.4. As a consequence, the NP corrections are sensitive to the choice of jet algorithm and jet size.

To avoid statistical fluctuations in less populated regions of phase space, the NP factors are usually parameterised by a simple polynomial function:

$$f(x) = p_0 + \frac{p_1}{x^{p_2}}. \quad (2.38)$$

Combining the three parameterised predictions for the whole range in rapidity leads to the curves shown in Fig. 2.29 right, exhibiting a similar size and shape versus p_T .

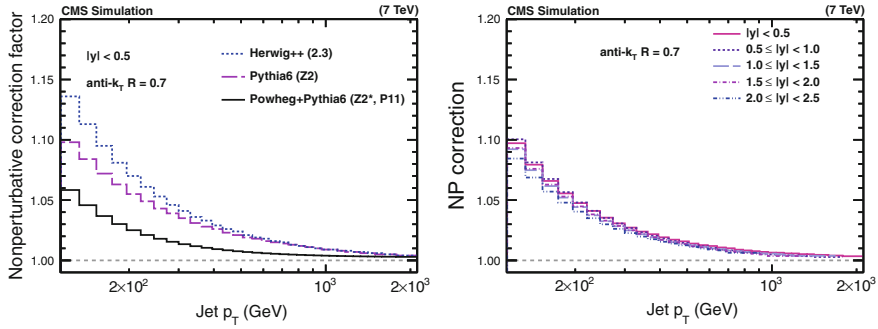


Fig. 2.29 *Left* NP corrections at central rapidity $|y| < 0.5$ for inclusive jets as a function of jet p_T using two LO+PS and the NLO+PS MC event generator POWHEG +PYTHIA6. *Right* Comparison of the combined NP factors in five regions of absolute jet rapidity. (Taken from Ref. [254])

Details with respect to particular analyses are presented in the relevant sections as appropriate.

2.6.5 Fast Interpolation Techniques

The processes of inclusive jet and dijet production at hadron colliders are known up to NLO since more than two decades from the (M)EKS [255–257], JETRAD [258], and NLOJET++ [259, 260] programs, where the latter also comprises 3-jet production at NLO. A calculation at NNLO is ongoing and at the time of writing is partially completed [261]. 4-jet and 5-jet production at NLO have become available recently [262–264].

All these programs, capable of providing cross sections fully differential in jet observables, are increasingly demanding in terms of CPU time consumption with higher orders and multiplicities. This prevents their direct use in fits of PDF parameters or the strong coupling constant. However, the CPU intensive part entering the calculation according to Eq. (2.20) is localised in the derivation of the partonic cross section

$$d\hat{\sigma}_{(ij \rightarrow X)}(x, x', \mu_f, \mu_r, \alpha_S(\mu_r)) \quad (2.39)$$

that depends on the PDFs and $\alpha_S(\mu_r)$ only indirectly via folding integrals. This fact enables the use of interpolation techniques to separate the time-consuming part from the PDF and $\alpha_S(\mu_r)$ dependence. To factorise for example the PDF dependence from the convolution, the PDFs are expressed as a sum of eigenfunctions (or interpolation kernels) on a grid in the convolution variable x as

$$f_{i/p}(x) \approx \sum_a f_{i/p}(x_a) \cdot E_a(x), \quad (2.40)$$

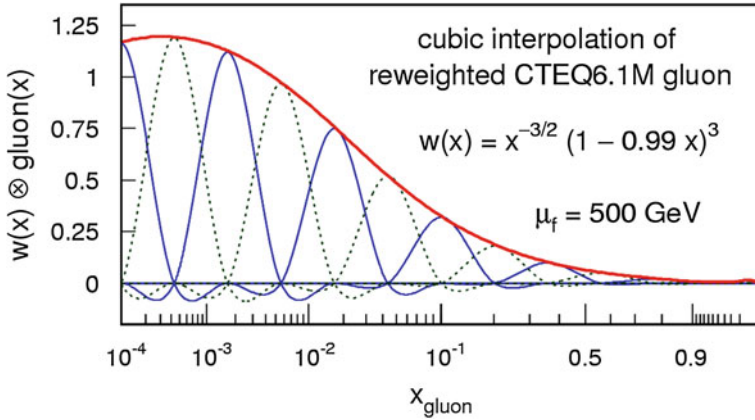


Fig. 2.30 Cubic interpolation of the gluon PDF in FASTNLO. $w(x)$ is an additional weight function to reduce PDF curvature and improve the approximation quality. (Illustration courtesy of M. Wobisch)

where a numbers the support nodes x_a , $f_{i/p}(x_a)$ assumes a fixed value, and $E_a(x)$ is the a -th eigenfunction. The set of eigenfunctions $\{E_a(x)\}$ must satisfy the relations

$$\begin{aligned} E_a(x_b) &= \delta_{ab}, \quad \forall a, b \\ \sum_a E_a(x) &= 1, \quad \forall x. \end{aligned} \quad (2.41)$$

A pictorial representation of this procedure employing cubic interpolation kernels is shown in Fig. 2.30.

Replacing $f_{i/p}(x)$ in Eq. (2.20) by the sum of Eq. (2.40) and performing the convolution with the partonic cross section once, the result can be written as a sum of terms, where a change in PDF only requires to adapt the factors $f_{i/p}(x_a)$, which is a very fast operation. For hadron-hadron collisions the same technique can easily be extended to both PDFs $f_{i/p}(x)$ and $f_{j/p}(x')$ giving a two-dimensional grid of support nodes (x_a, x_b) with PDF specific factors $f_{i/p}(x_a)$ and $f_{j/p}(x_b)$.

The quality of this approximation is determined by the number and distribution of support points, and the shape of the interpolation kernels in comparison to the shape of the PDFs and the distribution of the partonic cross section over the phase space. Two possibilities for optimisation are indicated in Fig. 2.30:

1. The support nodes are not evenly distributed in x but proportional to $\sqrt{(\log_{10}(x))}$.
2. An additional weight function $w(x)$ has been applied to reduce in a generic way the curvature of the PDFs, which improves the approximation quality.

Finally, the dependence on μ_r and μ_f can be addressed in the same way as the interpolation in x , where, however, the interpolation kernels and parameters can be optimised separately. In total, the equivalent of Eq. (2.20) then reads

$$d\sigma_{(pp \rightarrow X)} = \sum_{n,i,j,a,b,c} \alpha_s^n(\mu_c) \cdot f_{i/p}(x_a, \mu_c) \cdot f_{j/p}(x_b, \mu_c) \cdot d\tilde{\sigma}_{n,i,j,a,b,c}^{(ij \rightarrow X)}, \quad (2.42)$$

where the sum runs over the powers n of α_s , the parton flavours i and j , the x -interpolation nodes a and b , and the μ -interpolation nodes c . The time-consuming ($\mathcal{O}(kh)$) convolution has to be performed only once to compute and tabulate the coefficients

$$d\tilde{\sigma}_{n,i,j,a,b,c}^{(ij \rightarrow X)} = \int dx dx' E_a(x) \cdot E_b(x') \cdot E_c(\mu) \times d\hat{\sigma}_{(ij \rightarrow X)}^n(x, x', \mu), \quad (2.43)$$

that fully contain the information on observable definition and phase space restrictions. The evaluation of the sum of products in Eq. (2.42) only requires milliseconds.

This technique of *fast interpolation grids* introduced above hence can be exploited to reduce by many orders of magnitude the amount of CPU time to invest for repeated evaluations of higher-order cross sections with modified assumptions on PDFs, scales μ , or the value and evolution of α_s . Two independent implementations of this technique exist: FASTNLO [265, 266] and APPLGRID [267, 268], both of which are interfaced to various theory programs and utilised in fits with the XFITTER framework. The packages differ in their interpolation and optimisation strategies, but both of them construct tables with grids for each bin of an observable in two steps. In a first step the accessible phase space in momentum fraction x and scale μ is explored and the partonic subprocesses that contribute and need to be differentiated must be identified. This serves to optimise the table size by eliminating empty regions in x and μ as well as reducing the number of subprocesses to store as compared to $11 \cdot 11$ linear combinations in a full flavour basis without counting top quarks. Only in the second step the grid is filled for the requested observables and binning. The approximation quality can easily be checked by a comparison to histograms simultaneously filled with the full cross section. Alternatively, the dependence on the number of support nodes could be studied, as for an infinite number the approximation bias must approach zero.

For simplicity, μ_r and μ_f have been set equal in the formulae above. However, it is perfectly possible to differentiate between the two and in an update to the FASTNLO framework [269, 270] it is even possible to separately store terms proportional to $\log(\mu_r^2)^s \cdot \log(\mu_f^2)^t$ as they appear in the coefficients of a perturbative expansion. At NLO, the only combinations possible are $s = t = 0$, $s = 1, t = 0$, and $s = 0, t = 1$.

References

1. M.G. Holloway, C.P. Baker, Note on the origin of the term “barn”, Technical report, LAMS-523, Los Alamos National Laboratory, 1947. Report submitted: 13 September 1944. Report issued: 5 March 1947
2. D. Haitz, Precision Measurements of Proton Structure and Jet Energy Scale with the CMS Detector at the LHC. PhD thesis, KIT (Karlsruher Institut für Technologie), Jun, 2016

3. J. Chadwick, Possible existence of a neutron. *Nature* **129**, 312 (1932). doi:[10.1038/129312a0](https://doi.org/10.1038/129312a0)
4. P.A.M. Dirac, The quantum theory of the electron. *Proc. Roy. Soc. Lond. A* **117**, 610 (1928). doi:[10.1098/rspa.1928.0023](https://doi.org/10.1098/rspa.1928.0023)
5. C.D. Anderson, The positive electron. *Phys. Rev.* **43**, 491 (1933). doi:[10.1103/PhysRev.43.491](https://doi.org/10.1103/PhysRev.43.491)
6. S.H. Neddermeyer, C.D. Anderson, Note on the nature of cosmic ray particles. *Phys. Rev.* **51**, 884 (1937). doi:[10.1103/PhysRev.51.884](https://doi.org/10.1103/PhysRev.51.884)
7. H. Yukawa, On the interaction of elementary particles I. *Proc. Phys. Math. Soc. Jap.* **17**, 48 (1935). doi:[10.1143/PTPS.1.1](https://doi.org/10.1143/PTPS.1.1)
8. C.M.G. Lattes, G.P.S. Occhialini, C.F. Powell, Observations on the tracks of slow mesons in photographic emulsions. 1. *Nature* **160**, 453 (1947). doi:[10.1038/160453a0](https://doi.org/10.1038/160453a0)
9. C.M.G. Lattes, G.P.S. Occhialini, C.F. Powell, Observations on the tracks of slow mesons in photographic emulsions. 2. *Nature* **160**, 486 (1947). doi:[10.1038/160486a0](https://doi.org/10.1038/160486a0)
10. R. Cahn, G. Goldhaber, *The Experimental Foundations of Particle Physics*, 2nd edn. (Cambridge University Press, Cambridge, 2009)
11. V.E. Barnes et al., Observation of a hyperon with strangeness -3. *Phys. Rev. Lett.* **12**, 204 (1964). doi:[10.1103/PhysRevLett.12.204](https://doi.org/10.1103/PhysRevLett.12.204)
12. M. Gell-Mann, A schematic model of baryons and mesons. *Phys. Lett.* **8**, 214 (1964). doi:[10.1016/S0031-9163\(64\)92001-3](https://doi.org/10.1016/S0031-9163(64)92001-3)
13. G. Zweig, *An SU_3 model for strong interaction symmetry and its breaking; Version 1*. Technical report, CERN-TH-401, CERN, Geneva, 1964
14. G. Zweig, *An SU_3 model for strong interaction symmetry and its breaking; Version 2*. Technical report, CERN-TH-412, CERN, Geneva, 1964
15. M. Gell-Mann, Quarks, color, and QCD, in *Proceedings, Workshop on QCD—20 Years Later*, vol. C920609, p. 3. Aachen, Germany, 9–13 June 1992
16. Creative Commons License. CC-BY-SA-3.0, <http://creativecommons.org/licenses/by-sa/3.0/>
17. E.D. Bloom et al., High-energy inelastic ep scattering at 6-degrees and 10-degrees. *Phys. Rev. Lett.* **23**, 930 (1969). doi:[10.1103/PhysRevLett.23.930](https://doi.org/10.1103/PhysRevLett.23.930)
18. M. Breidenbach et al., Observed behavior of highly inelastic electron-proton scattering. *Phys. Rev. Lett.* **23**, 935 (1969). doi:[10.1103/PhysRevLett.23.935](https://doi.org/10.1103/PhysRevLett.23.935)
19. J.D. Bjorken, Asymptotic sum rules at infinite momentum. *Phys. Rev.* **179**, 1547 (1969). doi:[10.1103/PhysRev.179.1547](https://doi.org/10.1103/PhysRev.179.1547)
20. G. 't Hooft, M.J.G. Veltman, Regularization and renormalization of gauge fields. *Nucl. Phys. B* **44** (1972) 189. doi:[10.1016/0550-3213\(72\)90279-9](https://doi.org/10.1016/0550-3213(72)90279-9)
21. H. Fritzsch, M. Gell-Mann, Current algebra: quarks and what else?, in *Proceedings, 16th International Conference on High-Energy Physics (ICHEP)*, vol. C720906V2, p. 135. Batavia, IL, USA, 6–13 Sept 1972, [arXiv:hep-ph/0208010](https://arxiv.org/abs/hep-ph/0208010)
22. O.W. Greenberg, Spin and unitary spin independence in a paraquark model of baryons and mesons. *Phys. Rev. Lett.* **13**, 598 (1964). doi:[10.1103/PhysRevLett.13.598](https://doi.org/10.1103/PhysRevLett.13.598)
23. M. Gell-Mann, Symmetries of baryons and mesons. *Phys. Rev.* **125**, 1067 (1962). doi:[10.1103/PhysRev.125.1067](https://doi.org/10.1103/PhysRev.125.1067)
24. D.J. Gross, F. Wilczek, Ultraviolet behavior of nonabelian gauge theories. *Phys. Rev. Lett.* **30**, 1343 (1973). doi:[10.1103/PhysRevLett.30.1343](https://doi.org/10.1103/PhysRevLett.30.1343)
25. D.J. Gross, F. Wilczek, Asymptotically free gauge theories. 1. *Phys. Rev. D* **8**, 3633 (1973). doi:[10.1103/PhysRevD.8.3633](https://doi.org/10.1103/PhysRevD.8.3633)
26. D.J. Gross, F. Wilczek, Asymptotically free gauge theories. 2. *Phys. Rev. D* **9**, 980 (1974). doi:[10.1103/PhysRevD.9.980](https://doi.org/10.1103/PhysRevD.9.980)
27. H.D. Politzer, Reliable perturbative results for strong interactions? *Phys. Rev. Lett.* **30**, 1346 (1973). doi:[10.1103/PhysRevLett.30.1346](https://doi.org/10.1103/PhysRevLett.30.1346)
28. K.A. Olive and others (Particle Data Group), Review of particle physics. *Chin. Phys. C* **38** (2014) 090001. doi:[10.1088/1674-1137/38/9/090001](https://doi.org/10.1088/1674-1137/38/9/090001)
29. JabRef Development Team, JabRef (2003), <http://www.jabref.org/>. Accessed 24 May 2016
30. M.E. Peskin, D.V. Schroeder, *An Introduction to Quantum Field Theory (Frontiers in Physics)* (Westview Press, Boulder, CO, 1995)

31. I.J. Aitchison, A.J. Hey, *Gauge Theories in Particle Physics: A Practical Introduction*, Fourth Edition - 2 Volume set. 4th edn. 12 (CRC Press, 2012)
32. G.F. Sterman, *An Introduction to Quantum Field Theory* (Cambridge University Press, 1993)
33. C. Itzykson, J.-B. Zuber, *Quantum Field Theory* (Dover Publications, 2006)
34. J.D. Bjorken, S.D. Drell, *Relativistic Quantum Fields*, 1st edn. (Mcgraw-Hill College, 1965)
35. G. Dissertori, I.G. Knowles, M. Schmelling, *Quantum Chromodynamics: High Energy Experiments and Theory*, 2nd edn. (Oxford University Press, 2009)
36. F.J. Ynduráin, *The Theory of Quark and Gluon Interactions*, 4th edn. Texts and monographs in physics (Springer, Berlin, 2006)
37. R.K. Ellis, W.J. Stirling, B.R. Webber, *QCD and Collider Physics (Nuclear Physics and Cosmology)* (Cambridge University Press, Cambridge, Cambridge Monographs on Particle Physics, 1996)
38. Y.L. Dokshitzer, V.A. Khoze, A.H. Mueller, S.I. Troian, *Basics of Perturbative QCD*. Editions Frontieres, Dec 1991
39. T. Muta, *Foundations of Quantum Chromodynamics: An Introduction to Perturbative Methods in Gauge Theories* (World Scientific, 1987)
40. CTEQ Collaboration, Handbook of perturbative QCD. Rev. Mod. Phys. **67**, 157 (1995). doi:[10.1103/RevModPhys.67.157](https://doi.org/10.1103/RevModPhys.67.157)
41. D.W. Duke, R.G. Roberts, Determinations of the QCD strong coupling α_s and the scale Λ_{QCD} . Phys. Rept. **120**, 275 (1985). doi:[10.1016/0370-1573\(85\)90112-7](https://doi.org/10.1016/0370-1573(85)90112-7)
42. G. Altarelli, Partons in quantum chromodynamics. Phys. Rept. **81**, 1 (1982). doi:[10.1016/0370-1573\(82\)90127-2](https://doi.org/10.1016/0370-1573(82)90127-2)
43. A.H. Mueller, Perturbative QCD at high-energies. Phys. Rept. **73**, 237 (1981). doi:[10.1016/0370-1573\(81\)90030-2](https://doi.org/10.1016/0370-1573(81)90030-2)
44. R.P. Feynman, *Photon-Hadron Interactions* (Westview Press, 1998)
45. J. Collins, *Foundations of Perturbative QCD, Nuclear Physics and Cosmology* (Cambridge University Press, Cambridge, Cambridge Monographs on Particle Physics, 2011)
46. S. Moch, Hard QCD at hadron colliders. J. Phys. G **35**, 073001 (2008). doi:[10.1088/0954-3899/35/7/073001](https://doi.org/10.1088/0954-3899/35/7/073001). arXiv:0803.0457
47. J.M. Campbell, J.W. Huston, W.J. Stirling, Hard interactions of quarks and gluons: a primer for LHC physics. Rept. Prog. Phys. **70**, 89 (2007). doi:[10.1088/0034-4885/70/1/R02](https://doi.org/10.1088/0034-4885/70/1/R02). arXiv:hep-ph/0611148
48. R. Alemany-Fernandez et al., *The Large Hadron Collider: Harvest of Run 1*, 1st edn. (Springer, Berlin, Germany, 2015)
49. R.M. Barnett et al., *Physics at the Terascale*, 1st edn. (Wiley-VCH Verlag GmbH & Co. KGaA, Weinheim, Germany, 2011)
50. H. Fritzsch, M. Gell-Mann (eds.), *50 Years of Quarks* (World Scientific Publishing Co. Pte. Ltd., 2015)
51. P.M. Zerwas, H.A. Kastrup (eds.), *QCD: 20 Years Later: Aachen, June 9–13, 1992* (World Scientific Publishing Co. Pte. Ltd., 1993)
52. D. Binosi, L. Theussl, JaxoDraw: a graphical user interface for drawing Feynman diagrams. Comput. Phys. Commun. **161**, 76 (2004). doi:[10.1016/j.cpc.2004.05.001](https://doi.org/10.1016/j.cpc.2004.05.001). arXiv:hep-ph/0309015
53. L.D. Faddeev, V.N. Popov, Feynman diagrams for the yang-mills field. Phys. Lett. B **25**, 29 (1967). doi:[10.1016/0370-2693\(67\)90067-6](https://doi.org/10.1016/0370-2693(67)90067-6)
54. R.D. Peccei, H.R. Quinn, CP conservation in the presence of pseudoparticles. Phys. Rev. Lett. **38**, 1440 (1977). doi:[10.1103/PhysRevLett.38.1440](https://doi.org/10.1103/PhysRevLett.38.1440)
55. R.D. Peccei, H.R. Quinn, Constraints imposed by CP conservation in the presence of pseudoparticles. Phys. Rev. D **16**, 1791 (1977). doi:[10.1103/PhysRevD.16.1791](https://doi.org/10.1103/PhysRevD.16.1791)
56. G. 't Hooft, The Glorious days of physics: renormalization of gauge theories, arXiv:hep-th/9812203
57. T. van Ritbergen, J.A.M. Vermaseren, S.A. Larin, The four-loop β -function in quantum chromodynamics. Phys. Lett. B **400**, 379 (1997). doi:[10.1016/S0370-2693\(97\)00370-5](https://doi.org/10.1016/S0370-2693(97)00370-5). arXiv:hep-ph/9701390

58. G. 't Hooft, Dimensional regularization and the renormalization group. Nucl. Phys. B **61** (1973) 455. doi:[10.1016/0550-3213\(73\)90376-3](https://doi.org/10.1016/0550-3213(73)90376-3)
59. W.A. Bardeen, A.J. Buras, D.W. Duke, T. Muta, Deep inelastic scattering beyond the leading order in asymptotically free gauge theories. Phys. Rev. D **18**, 3998 (1978). doi:[10.1103/PhysRevD.18.3998](https://doi.org/10.1103/PhysRevD.18.3998)
60. J. Beringer and others (Particle Data Group), Review of particle physics. Phys. Rev. D **86** (2012) 010001. doi:[10.1103/PhysRevD.86.010001](https://doi.org/10.1103/PhysRevD.86.010001)
61. S. Durr et al., Ab-Initio Determination of Light Hadron Masses. Science **322**, 1224 (2008). doi:[10.1126/science.1163233](https://doi.org/10.1126/science.1163233). arXiv:[0906.3599](https://arxiv.org/abs/0906.3599)
62. J.C. Collins, D.E. Soper, G. Sterman, *Factorization of Hard Processes in QCD*, volume 5 of Advanced Series on Directions in High Energy Physics, Ch. 1, p. 1, (World Scientific Pub Co Inc, 1988), arXiv:[hep-ph/0409313](https://arxiv.org/abs/hep-ph/0409313). doi:[10.1142/9789814503266_0001](https://doi.org/10.1142/9789814503266_0001)
63. J.R. Andersen et al., Les Houches 2013: Physics at TeV Colliders: Standard Model Working Group Report, arXiv:[1405.1067](https://arxiv.org/abs/1405.1067)
64. S. Dittmaier, A. Huss, C. Speckner, Weak radiative corrections to dijet production at hadron colliders. JHEP **11**, 095 (2012). doi:[10.1007/JHEP11\(2012\)095](https://doi.org/10.1007/JHEP11(2012)095). arXiv:[1210.0438](https://arxiv.org/abs/1210.0438)
65. V.N. Gribov, L.N. Lipatov, Deep inelastic ep scattering in perturbation theory. Sov. J. Nucl. Phys. **15**, 438 (1972)
66. L.N. Lipatov, The parton model and perturbation theory. Sov. J. Nucl. Phys. **20** (1975) 94. [Yad. Fiz.20,181(1974)]
67. G. Altarelli, G. Parisi, Asymptotic Freedom in Parton Language. Nucl. Phys. B **126**, 298 (1977). doi:[10.1016/0550-3213\(77\)90384-4](https://doi.org/10.1016/0550-3213(77)90384-4)
68. Y.L. Dokshitzer, Calculation of the Structure Functions for Deep Inelastic Scattering and e+ e- Annihilation by Perturbation Theory in Quantum Chromodynamics. Sov. Phys. JETP **46**, 641 (1977)
69. S. Moch, J.A.M. Vermaseren, A. Vogt, The three loop splitting functions in QCD: the nonsinglet case. Nucl. Phys. B **688**, 101 (2004). doi:[10.1016/j.nuclphysb.2004.03.030](https://doi.org/10.1016/j.nuclphysb.2004.03.030). arXiv:[hep-ph/0403192](https://arxiv.org/abs/hep-ph/0403192)
70. A. Vogt, S. Moch, J.A.M. Vermaseren, The three-loop splitting functions in QCD: the singlet case. Nucl. Phys. B **691**, 129 (2004). doi:[10.1016/j.nuclphysb.2004.04.024](https://doi.org/10.1016/j.nuclphysb.2004.04.024). arXiv:[hep-ph/0404111](https://arxiv.org/abs/hep-ph/0404111)
71. E.A. Kuraev, L.N. Lipatov, V.S. Fadin, The pomeranchuk singularity in nonabelian gauge theories. Sov. Phys. JETP **45** (1977) 199. [Zh. Eksp. Teor. Fiz.72,377(1977)]
72. I.I. Balitsky, L.N. Lipatov, The pomeranchuk singularity in quantum chromodynamics. Sov. J. Nucl. Phys. **28** (1978) 822. [Yad. Fiz.28,1597(1978)]
73. W.J. Stirling, Parton luminosity and cross section plots. Private communication, 2016. <http://www.hep.ph.ic.ac.uk/~wstirling/plots/plots.html>
74. C. Buttar et al., The QCD, EW, and Higgs Working Group: Summary Report, in *Proceedings, 4th Les Houches Workshop 2005 on Physics at TeV colliders (Les Houches 2005)*. Les Houches, France, 2-20 May 2005. arXiv:[hep-ph/0604120](https://arxiv.org/abs/hep-ph/0604120)
75. S.D. Drell, T.-M. Yan, Partons and their applications at high-energies. Annals Phys. **66**, 578 (1971). doi:[10.1016/0003-4916\(71\)90071-6](https://doi.org/10.1016/0003-4916(71)90071-6)
76. S.M. Berman, J.D. Bjorken, J.B. Kogut, Inclusive processes at high transverse momentum. Phys. Rev. D **4**, 3388 (1971). doi:[10.1103/PhysRevD.4.3388](https://doi.org/10.1103/PhysRevD.4.3388)
77. F. Halzen, D.M. Scott, energy flow: testing QCD without structure functions, in *Proceedings, 11th International Symposium on Multiparticle Dynamics (ISMD)*, p. 0593. Bruges, Belgium, 22-27 June 1980
78. S.D. Drell, D.J. Levy, T.-M. Yan, A theory of deep-inelastic lepton-nucleon scattering and lepton-pair annihilation processes. I. Phys. Rev. **187**, 2159 (1969). doi:[10.1103/PhysRev.187.2159](https://doi.org/10.1103/PhysRev.187.2159)
79. S.D. Drell, D.J. Levy, T.-M. Yan, A theory of deep-inelastic lepton-nucleon scattering and lepton-pair annihilation processes. III. deep-inelastic electron-positron annihilation. Phys. Rev. D **1**, 1617 (1970). doi:[10.1103/PhysRevD.1.1617](https://doi.org/10.1103/PhysRevD.1.1617)

80. N. Cabibbo, G. Parisi, M. Testa, Hadron production in e^+e^- collisions. *Lett. Nuovo Cim.* **4S1** (1970) 35. doi:[10.1007/BF02755392](https://doi.org/10.1007/BF02755392). [*Lett. Nuovo Cim.*4,35(1970)]
81. J.D. Bjorken, S.J. Brodsky, Statistical model for electron-positron annihilation Into hadrons. *Phys. Rev. D* **1**, 1416 (1970). doi:[10.1103/PhysRevD.1.1416](https://doi.org/10.1103/PhysRevD.1.1416)
82. R.P. Feynman, R.D. Field, G.C. Fox, Quantum-chromodynamic approach for the large-transverse- momentum production of particles and jets. *Phys. Rev. D* **18**, 3320 (1978). doi:[10.1103/PhysRevD.18.3320](https://doi.org/10.1103/PhysRevD.18.3320)
83. A.V. Belitsky, G.P. Korchemsky, G.F. Sterman, Energy flow in QCD and event shape functions. *Phys. Lett. B* **515**, 297 (2001). doi:[10.1016/S0370-2693\(01\)00899-1](https://doi.org/10.1016/S0370-2693(01)00899-1). [arXiv:hep-ph/0106308](https://arxiv.org/abs/hep-ph/0106308)
84. A. Ali, G. Kramer, Jets and QCD: a historical review of the discovery of the quark and gluon jets and its impact on QCD. *Eur. Phys. J. H* **36**, 245 (2011). doi:[10.1140/epjh/e2011-10047-1](https://doi.org/10.1140/epjh/e2011-10047-1). [arXiv:1012.2288](https://arxiv.org/abs/1012.2288)
85. P. Söding, On the discovery of the gluon. *Eur. Phys. J. H* **35**, 3 (2010). doi:[10.1140/epjh/e2010-00002-5](https://doi.org/10.1140/epjh/e2010-00002-5)
86. B.R. Stella, H.-J. Meyer, Y(9.46 GeV) and the gluon discovery (a critical recollection of PLUTO results). *Eur. Phys. J. H* **36**, 203 (2011). doi:[10.1140/epjh/e2011-10029-3](https://doi.org/10.1140/epjh/e2011-10029-3). [arXiv:1008.1869](https://arxiv.org/abs/1008.1869)
87. ATLAS Collaboration, Observation of a new particle in the search for the Standard Model Higgs boson with the ATLAS detector at the LHC. *Phys. Lett. B* **716** (2012) 1. doi:[10.1016/j.physletb.2012.08.020](https://doi.org/10.1016/j.physletb.2012.08.020), [arXiv:1207.7214](https://arxiv.org/abs/1207.7214)
88. CMS Collaboration, Observation of a new boson at a mass of 125 GeV with the CMS experiment at the LHC. *Phys. Lett. B* **716**, 30 (2012). doi:[10.1016/j.physletb.2012.08.021](https://doi.org/10.1016/j.physletb.2012.08.021). [arXiv:1207.7235](https://arxiv.org/abs/1207.7235)
89. CDF Collaboration, Observation of top quark production in $\bar{p}p$ collisions. *Phys. Rev. Lett.* **74**, 2626 (1995). doi:[10.1103/PhysRevLett.74.2626](https://doi.org/10.1103/PhysRevLett.74.2626). [arXiv:hep-ex/9503002](https://arxiv.org/abs/hep-ex/9503002)
90. D0 Collaboration, Observation of the top quark. *Phys. Rev. Lett.* **74**, 2632 (1995). doi:[10.1103/PhysRevLett.74.2632](https://doi.org/10.1103/PhysRevLett.74.2632). [arXiv:hep-ex/9503003](https://arxiv.org/abs/hep-ex/9503003)
91. H.U. Bengtsson, The Lund Monte Carlo for high p_T physics. *Comput. Phys. Commun.* **31**, 323 (1984). doi:[10.1016/0010-4655\(84\)90018-3](https://doi.org/10.1016/0010-4655(84)90018-3)
92. T. Sjöstrand, The Lund Monte Carlo for jet fragmentation. *Comput. Phys. Commun.* **27**, 243 (1982). doi:[10.1016/0010-4655\(82\)90175-8](https://doi.org/10.1016/0010-4655(82)90175-8)
93. T. Sjöstrand, High-energy physics event generation with PYTHIA 5.7 and JETSET 7.4. *Comput. Phys. Commun.* **82**, 74 (1994). doi:[10.1016/0010-4655\(94\)90132-5](https://doi.org/10.1016/0010-4655(94)90132-5)
94. T. Sjöstrand, S. Mrenna, P.Z. Skands, PYTHIA 6.4 Physics and Manual. *JHEP* **05** (2006) 026. doi:[10.1088/1126-6708/2006/05/026](https://doi.org/10.1088/1126-6708/2006/05/026), [arXiv:hep-ph/0603175](https://arxiv.org/abs/hep-ph/0603175)
95. G. Marchesini, B.R. Webber, Monte carlo simulation of general hard processes with coherent QCD radiation. *Nucl. Phys. B* **310**, 461 (1988). doi:[10.1016/0550-3213\(88\)90089-2](https://doi.org/10.1016/0550-3213(88)90089-2)
96. G. Marchesini et al., HERWIG: a Monte Carlo event generator for simulating hadron emission reactions with interfering gluons. Version 5.1 - April 1991. *Comput. Phys. Commun.* **67**, 465 (1992). doi:[10.1016/0010-4655\(92\)90055-4](https://doi.org/10.1016/0010-4655(92)90055-4)
97. G. Corcella et al., HERWIG 6: an Event generator for hadron emission reactions with interfering gluons (including supersymmetric processes). *JHEP* **01**, 010 (2001). doi:[10.1088/1126-6708/2001/01/010](https://doi.org/10.1088/1126-6708/2001/01/010). [arXiv:hep-ph/0011363](https://arxiv.org/abs/hep-ph/0011363)
98. G. Corcella et al., HERWIG 6.5 release note, [arXiv:hep-ph/0210213](https://arxiv.org/abs/hep-ph/0210213)
99. T. Sjöstrand, S. Mrenna, P.Z. Skands, A. Brief, Introduction to PYTHIA 8.1. *Comput. Phys. Commun.* **178**, 852 (2008). doi:[10.1016/j.cpc.2008.01.036](https://doi.org/10.1016/j.cpc.2008.01.036). [arXiv:0710.3820](https://arxiv.org/abs/0710.3820)
100. T. Sjöstrand et al., An Introduction to PYTHIA 8.2. *Comput. Phys. Commun.* **191**, 159 (2015). doi:[10.1016/j.cpc.2015.01.024](https://doi.org/10.1016/j.cpc.2015.01.024). [arXiv:1410.3012](https://arxiv.org/abs/1410.3012)
101. M. Bähr et al., Herwig++ physics and manual. *Eur. Phys. J. C* **58**, 639 (2008). doi:[10.1140/epjc/s10052-008-0798-9](https://doi.org/10.1140/epjc/s10052-008-0798-9). [arXiv:0803.0883](https://arxiv.org/abs/0803.0883)
102. J. Bellm et al., Herwig 7.0 / Herwig++ 3.0 Release Note, [arXiv:1512.01178](https://arxiv.org/abs/1512.01178)
103. T. Gleisberg et al., Event generation with SHERPA 1.1. *JHEP* **02** (2009) 007. doi:[10.1088/1126-6708/2009/02/007](https://doi.org/10.1088/1126-6708/2009/02/007), [arXiv:0811.4622](https://arxiv.org/abs/0811.4622)

104. A. Buckley et al., General-purpose event generators for LHC physics. *Phys. Rept.* **504**, 145 (2011). doi:[10.1016/j.physrep.2011.03.005](https://doi.org/10.1016/j.physrep.2011.03.005). [arXiv:1101.2599](https://arxiv.org/abs/1101.2599)
105. S. Gieseke, Z. Nagy, *Monte Carlo Generators and Fixed-order Calculations: Predicting the (Un)Expected*, 1st edn. Ch. 5, p. 97. Wiley-VCH Verlag GmbH & Co. KGaA, Weinheim, Germany, April, 2011. doi:[10.1002/9783527634965.ch5](https://doi.org/10.1002/9783527634965.ch5)
106. S. Gieseke, Simulation of jets at colliders. *Prog. Part. Nucl. Phys.* **72**, 155 (2013). doi:[10.1016/j.pnpnp.2013.04.001](https://doi.org/10.1016/j.pnpnp.2013.04.001)
107. S. Höche, Introduction to parton-shower event generators, in *Proceedings, Theoretical Advanced Study Institute in Elementary Particle Physics: Journeys Through the Precision Frontier: Amplitudes for Colliders (TASI 2014)*. Boulder, CO, USA, 2–27 June 2014. [arXiv:1411.4085](https://arxiv.org/abs/1411.4085)
108. M.A. Dobbs et al., Les Houches guidebook to Monte Carlo generators for hadron collider physics, in *Proceedings, 3rd Les Houches Workshop 2003 on Physics at TeV colliders (Les Houches 2003)*, p. 411. Les Houches, France, May 26–June 2, 2003. [arXiv:hep-ph/0403045](https://arxiv.org/abs/hep-ph/0403045)
109. I.G. Knowles, A linear algorithm for calculating spin correlations in hadronic collisions. *Comput. Phys. Commun.* **58**, 271 (1990). doi:[10.1016/0010-4655\(90\)90063-7](https://doi.org/10.1016/0010-4655(90)90063-7)
110. I.G. Knowles, Spin correlations in parton–parton scattering. *Nucl. Phys. B* **310**, 571 (1988). doi:[10.1016/0550-3213\(88\)90092-2](https://doi.org/10.1016/0550-3213(88)90092-2)
111. M. Bengtsson, T. Sjöstrand, A comparative study of coherent and noncoherent parton shower evolution. *Nucl. Phys. B* **289**, 810 (1987). doi:[10.1016/0550-3213\(87\)90407-X](https://doi.org/10.1016/0550-3213(87)90407-X)
112. M. Bengtsson, T. Sjöstrand, Coherent parton showers versus matrix elements: implications of PETRA - PEP Data. *Phys. Lett. B* **185**, 435 (1987). doi:[10.1016/0370-2693\(87\)91031-8](https://doi.org/10.1016/0370-2693(87)91031-8)
113. T. Sjöstrand, P.Z. Skands, Transverse-momentum-ordered showers and interleaved multiple interactions. *Eur. Phys. J. C* **39**, 129 (2005). doi:[10.1140/epjc/s2004-02084-y](https://doi.org/10.1140/epjc/s2004-02084-y). [arXiv:hep-ph/0408302](https://arxiv.org/abs/hep-ph/0408302)
114. S. Gieseke, P. Stephens, B. Webber, New formalism for QCD parton showers. *JHEP* **12**, 045 (2003). doi:[10.1088/1126-6708/2003/12/045](https://doi.org/10.1088/1126-6708/2003/12/045). [arXiv:hep-ph/0310083](https://arxiv.org/abs/hep-ph/0310083)
115. J.-C. Winter, F. Krauss, Initial-state showering based on colour dipoles connected to incoming parton lines. *JHEP* **07**, 040 (2008). doi:[10.1088/1126-6708/2008/07/040](https://doi.org/10.1088/1126-6708/2008/07/040). [arXiv:0712.3913](https://arxiv.org/abs/0712.3913)
116. S. Schumann, F. Krauss, A parton shower algorithm based on Catani-Seymour dipole factorisation. *JHEP* **03**, 038 (2008). doi:[10.1088/1126-6708/2008/03/038](https://doi.org/10.1088/1126-6708/2008/03/038). [arXiv:0709.1027](https://arxiv.org/abs/0709.1027)
117. G. Gustafson, U. Petterson, Dipole formulation of QCD cascades. *Nucl. Phys. B* **306**, 746 (1988). doi:[10.1016/0550-3213\(88\)90441-5](https://doi.org/10.1016/0550-3213(88)90441-5)
118. B. Andersson, G. Gustafson, G. Ingelman, T. Sjöstrand, Parton fragmentation and string dynamics. *Phys. Rept.* **97**, 31 (1983). doi:[10.1016/0370-1573\(83\)90080-7](https://doi.org/10.1016/0370-1573(83)90080-7)
119. B. Andersson, G. Gustafson, B. Söderberg, A general model for jet fragmentation. *Z. Phys. C* **20**, 317 (1983). doi:[10.1007/BF01407824](https://doi.org/10.1007/BF01407824)
120. T. Sjöstrand, The merging of jets. *Phys. Lett. B* **142**, 420 (1984). doi:[10.1016/0370-2693\(84\)91354-6](https://doi.org/10.1016/0370-2693(84)91354-6)
121. B.R. Webber, A QCD Model for jet fragmentation including soft gluon interference. *Nucl. Phys. B* **238**, 492 (1984). doi:[10.1016/0550-3213\(84\)90333-X](https://doi.org/10.1016/0550-3213(84)90333-X)
122. J.-C. Winter, F. Krauss, G. Soff, A modified cluster hadronization model. *Eur. Phys. J. C* **36**, 381 (2004). doi:[10.1140/epjc/s2004-01960-8](https://doi.org/10.1140/epjc/s2004-01960-8). [arXiv:hep-ph/0311085](https://arxiv.org/abs/hep-ph/0311085)
123. CDF Collaboration, Charged jet evolution and the underlying event in $p\bar{p}$ collisions at 1.8 TeV. *Phys. Rev. D* **65**, 092002 (2002). doi:[10.1103/PhysRevD.65.092002](https://doi.org/10.1103/PhysRevD.65.092002)
124. CDF Collaboration, The underlying event in hard interactions at the Tevatron $p\bar{p}$ collider. *Phys. Rev. D* **70**, 072002 (2004). doi:[10.1103/PhysRevD.70.072002](https://doi.org/10.1103/PhysRevD.70.072002). [arXiv:hep-ex/0404004](https://arxiv.org/abs/hep-ex/0404004)
125. CDF Collaboration, Studying the Underlying Event in Drell-Yan and High Transverse Momentum Jet Production at the Tevatron. *Phys. Rev. D* **82**, 034001 (2010). doi:[10.1103/PhysRevD.82.034001](https://doi.org/10.1103/PhysRevD.82.034001). [arXiv:1003.3146](https://arxiv.org/abs/1003.3146)
126. CDF Collaboration, Study of the energy dependence of the underlying event in proton-antiproton collisions. *Phys. Rev. D* **92**, 092009 (2015). doi:[10.1103/PhysRevD.92.092009](https://doi.org/10.1103/PhysRevD.92.092009). [arXiv:1508.05340](https://arxiv.org/abs/1508.05340)

127. ATLAS Collaboration, Measurement of underlying event characteristics using charged particles in pp collisions at $\sqrt{s} = 900$ GeV and 7 TeV with the ATLAS detector. *Phys. Rev. D* **83** (2011) 112001. doi:[10.1103/PhysRevD.83.112001](https://doi.org/10.1103/PhysRevD.83.112001), arXiv:[1012.0791](https://arxiv.org/abs/1012.0791)
128. ATLAS Collaboration, Measurements of underlying-event properties using neutral and charged particles in pp collisions at 900 GeV and 7 TeV with the ATLAS detector at the LHC. *Eur. Phys. J. C* **71** (2011) 1636. doi:[10.1140/epjc/s10052-011-1636-z](https://doi.org/10.1140/epjc/s10052-011-1636-z), arXiv:[1103.1816](https://arxiv.org/abs/1103.1816)
129. ATLAS Collaboration, Measurement of the underlying event in jet events from 7 TeV proton-proton collisions with the ATLAS detector. *Eur. Phys. J. C* **74** (2014) 2965. doi:[10.1140/epjc/s10052-014-2965-5](https://doi.org/10.1140/epjc/s10052-014-2965-5), arXiv:[1406.0392](https://arxiv.org/abs/1406.0392)
130. ATLAS Collaboration, Measurement of distributions sensitive to the underlying event in inclusive Z-boson production in pp collisions at $\sqrt{s} = 7$ TeV with the ATLAS detector. *Eur. Phys. J. C* **74** (2014) 319. doi:[10.1140/epjc/s10052-014-3195-6](https://doi.org/10.1140/epjc/s10052-014-3195-6), arXiv:[1409.3433](https://arxiv.org/abs/1409.3433)
131. CMS Collaboration, First measurement of the underlying event activity at the LHC with $\sqrt{s} = 0.9$ TeV. *Eur. Phys. J. C* **70**, 555 (2010). doi:[10.1140/epjc/s10052-010-1453-9](https://doi.org/10.1140/epjc/s10052-010-1453-9). arXiv:[1006.2083](https://arxiv.org/abs/1006.2083)
132. CMS Collaboration, Measurement of the underlying event activity at the LHC with $\sqrt{s} = 7$ TeV and comparison with $\sqrt{s} = 0.9$ TeV. *JHEP* **09** (2011) 109. doi:[10.1007/JHEP09\(2011\)109](https://doi.org/10.1007/JHEP09(2011)109), arXiv:[1107.0330](https://arxiv.org/abs/1107.0330)
133. CMS Collaboration, Measurement of the underlying event in the Drell-Yan process in proton-proton collisions at $\sqrt{s} = 7$ TeV. *Eur. Phys. J. C* **72**, 2080 (2012). doi:[10.1140/epjc/s10052-012-2080-4](https://doi.org/10.1140/epjc/s10052-012-2080-4). arXiv:[1204.1411](https://arxiv.org/abs/1204.1411)
134. CMS Collaboration, Study of the underlying event at forward rapidity in pp collisions at $\sqrt{s} = 0.9, 2.76$, and 7 TeV. *JHEP* **04** (2013) 072. doi:[10.1007/JHEP04\(2013\)072](https://doi.org/10.1007/JHEP04(2013)072), arXiv:[1302.2394](https://arxiv.org/abs/1302.2394)
135. CMS Collaboration, Measurement of the underlying event activity using charged-particle jets in proton-proton collisions at $\sqrt{s} = 2.76$ TeV. *JHEP* **09** (2015) 137. doi:[10.1007/JHEP09\(2015\)137](https://doi.org/10.1007/JHEP09(2015)137), arXiv:[1507.07229](https://arxiv.org/abs/1507.07229)
136. ALICE Collaboration, Underlying Event measurements in pp collisions at $\sqrt{s} = 0.9$ and 7 TeV with the ALICE experiment at the LHC. *JHEP* **07** (2012) 116. doi:[10.1007/JHEP07\(2012\)116](https://doi.org/10.1007/JHEP07(2012)116), arXiv:[1112.2082](https://arxiv.org/abs/1112.2082)
137. D. Piparo, Statistical Combination of Higgs Decay Channels and Determination of the Jet-Energy Scale of the CMS Experiment at the LHC. PhD thesis, KIT (Karlsruher Institut für Technologie), Nov 2010
138. T. Sjöstrand, M. van Zijl, A multiple interaction model for the event structure in hadron collisions. *Phys. Rev. D* **36**, 2019 (1987). doi:[10.1103/PhysRevD.36.2019](https://doi.org/10.1103/PhysRevD.36.2019)
139. T. Sjöstrand, P.Z. Skands, Multiple interactions and the structure of beam remnants. *JHEP* **03**, 053 (2004). doi:[10.1088/1126-6708/2004/03/053](https://doi.org/10.1088/1126-6708/2004/03/053). arXiv:[hep-ph/0402078](https://arxiv.org/abs/hep-ph/0402078)
140. M. Bähr, S. Gieseke, M.H. Seymour, Simulation of multiple partonic interactions in Herwig++. *JHEP* **07**, 076 (2008). doi:[10.1088/1126-6708/2008/07/076](https://doi.org/10.1088/1126-6708/2008/07/076). arXiv:[0803.3633](https://arxiv.org/abs/0803.3633)
141. A. Buckley et al., Rivet user manual. *Comput. Phys. Commun.* **184**, 2803 (2013). doi:[10.1016/j.cpc.2013.05.021](https://doi.org/10.1016/j.cpc.2013.05.021). arXiv:[1003.0694](https://arxiv.org/abs/1003.0694)
142. A. Buckley et al., Systematic event generator tuning for the LHC. *Eur. Phys. J. C* **65**, 331 (2010). doi:[10.1140/epjc/s10052-009-1196-7](https://doi.org/10.1140/epjc/s10052-009-1196-7). arXiv:[0907.2973](https://arxiv.org/abs/0907.2973)
143. H. Abramowicz et al., Summary of the Workshop on Multi-Parton Interactions (MPI@LHC 2012), arXiv:[1306.5413](https://arxiv.org/abs/1306.5413)
144. S. Plätzer, M. Diehl (eds.), in *Proceedings of the 3rd International Workshop on Multiple Partonic Interactions at the LHC (MPI@LHC 2011)*, Hamburg, Germany, 21–25 Nov, DESY. DESY, Hamburg, Germany, (2011). doi:[10.3204/DESY-PROC-2012-03](https://doi.org/10.3204/DESY-PROC-2012-03)
145. P. Bartalini, L. Fanó (eds.), in *Proceedings of the 1st International Workshop on Multiple Partonic Interactions at the LHC (MPI@LHC 2008)*, Perugia, Italy, 27–31 Oct (2008). arXiv:[1003.4220](https://arxiv.org/abs/1003.4220)
146. CMS Collaboration, Event generator tunes obtained from underlying event and multiparton scattering measurements. *Eur. Phys. J. C* **76**, 155 (2015). doi:[10.1140/epjc/s10052-016-3988-x](https://doi.org/10.1140/epjc/s10052-016-3988-x). arXiv:[1512.00815](https://arxiv.org/abs/1512.00815)

147. CDF Collaboration, R. Field, The Energy Dependence of the Underlying Event in Hadronic Collisions, in *Proceedings, The 2013 European Physical Society Conference on High Energy Physics (EPS-HEP 2013)*, volume EPS-HEP2013, p. 422. Stockholm, Sweden, 18-24 July 2013
148. ATLAS Collaboration, New ATLAS event generator tunes to 2010 *data*, Technical report ATL-PHYS-PUB-2011-008, CERN, Geneva, 2011
149. P.Z. Skands, Tuning Monte Carlo Generators: The Perugia Tunes. *Phys. Rev. D* **82**, 074018 (2010). doi:[10.1103/PhysRevD.82.074018](https://doi.org/10.1103/PhysRevD.82.074018). arXiv:[1005.3457](https://arxiv.org/abs/1005.3457)
150. J.M. Katzy, QCD Monte-Carlo model tunes for the LHC. *Prog. Part. Nucl. Phys.* **73**, 141 (2013). doi:[10.1016/j.ppnp.2013.08.002](https://doi.org/10.1016/j.ppnp.2013.08.002)
151. S. Catani, F. Krauss, R. Kuhn, B.R. Webber, QCD matrix elements + parton showers. *JHEP* **11**, 063 (2001). doi:[10.1088/1126-6708/2001/11/063](https://doi.org/10.1088/1126-6708/2001/11/063). arXiv:[hep-ph/0109231](https://arxiv.org/abs/hep-ph/0109231)
152. F. Krauss, Matrix elements and parton showers in hadronic interactions. *JHEP* **08**, 015 (2002). doi:[10.1088/1126-6708/2002/08/015](https://doi.org/10.1088/1126-6708/2002/08/015). arXiv:[hep-ph/0205283](https://arxiv.org/abs/hep-ph/0205283)
153. L. Lönnblad, Correcting the color dipole cascade model with fixed order matrix elements. *JHEP* **05**, 046 (2002). doi:[10.1088/1126-6708/2002/05/046](https://doi.org/10.1088/1126-6708/2002/05/046). arXiv:[hep-ph/0112284](https://arxiv.org/abs/hep-ph/0112284)
154. M.L. Mangano, M. Moretti, F. Piccinini, M. Treccani, Matching matrix elements and shower evolution for top-quark production in hadronic collisions. *JHEP* **01**, 013 (2007). doi:[10.1088/1126-6708/2007/01/013](https://doi.org/10.1088/1126-6708/2007/01/013). arXiv:[hep-ph/0611129](https://arxiv.org/abs/hep-ph/0611129)
155. J. Alwall et al., Comparative study of various algorithms for the merging of parton showers and matrix elements in hadronic collisions. *Eur. Phys. J. C* **53**, 473 (2008). doi:[10.1140/epjc/s10052-007-0490-5](https://doi.org/10.1140/epjc/s10052-007-0490-5). arXiv:[0706.2569](https://arxiv.org/abs/0706.2569)
156. S. Catani, M.H. Seymour, A General algorithm for calculating jet cross-sections in NLO QCD. *Nucl. Phys. B* **485**, 291 (1997). doi:[10.1016/S0550-3213\(96\)00589-5](https://doi.org/10.1016/S0550-3213(96)00589-5). arXiv:[hep-ph/9605323](https://arxiv.org/abs/hep-ph/9605323)
157. S. Frixione, Z. Kunszt, A. Signer, Three jet cross-sections to next-to-leading order. *Nucl. Phys. B* **467**, 399 (1996). doi:[10.1016/0550-3213\(96\)00110-1](https://doi.org/10.1016/0550-3213(96)00110-1). arXiv:[hep-ph/9512328](https://arxiv.org/abs/hep-ph/9512328)
158. D.A. Kosower, Antenna factorization of gauge theory amplitudes. *Phys. Rev. D* **57**, 5410 (1998). doi:[10.1103/PhysRevD.57.5410](https://doi.org/10.1103/PhysRevD.57.5410). arXiv:[hep-ph/9710213](https://arxiv.org/abs/hep-ph/9710213)
159. Z. Nagy, D.E. Soper, General subtraction method for numerical calculation of one-loop QCD matrix elements. *JHEP* **09**, 055 (2003). doi:[10.1088/1126-6708/2003/09/055](https://doi.org/10.1088/1126-6708/2003/09/055). arXiv:[hep-ph/0308127](https://arxiv.org/abs/hep-ph/0308127)
160. S. Frixione, B.R. Webber, Matching NLO QCD computations and parton shower simulations. *JHEP* **06**, 029 (2002). doi:[10.1088/1126-6708/2002/06/029](https://doi.org/10.1088/1126-6708/2002/06/029). arXiv:[hep-ph/0204244](https://arxiv.org/abs/hep-ph/0204244)
161. P. Nason, A New method for combining NLO QCD with shower Monte Carlo algorithms. *JHEP* **11**, 040 (2004). doi:[10.1088/1126-6708/2004/11/040](https://doi.org/10.1088/1126-6708/2004/11/040). arXiv:[hep-ph/0409146](https://arxiv.org/abs/hep-ph/0409146)
162. S. Frixione, P. Nason, C. Oleari, Matching NLO QCD computations with Parton Shower simulations: the POWHEG method. *JHEP* **11**, 070 (2007). doi:[10.1088/1126-6708/2007/11/070](https://doi.org/10.1088/1126-6708/2007/11/070). arXiv:[0709.2092](https://arxiv.org/abs/0709.2092)
163. S. Alioli, P. Nason, C. Oleari, E. Re, A general framework for implementing NLO calculations in shower Monte Carlo programs: the POWHEG BOX. *JHEP* **06**, 043 (2010). doi:[10.1007/JHEP06\(2010\)043](https://doi.org/10.1007/JHEP06(2010)043). arXiv:[1002.2581](https://arxiv.org/abs/1002.2581)
164. S. Höche, F. Krauss, M. Schönherr, F. Siegert, A critical appraisal of NLO+PS matching methods. *JHEP* **09**, 049 (2012). doi:[10.1007/JHEP09\(2012\)049](https://doi.org/10.1007/JHEP09(2012)049). arXiv:[1111.1220](https://arxiv.org/abs/1111.1220)
165. J. Alwall et al., The automated computation of tree-level and next-to-leading order differential cross sections, and their matching to parton shower simulations. *JHEP* **07**, 079 (2014). doi:[10.1007/JHEP07\(2014\)079](https://doi.org/10.1007/JHEP07(2014)079). arXiv:[1405.0301](https://arxiv.org/abs/1405.0301)
166. K. Hamilton, P. Nason, Improving NLO-parton shower matched simulations with higher order matrix elements. *JHEP* **06**, 039 (2010). doi:[10.1007/JHEP06\(2010\)039](https://doi.org/10.1007/JHEP06(2010)039). arXiv:[1004.1764](https://arxiv.org/abs/1004.1764)
167. S. Höche, F. Krauss, M. Schönherr, F. Siegert, NLO matrix elements and truncated showers. *JHEP* **08**, 123 (2011). doi:[10.1007/JHEP08\(2011\)123](https://doi.org/10.1007/JHEP08(2011)123). arXiv:[1009.1127](https://arxiv.org/abs/1009.1127)
168. S. Höche, F. Krauss, M. Schönherr, F. Siegert, QCD matrix elements + parton showers: the NLO case. *JHEP* **04**, 027 (2013). doi:[10.1007/JHEP04\(2013\)027](https://doi.org/10.1007/JHEP04(2013)027). arXiv:[1207.5030](https://arxiv.org/abs/1207.5030)
169. L. Lönnblad, S. Prestel, Merging multi-leg NLO matrix elements with parton showers. *JHEP* **03**, 166 (2013). doi:[10.1007/JHEP03\(2013\)166](https://doi.org/10.1007/JHEP03(2013)166). arXiv:[1211.7278](https://arxiv.org/abs/1211.7278)

170. K. Hamilton, P. Nason, C. Oleari, G. Zanderighi, Merging H/W/Z + 0 and 1 jet at NLO with no merging scale: a path to parton shower + NNLO matching. *JHEP* **05**, 082 (2013). doi:[10.1007/JHEP05\(2013\)082](https://doi.org/10.1007/JHEP05(2013)082). [arXiv:1212.4504](https://arxiv.org/abs/1212.4504)
171. S. Höche et al., Next-to-leading order QCD predictions for top-quark pair production with up to two jets merged with a parton shower. *Phys. Lett. B* **748**, 74 (2015). doi:[10.1016/j.physletb.2015.06.060](https://doi.org/10.1016/j.physletb.2015.06.060). [arXiv:1402.6293](https://arxiv.org/abs/1402.6293)
172. G.F. Sterman, S. Weinberg, Jets from quantum chromodynamics. *Phys. Rev. Lett.* **39**, 1436 (1977). doi:[10.1103/PhysRevLett.39.1436](https://doi.org/10.1103/PhysRevLett.39.1436)
173. JADE Collaboration, Experimental studies on multi-jet production in e+ e- annihilation at PETRA energies. *Z. Phys. C* **33**, 23 (1986). doi:[10.1007/BF01410449](https://doi.org/10.1007/BF01410449)
174. B. Flaughner and K. Meier, A Compilation of jet finding algorithms, in *Proceedings, 5th DPF Summer Study on High-energy Physics: Research Directions for the Decade (Snowmass 90)*, p. 128. Snowmass, CO, USA, June 25–July 13, 1990
175. J. E. Huth et al., Towards a standardization of jet definitions, in *Proceedings, 5th DPF Summer Study on High-energy Physics: Research Directions for the Decade (Snowmass 90)*, p. 134. Snowmass, CO, USA, June 25–July 13, 1990
176. G.C. Blazey et al., Run II jet physics, in *Proceedings, Physics at Run II: QCD and Weak Boson Physics Workshop*, p. 47. Batavia, IL, USA, March 4–6, June 3–4, November 4–6, 1999. [arXiv:hep-ex/0005012](https://arxiv.org/abs/hep-ex/0005012)
177. C. Buttar et al., Standard Model Handles and Candles Working Group: Tools and Jets Summary Report, in *Proceedings, 5th Les Houches Workshop 2007 on Physics at TeV colliders (Les Houches 2007)*, p. 121. Les Houches, France, 11–29 June 2007. [arXiv:0803.0678](https://arxiv.org/abs/0803.0678)
178. G.P. Salam, Towards jetography. *Eur. Phys. J. C* **67**, 637 (2010). doi:[10.1140/epjc/s10052-010-1314-6](https://doi.org/10.1140/epjc/s10052-010-1314-6). [arXiv:0906.1833](https://arxiv.org/abs/0906.1833)
179. M. Cacciari, G.P. Salam, G. Soyez, FastJet user manual. *Eur. Phys. J. C* **72**, 1896 (2012). doi:[10.1140/epjc/s10052-012-1896-2](https://doi.org/10.1140/epjc/s10052-012-1896-2). [arXiv:1111.6097](https://arxiv.org/abs/1111.6097)
180. CDF Collaboration, Measurement of the inclusive jet cross section at the Fermilab Tevatron $p\bar{p}$ collider using a cone-based jet algorithm. *Phys. Rev. D* **78**, 052006 (2008). doi:[10.1103/PhysRevD.78.052006](https://doi.org/10.1103/PhysRevD.78.052006), [arXiv:0807.2204](https://arxiv.org/abs/0807.2204)
181. D0 Collaboration, Measurement of the inclusive jet cross section in $p\bar{p}$ collisions at $\sqrt{s} = 1.96$ TeV. *Phys. Rev. D* **85** (2012) 052006. doi:[10.1103/PhysRevD.85.052006](https://doi.org/10.1103/PhysRevD.85.052006), [arXiv:1110.3771](https://arxiv.org/abs/1110.3771). Long author list—awaiting processing
182. G.P. Salam, G. Soyez, A practical Seedless Infrared-Safe Cone jet algorithm. *JHEP* **05**, 086 (2007). doi:[10.1088/1126-6708/2007/05/086](https://doi.org/10.1088/1126-6708/2007/05/086). [arXiv:0704.0292](https://arxiv.org/abs/0704.0292)
183. S. Catani, B.R. Webber, Infrared safe but infinite: soft gluon divergences inside the physical region. *JHEP* **10**, 005 (1997). doi:[10.1088/1126-6708/1997/10/005](https://doi.org/10.1088/1126-6708/1997/10/005). [arXiv:hep-ph/9710333](https://arxiv.org/abs/hep-ph/9710333)
184. T. Hebbeker, Tests of quantum chromodynamics in hadronic decays of Z^0 bosons produced in e^+e^- annihilation. *Phys. Rept.* **217**, 69 (1992). doi:[10.1016/0370-1573\(92\)90181-X](https://doi.org/10.1016/0370-1573(92)90181-X)
185. S. Catani et al., New clustering algorithm for multi - jet cross-sections in e+ e- annihilation. *Phys. Lett. B* **269**, 432 (1991). doi:[10.1016/0370-2693\(91\)90196-W](https://doi.org/10.1016/0370-2693(91)90196-W)
186. M. Dasgupta, L. Magnea, G.P. Salam, Non-perturbative QCD effects in jets at hadron colliders. *JHEP* **02**, 055 (2008). doi:[10.1088/1126-6708/2008/02/055](https://doi.org/10.1088/1126-6708/2008/02/055). [arXiv:0712.3014](https://arxiv.org/abs/0712.3014)
187. UA1 Collaboration, Hadronic Jet Production at the CERN Proton-Antiproton Collider. *Phys. Lett. B* **132**, 214 (1983). doi:[10.1016/0370-2693\(83\)90254-X](https://doi.org/10.1016/0370-2693(83)90254-X)
188. UA2 Collaboration, Observation of very large transverse momentum jets at the CERN $\bar{p}p$ Collider. *Phys. Lett. B* **118**, 203 (1982). doi:[10.1016/0370-2693\(82\)90629-3](https://doi.org/10.1016/0370-2693(82)90629-3)
189. UA2 Collaboration, Measurement of production and properties of jets at the CERN anti-p p collider. *Z. Phys. C* **20**, 117 (1983). doi:[10.1007/BF01573214](https://doi.org/10.1007/BF01573214)
190. M. Cacciari, G.P. Salam, Dispelling the N^3 myth for the k_t jet-finder. *Phys. Lett. B* **641**, 57 (2006). doi:[10.1016/j.physletb.2006.08.037](https://doi.org/10.1016/j.physletb.2006.08.037). [arXiv:hep-ph/0512210](https://arxiv.org/abs/hep-ph/0512210)
191. S.D. Ellis, J. Huston, M. Tönnemann, On building better cone jet algorithms. *eConf* **C010630** (2001) 513, [arXiv:hep-ph/0111434](https://arxiv.org/abs/hep-ph/0111434)
192. J. Berger, Search for the Higgs Boson Produced via Vector-Boson Fusion in the Decay Channel $H \rightarrow \tau\tau$. PhD thesis, KIT (Karlsruher Institut für Technologie), Jun, 2014

193. M. Cacciari, G.P. Salam, G. Soyez, The catchment area of jets. JHEP **04**, 005 (2008). doi:[10.1088/1126-6708/2008/04/005](https://doi.org/10.1088/1126-6708/2008/04/005). arXiv:[0802.1188](https://arxiv.org/abs/0802.1188)
194. S.D. Ellis, D.E. Soper, Successive combination jet algorithm for hadron collisions. Phys. Rev. D **48**, 3160 (1993). doi:[10.1103/PhysRevD.48.3160](https://doi.org/10.1103/PhysRevD.48.3160). arXiv:[hep-ph/9305266](https://arxiv.org/abs/hep-ph/9305266)
195. Y.L. Dokshitzer, G.D. Leder, S. Moretti, B.R. Webber, Better jet clustering algorithms. JHEP **08**, 001 (1997). doi:[10.1088/1126-6708/1997/08/001](https://doi.org/10.1088/1126-6708/1997/08/001). arXiv:[hep-ph/9707323](https://arxiv.org/abs/hep-ph/9707323)
196. M. Wobisch, T. Wengler, Hadronization corrections to jet cross-sections in deep inelastic scattering, in *Proceedings, Monte Carlo Generators for HERA Physics*. Hamburg, Germany, 1998–1999, 1998. arXiv:[hep-ph/9907280](https://arxiv.org/abs/hep-ph/9907280)
197. M. Cacciari, G.P. Salam, G. Soyez, The anti- k_t jet clustering algorithm. JHEP **04**, 063 (2008). doi:[10.1088/1126-6708/2008/04/063](https://doi.org/10.1088/1126-6708/2008/04/063). arXiv:[0802.1189](https://arxiv.org/abs/0802.1189)
198. CMS Collaboration, Measurement of the underlying event activity in pp collisions at $\sqrt{s} = 0.9$ and 7 TeV with the novel jet-area/median approach, JHEP **08** (2012) 130. doi:[10.1007/JHEP08\(2012\)130](https://doi.org/10.1007/JHEP08(2012)130), arXiv:[1207.2392](https://arxiv.org/abs/1207.2392)
199. R. Barlow et al., *Data Analysis in High Energy Physics*, 1st edn. (Wiley-VCH Verlag GmbH & Co. KGaA, Weinheim, Germany, 2013)
200. F.I. Olness, D.E. Soper, Correlated theoretical uncertainties for the one-jet inclusive cross section. Phys. Rev. D **81**, 035018 (2010). doi:[10.1103/PhysRevD.81.035018](https://doi.org/10.1103/PhysRevD.81.035018). arXiv:[0907.5052](https://arxiv.org/abs/0907.5052)
201. C. Anastasiou, L.J. Dixon, K. Melnikov, F. Petriello, High precision QCD at hadron colliders: electroweak gauge boson rapidity distributions at NNLO. Phys. Rev. D **69**, 094008 (2004). doi:[10.1103/PhysRevD.69.094008](https://doi.org/10.1103/PhysRevD.69.094008). arXiv:[hep-ph/0312266](https://arxiv.org/abs/hep-ph/0312266)
202. M. Cacciari, N. Houdeau, Meaningful characterisation of perturbative theoretical uncertainties. JHEP **09**, 039 (2011). doi:[10.1007/JHEP09\(2011\)039](https://doi.org/10.1007/JHEP09(2011)039). arXiv:[1105.5152](https://arxiv.org/abs/1105.5152)
203. E. Bagnaschi, M. Cacciari, A. Guffanti, L. Jenniches, An extensive survey of the estimation of uncertainties from missing higher orders in perturbative calculations. JHEP **02**, 133 (2015). doi:[10.1007/JHEP02\(2015\)133](https://doi.org/10.1007/JHEP02(2015)133). arXiv:[1409.5036](https://arxiv.org/abs/1409.5036)
204. M. Cacciari et al., The t anti- t cross-section at 1.8 TeV and 1.96 TeV: A Study of the systematics due to parton densities and scale dependence. JHEP **04** (2004) 068. doi:[10.1088/1126-6708/2004/04/068](https://doi.org/10.1088/1126-6708/2004/04/068), arXiv:[hep-ph/0303085](https://arxiv.org/abs/hep-ph/0303085)
205. A. Banfi, G.P. Salam, G. Zanderighi, Phenomenology of event shapes at hadron colliders. JHEP **06**, 038 (2010). doi:[10.1007/JHEP06\(2010\)038](https://doi.org/10.1007/JHEP06(2010)038). arXiv:[1001.4082](https://arxiv.org/abs/1001.4082)
206. G. Grunberg, Renormalization Group Improved Perturbative QCD. Phys. Lett. B **95**, 70 (1980). doi:[10.1016/0370-2693\(80\)90402-5](https://doi.org/10.1016/0370-2693(80)90402-5). [Erratum: Phys. Lett. B **110**, 501(1982)]
207. J. Kubo, S. Sakakibara, Equivalence of the fastest apparent convergence criterion and the principle of minimal sensitivity in perturbative quantum chromodynamics. Phys. Rev. D **26**, 3656 (1982). doi:[10.1103/PhysRevD.26.3656](https://doi.org/10.1103/PhysRevD.26.3656)
208. P.M. Stevenson, Resolution of the renormalization scheme ambiguity in perturbative QCD. Phys. Lett. B **100**, 61 (1981). doi:[10.1016/0370-2693\(81\)90287-2](https://doi.org/10.1016/0370-2693(81)90287-2)
209. P.M. Stevenson, Optimized perturbation theory. Phys. Rev. D **23**, 2916 (1981). doi:[10.1103/PhysRevD.23.2916](https://doi.org/10.1103/PhysRevD.23.2916)
210. S.J. Brodsky, G.P. Lepage, P.B. Mackenzie, On the elimination of scale ambiguities in perturbative quantum chromodynamics. Phys. Rev. D **28**, 228 (1983). doi:[10.1103/PhysRevD.28.228](https://doi.org/10.1103/PhysRevD.28.228)
211. S.J. Brodsky, L. Di Giustino, Setting the renormalization scale in QCD: the principle of maximum conformality. Phys. Rev. D **86**, 085026 (2012). doi:[10.1103/PhysRevD.86.085026](https://doi.org/10.1103/PhysRevD.86.085026). arXiv:[1107.0338](https://arxiv.org/abs/1107.0338)
212. S.J. Brodsky, M. Mojaza, X.-G. Wu, Systematic scale-setting to all orders: the principle of maximum conformality and commensurate scale relations. Phys. Rev. D **89**, 014027 (2014). doi:[10.1103/PhysRevD.89.014027](https://doi.org/10.1103/PhysRevD.89.014027). arXiv:[1304.4631](https://arxiv.org/abs/1304.4631)
213. H.-Y. Bi et al., Degeneracy relations in QCD and the equivalence of two systematic all-orders methods for setting the renormalization scale. Phys. Lett. B **748** (2015) 13–18. doi:[10.1016/j.physletb.2015.06.056](https://doi.org/10.1016/j.physletb.2015.06.056), arXiv:[1505.04958](https://arxiv.org/abs/1505.04958)

214. M. Rubin, G.P. Salam, S. Sapeta, Giant QCD K-factors beyond NLO. JHEP **09**, 084 (2010). doi:[10.1007/JHEP09\(2010\)084](#). arXiv:[1006.2144](#)
215. A. David, G. Passarino, How well can we guess theoretical uncertainties? Phys. Lett. B **726**, 266 (2013). doi:[10.1016/j.physletb.2013.08.025](#). arXiv:[1307.1843](#)
216. CDF Collaboration, Inclusive jet cross section in $\bar{p}p$ collisions at $\sqrt{s} = 1.8$ TeV. Phys. Rev. Lett. **77**, 438 (1996). doi:[10.1103/PhysRevLett.77.438](#). arXiv:[hep-ex/9601008](#)
217. J. Huston et al., Large transverse momentum jet production and the gluon distribution inside the proton. Phys. Rev. Lett. **77**, 444 (1996). doi:[10.1103/PhysRevLett.77.444](#). arXiv:[hep-ph/9511386](#)
218. A.D. Martin, W.J. Stirling, R.S. Thorne, G. Watt, Parton distributions for the LHC. Eur. Phys. J. C **63**, 189 (2009). doi:[10.1140/epjc/s10052-009-1072-5](#). arXiv:[0901.0002](#)
219. S. Dulat et al., New parton distribution functions from a global analysis of quantum chromodynamics. Phys. Rev. D **93**, 033006 (2016). doi:[10.1103/PhysRevD.93.033006](#). arXiv:[1506.07443](#)
220. E. Laenen, S. Riemersma, J. Smith, W.L. van Neerven, On the heavy quark content of the nucleon. Phys. Lett. B **291**, 325 (1992). doi:[10.1016/0370-2693\(92\)91053-C](#)
221. E. Laenen, S. Riemersma, J. Smith, W.L. van Neerven, Complete $O(\alpha_s)$ corrections to heavy flavor structure functions in electroproduction. Nucl. Phys. B **392**, 162 (1993). doi:[10.1016/0550-3213\(93\)90201-Y](#)
222. S. Riemersma, J. Smith, W.L. van Neerven, Rates for inclusive deep inelastic electroproduction of charm quarks at HERA. Phys. Lett. B **347**, 143 (1995). doi:[10.1016/0370-2693\(95\)00036-K](#). arXiv:[hep-ph/9411431](#)
223. R. S. Thorne, W.K. Tung, PQCD Formulations with Heavy Quark Masses and Global Analysis, in *Proceedings, 4th Workshop on the Implications of HERA for LHC Physics (HERA and the LHC)*. Geneva, Switzerland, 26–30 May 2008. arXiv:[0809.0714](#)
224. N. Arkani-Hamed, T. Han, M. Mangano, L.-T. Wang, Physics Opportunities of a 100 TeV Proton-Proton Collider, arXiv:[1511.06495](#)
225. S. Alekhin, J. Blümlein, S. Moch, Parton distribution functions and benchmark cross sections at NNLO. Phys. Rev. D **86**, 054009 (2012). doi:[10.1103/PhysRevD.86.054009](#). arXiv:[1202.2281](#)
226. J.F. Owens, A. Accardi, W. Melnitchouk, Global parton distributions with nuclear and finite- Q^2 corrections. Phys. Rev. D **87**, 094012 (2013). doi:[10.1103/PhysRevD.87.094012](#). arXiv:[1212.1702](#)
227. H.-L. Lai et al., New parton distributions for collider physics. Phys. Rev. D **82**, 074024 (2010). doi:[10.1103/PhysRevD.82.074024](#). arXiv:[1007.2241](#)
228. H1 and ZEUS Collaborations, Combined measurement and QCD analysis of the inclusive $e^\pm p$ scattering cross sections at HERA. J. High Energy Phys. **01**, 109 (2010). doi:[10.1007/JHEP01\(2010\)109](#). arXiv:[0911.0884](#)
229. M. Glück, P. Jimenez-Delgado, E. Reya, Dynamical parton distributions of the nucleon and very small- x physics. Eur. Phys. J. C **53**, 355 (2008). doi:[10.1140/epjc/s10052-007-0462-9](#). arXiv:[0709.0614](#)
230. M. Glück, P. Jimenez-Delgado, E. Reya, C. Schuck, On the role of heavy flavor parton distributions at high energy colliders. Phys. Lett. B **664**, 133 (2008). doi:[10.1016/j.physletb.2008.04.063](#). arXiv:[0801.3618](#)
231. A.D. Martin, W.J. Stirling, R.S. Thorne, G. Watt, Uncertainties on α_s in global PDF analyses and implications for predicted hadronic cross sections. Eur. Phys. J. C **64**, 653 (2009). doi:[10.1140/epjc/s10052-009-1164-2](#). arXiv:[0905.3531](#)
232. R.D. Ball et al., Impact of heavy quark masses on parton distributions and LHC phenomenology. Nucl. Phys. B **849**, 296 (2011). doi:[10.1016/j.nuclphysb.2011.03.021](#). arXiv:[1101.1300](#)
233. R.D. Ball et al., Parton distributions with LHC data. Nucl. Phys. B **867**, 244 (2013). doi:[10.1016/j.nuclphysb.2012.10.003](#). arXiv:[1207.1303](#)
234. A. Accardi et al., Constraints on large- x parton distributions from new weak boson production and deep-inelastic scattering data, arXiv:[1602.03154](#)

235. H1 and ZEUS Collaborations, Combination of measurements of inclusive deep inelastic $e^\pm p$ scattering cross sections and QCD analysis of HERA data. *Eur. Phys. J. C* **75** (2015) 580. doi:[10.1140/epjc/s10052-015-3710-4](https://doi.org/10.1140/epjc/s10052-015-3710-4), [arXiv:1506.06042](https://arxiv.org/abs/1506.06042)
236. P. Jimenez-Delgado, E. Reya, Delineating parton distributions and the strong coupling. *Phys. Rev. D* **89**, 074049 (2014). doi:[10.1103/PhysRevD.89.074049](https://doi.org/10.1103/PhysRevD.89.074049). [arXiv:1403.1852](https://arxiv.org/abs/1403.1852)
237. L.A. Harland-Lang, A.D. Martin, P. Motylinski, R.S. Thorne, Parton distributions in the LHC era: MMHT 2014 PDFs. *Eur. Phys. J. C* **75**, 204 (2015). doi:[10.1140/epjc/s10052-015-3397-6](https://doi.org/10.1140/epjc/s10052-015-3397-6). [arXiv:1412.3989](https://arxiv.org/abs/1412.3989)
238. NNPDF Collaboration, Parton distributions for the LHC Run II. *JHEP* **04** (2015) 040. doi:[10.1007/JHEP04\(2015\)040](https://doi.org/10.1007/JHEP04(2015)040), [arXiv:1410.8849](https://arxiv.org/abs/1410.8849)
239. M.R. Whalley, D. Bourilkov, R.C. Group, The Les Houches Accord PDFs (LHAPDF) and LHAGLUE, in *Proceedings, HERA and the LHC: A Workshop on the implications of HERA for LHC physics: Vol. B*. Geneva, Switzerland and Hamburg, Germany, 26–27 March, 11–13 Oct, 21–24 March, 2004–2005. [arXiv:hep-ph/0508110](https://arxiv.org/abs/hep-ph/0508110)
240. A. Buckley et al., LHAPDF6: parton density access in the LHC precision era. *Eur. Phys. J. C* **75**, 132 (2015). doi:[10.1140/epjc/s10052-015-3318-8](https://doi.org/10.1140/epjc/s10052-015-3318-8). [arXiv:1412.7420](https://arxiv.org/abs/1412.7420)
241. D. Stump et al., Uncertainties of predictions from parton distribution functions. 1. The Lagrange multiplier method. *Phys. Rev. D* **65**, 014012 (2001). doi:[10.1103/PhysRevD.65.014012](https://doi.org/10.1103/PhysRevD.65.014012). [arXiv:hep-ph/0101051](https://arxiv.org/abs/hep-ph/0101051)
242. J. Pumplin et al., Uncertainties of predictions from parton distribution functions. 2. The Hessian method. *Phys. Rev. D* **65**, 014013 (2001). doi:[10.1103/PhysRevD.65.014013](https://doi.org/10.1103/PhysRevD.65.014013). [arXiv:hep-ph/0101032](https://arxiv.org/abs/hep-ph/0101032)
243. W.T. Giele, S. Keller, Implications of hadron collider observables on parton distribution function uncertainties. *Phys. Rev. D* **58**, 094023 (1998). doi:[10.1103/PhysRevD.58.094023](https://doi.org/10.1103/PhysRevD.58.094023). [arXiv:hep-ph/9803393](https://arxiv.org/abs/hep-ph/9803393)
244. W.T. Giele, S.A. Keller, D.A. Kosower, Parton distribution function uncertainties, [arXiv:hep-ph/0104052](https://arxiv.org/abs/hep-ph/0104052)
245. NNPDF Collaboration, A determination of parton distributions with faithful uncertainty estimation. *Nucl. Phys. B* **809** (2009) 1. doi:[10.1016/j.nuclphysb.2008.09.037](https://doi.org/10.1016/j.nuclphysb.2008.09.037), [arXiv:0808.1231](https://arxiv.org/abs/0808.1231)
246. S. Alekhin et al., HERAFitter. *Eur. Phys. J. C* **75**, 304 (2015). doi:[10.1140/epjc/s10052-015-3480-z](https://doi.org/10.1140/epjc/s10052-015-3480-z). [arXiv:1410.4412](https://arxiv.org/abs/1410.4412)
247. M. Botje et al., The PDF4LHC Working Group Interim Recommendations, [arXiv:1101.0538](https://arxiv.org/abs/1101.0538)
248. J. Butterworth et al., PDF4LHC recommendations for LHC Run II. *J. Phys. G* **43**, 023001 (2016). doi:[10.1088/0954-3899/43/2/023001](https://doi.org/10.1088/0954-3899/43/2/023001). [arXiv:1510.03865](https://arxiv.org/abs/1510.03865)
249. C. Bourrely, J. Soffer, F. Buccella, A Statistical approach for polarized parton distributions. *Eur. Phys. J. C* **23**, 487 (2002). doi:[10.1007/s100520100855](https://doi.org/10.1007/s100520100855). [arXiv:hep-ph/0109160](https://arxiv.org/abs/hep-ph/0109160)
250. C. Bourrely, J. Soffer, New developments in the statistical approach of parton distributions: tests and predictions up to LHC energies. *Nucl. Phys. A* **941**, 307 (2015). doi:[10.1016/j.nuclphysa.2015.06.018](https://doi.org/10.1016/j.nuclphysa.2015.06.018). [arXiv:1502.02517](https://arxiv.org/abs/1502.02517)
251. SM and NLO Multileg Working Group Collaboration, T. Binoth et al., The SM and NLO Multileg Working Group: Summary report, in *Proceedings, 6th Les Houches Workshop 2009 on Physics at TeV colliders (Les Houches 2009; dedicated to Thomas Binoth)*, p. 21. Les Houches, France, 8–26 June 2010. [arXiv:1003.1241](https://arxiv.org/abs/1003.1241)
252. H.-L. Lai et al., Uncertainty induced by the QCD coupling in the CTEQ global analysis of parton distributions. *Phys. Rev. D* **82**, 054021 (2010). doi:[10.1103/PhysRevD.82.054021](https://doi.org/10.1103/PhysRevD.82.054021). [arXiv:1004.4624](https://arxiv.org/abs/1004.4624)
253. F. Demartin et al., The impact of PDF and alphas uncertainties on Higgs Production in gluon fusion at hadron colliders. *Phys. Rev. D* **82**, 014002 (2010). doi:[10.1103/PhysRevD.82.014002](https://doi.org/10.1103/PhysRevD.82.014002). [arXiv:1004.0962](https://arxiv.org/abs/1004.0962)
254. CMS Collaboration, Constraints on parton distribution functions and extraction of the strong coupling constant from the inclusive jet cross section in pp collisions at $\sqrt{s} = 7$ TeV. *Eur. Phys. J. C* **75**, 288 (2015). doi:[10.1140/epjc/s10052-015-3499-1](https://doi.org/10.1140/epjc/s10052-015-3499-1). [arXiv:1410.6765](https://arxiv.org/abs/1410.6765)
255. S.D. Ellis, Z. Kunszt, D.E. Soper, One-jet inclusive cross section at order α_s^3 : quarks and gluons. *Phys. Rev. Lett.* **64**, 2121 (1990). doi:[10.1103/PhysRevLett.64.2121](https://doi.org/10.1103/PhysRevLett.64.2121)

256. S.D. Ellis, Z. Kunszt, D.E. Soper, Two-jet production in hadron collisions at order α_s^3 in QCD. *Phys. Rev. Lett.* **69**, 1496 (1992). doi:[10.1103/PhysRevLett.69.1496](https://doi.org/10.1103/PhysRevLett.69.1496)
257. J. Gao et al., MEKS: a program for computation of inclusive jet cross sections at hadron colliders. *Comput. Phys. Commun.* **184**, 1626 (2013). doi:[10.1016/j.cpc.2013.01.022](https://doi.org/10.1016/j.cpc.2013.01.022). [arXiv:1207.0513](https://arxiv.org/abs/1207.0513)
258. W.T. Giele, E.W.N. Glover, D.A. Kosower, Higher order corrections to jet cross-sections in hadron colliders. *Nucl. Phys. B* **403**, 633 (1993). doi:[10.1016/0550-3213\(93\)90365-V](https://doi.org/10.1016/0550-3213(93)90365-V). [arXiv:hep-ph/9302225](https://arxiv.org/abs/hep-ph/9302225)
259. Z. Nagy, Three jet cross-sections in hadron hadron collisions at next-to-leading order. *Phys. Rev. Lett.* **88**, 122003 (2002). doi:[10.1103/PhysRevLett.88.122003](https://doi.org/10.1103/PhysRevLett.88.122003). [arXiv:hep-ph/0110315](https://arxiv.org/abs/hep-ph/0110315)
260. Z. Nagy, Next-to-leading order calculation of three-jet observables in hadron hadron collisions. *Phys. Rev. D* **68**, 094002 (2003). doi:[10.1103/PhysRevD.68.094002](https://doi.org/10.1103/PhysRevD.68.094002). [arXiv:hep-ph/0307268](https://arxiv.org/abs/hep-ph/0307268)
261. J. Currie, A. Gehrmann-De Ridder, E.W.N. Glover, J. Pires, NNLO QCD corrections to jet production at hadron colliders from gluon scattering. *JHEP* **01** (2014) 110. doi:[10.1007/JHEP01\(2014\)110](https://doi.org/10.1007/JHEP01(2014)110), [arXiv:1310.3993](https://arxiv.org/abs/1310.3993)
262. Z. Bern et al., Four-jet production at the large hadron collider at next-to-leading order in QCD. *Phys. Rev. Lett.* **109**, 042001 (2012). doi:[10.1103/PhysRevLett.109.042001](https://doi.org/10.1103/PhysRevLett.109.042001). [arXiv:1112.3940](https://arxiv.org/abs/1112.3940)
263. S. Badger, B. Biedermann, P. Uwer, V. Yundin, NLO QCD corrections to multi-jet production at the LHC with a centre-of-mass energy of $\sqrt{s} = 8$ TeV. *Phys. Lett. B* **718**, 965 (2013). doi:[10.1016/j.physletb.2012.11.029](https://doi.org/10.1016/j.physletb.2012.11.029). [arXiv:1209.0098](https://arxiv.org/abs/1209.0098)
264. S. Badger, B. Biedermann, P. Uwer, V. Yundin, Next-to-leading order QCD corrections to five jet production at the LHC. *Phys. Rev. D* **89**, 034019 (2014). doi:[10.1103/PhysRevD.89.034019](https://doi.org/10.1103/PhysRevD.89.034019). [arXiv:1309.6585](https://arxiv.org/abs/1309.6585)
265. H1 Collaboration, Measurement and QCD analysis of jet cross-sections in deep-inelastic positron-proton collisions at \sqrt{s} of 300 GeV. *Eur. Phys. J. C* **19**, 289 (2001). doi:[10.1007/s100520100621](https://doi.org/10.1007/s100520100621). [arXiv:hep-ex/0010054](https://arxiv.org/abs/hep-ex/0010054)
266. T. Kluge, K. Rabbertz, M. Wobisch, FastNLO: Fast pQCD calculations for PDF fits, in *14th International Workshop on Deep Inelastic Scattering (DIS 2006)*, p. 483. Tsukuba, Japan, 20–24 April 2006. [arXiv:hep-ph/0609285](https://arxiv.org/abs/hep-ph/0609285). doi:[10.1142/9789812706706_0110](https://doi.org/10.1142/9789812706706_0110)
267. T. Carli, G.P. Salam, F. Siegert, A Posteriori inclusion of PDFs in NLO QCD final-state calculations, in *HERA and the LHC: A Workshop on the Implications of HERA for LHC Physics (Startup Meeting, CERN, 26–27 March 2004; Working Group Meeting, CERN, 17–21 Jan 2005; Final Meeting 21–24 Mar 2005)* CERN. Geneva, Switzerland 11–13, 2005 (2004). [arXiv:hep-ph/0510324](https://arxiv.org/abs/hep-ph/0510324)
268. T. Carli et al., A posteriori inclusion of parton density functions in NLO QCD final-state calculations at hadron colliders: the APPLGRID Project. *Eur. Phys. J. C* **66**, 503 (2010). doi:[10.1140/epjc/s10052-010-1255-0](https://doi.org/10.1140/epjc/s10052-010-1255-0). [arXiv:0911.2985](https://arxiv.org/abs/0911.2985)
269. D. Britzger, K. Rabbertz, F. Stober, M. Wobisch, New features in version 2 of the fastNLO project, in *Proceedings, XX. International Workshop on Deep-Inelastic Scattering and Related Subjects (DIS 2012)*, p. 217. Bonn, Germany, 26–30 March 2012. [arXiv:1208.3641](https://arxiv.org/abs/1208.3641). doi:[10.3204/DESY-PROC-2012-02/165](https://doi.org/10.3204/DESY-PROC-2012-02/165)
270. D.A. Britzger, Regularized Unfolding of Jet Cross Sections in Deep-Inelastic ep Scattering at HERA and Determination of the Strong Coupling Constant. PhD thesis, Universität Hamburg, June, 2013

Jet Physics at the LHC

The Strong Force beyond the TeV Scale

Rabbertz, K.

2017, XV, 214 p. 112 illus., 98 illus. in color., Hardcover

ISBN: 978-3-319-42113-1